COMPARISON OF DEFORMATIONS FROM 2D AND 3D FEM ANALYSIS WITH FIELD MEASUREMENTS OF A TOP DOWN DEEP EXCAVATION IN BAĞCILAR METRO STATION

A THESIS SUBMITTED TO
THE GRADUATE SCHOOL OF NATURAL AND APPLIED SCIENCES
OF
MIDDLE EAST TECHNICAL UNIVERSITY

BY

ABDULLAH ONUR USTAOĞLU

IN PARTIAL FULFILLMENT OF THE REQUIREMENTS
FOR
THE DEGREE OF MASTER OF SCIENCE
IN
CIVIL ENGINEERING

MAY 2015

Approval of the thesis:

COMPARISON OF DEFORMATIONS FROM 2D AND 3D FEM ANALYSIS WITH FIELD MEASUREMENTS OF A TOP DOWN DEEP EXCAVATION IN BAĞCILAR METRO STATION

submitted by **ABDULLAH ONUR USTAOĞLU** in partial fulfillment of the requirements for the degree of **Master of Science in Civil Engineering Department, Middle East Technical University** by,

Prof. Dr. Gülbin Dural Ünver
Dean, Graduate School of **Natural and Applied Sciences** _____

Prof. Dr. Ahmet Cevdet Yalçıner
Head of Department, **Civil Engineering** _____

Prof. Dr. Erdal Çokça
Supervisor, **Civil Engineering Dept., METU** _____

Examining Committee Members

Asst. Prof. Dr. Nejan Huvaj Sarıhan
Civil Engineering Dept., METU _____

Prof. Dr. Erdal Çokça
Civil Engineering Dept., METU _____

Asst. Prof. Dr. Onur Pekcan
Civil Engineering Dept., METU _____

Asst. Prof. Dr. Nabi Kartal Toker
Civil Engineering Dept., METU _____

Prof. Dr. Tamer Topal
Geological Engineering Dept., METU _____

Date: 05/05/2015

I hereby declare that all information in this document has been obtained and presented in accordance with academic rules and ethical conduct. I also declare that, as required by these rules and conduct, I have fully cited and referenced all material and results that are not original to this work.

Name, Last Name: ABDULLAH ONUR USTAOĞLU

Signature :

ABSTRACT

COMPARISON OF DEFORMATIONS FROM 2D AND 3D FEM ANALYSIS WITH FIELD MEASUREMENTS OF A TOP DOWN DEEP EXCAVATION IN BAĞCILAR METRO STATION

Ustaoğlu, Abdullah Onur

M.S., Department of Civil Engineering

Supervisor: Prof. Dr. Erdal Çokca

May 2015, 138 pages

In this thesis, 2D and 3D FEM analysis results are compared with field measurements of a top down deep excavation in Bağcılar Metro Station which is on the Otogar - Bağcılar Light Rail Transit Line in İstanbul. First, a literature review on deep excavations is performed. The soil formation observed in the project site is Güngören formation and the dominant soil type is silty clay. After selecting the soil parameters and soil models, 2D and 3D models of the excavation are analyzed by FEM programs PLAXIS2D and PLAXIS3D. Deformation measurements taken by inclinometers are compared with the calculated deformations from FEM. The thesis study shows that lateral displacements of 2D analysis are between 3 and 4 times larger than the inclinometer measurements and 3D analysis. Moreover, 3D analysis results and inclinometer measurements are approximately same.

Key Words: Diaphragm Wall, Finite Element Method (FEM) Analysis, Inclinometer, Deep Excavations, Lateral Deformations, Bağcılar Station, Silty Clay.

ÖZ

BAĞCILAR METRO İSTASYONU'NDAKİ YUKARIDAN AŞAĞIYA YAPILAN DERİN KAZI İÇİN 2 VE 3 BOYUTLU SONLU ELEMAN YÖNTEMİ ANALİZ SONUÇLARI İLE SAHADA YAPILAN DEFORMASYON ÖLÇÜM SONUÇLARININ KARŞILAŞTIRILMASI

Ustaoğlu, Abdullah Onur

Yüksek Lisans, İnşaat Mühendisliği Bölümü

Tez Yöneticisi: Prof. Dr. Erdal Çokca

Mayıs 2015, 138 sayfa

Bu tezde, İstanbul'da bulunan Otogar-Bağcılar raylı sistem hattında bulunan Bağcılar Metro İstasyonu'ndaki yukarıdan aşağıya yapılan derin kazı için, 2 ve 3 boyutlu sonlu eleman sistemi analiz sonuçları ile sahada yapılan ölçüm sonuçları karşılaştırılmıştır. İlk olarak derin kazılar hakkında genel literatür taraması yapılmıştır. Proje alanında Güngören formasyonu gözlemlenmiş ve baskın zemin tipi siltli kil olarak belirlenmiştir. Zemin parametreleri ve zemin modeli seçildikten sonra, PLAXIS2D ve PLAXIS3D adlı sonlu eleman sistemi analiz programları ile 2 ve 3 boyutlu analizler yapılmıştır. Daha sonra, analiz sonuçları ile sahada inklinometre vasıtasıyla yapılan deformasyon sonuçları karşılaştırılmıştır. Tez çalışması sonucunda, 2 boyutlu analizlerin yatay deplasman sonuçlarının, inklinometre ölçümlerinden ve 3 boyutlu analiz sonuçlarından 3 ve 4 kat arasında

büyük olduğu görülmüştür. Buna ek olarak, 3 boyutlu analiz sonuçları ve inklinometre ölçümlerinin yaklaşık olarak aynı olduğu gözlemlenmiştir.

Anahtar Kelimeler: Diyafram Duvar, Sonlu Elemanlar Metodu Analizleri, İnklinometre, Derin Kazılar, Yatay Deplasmanlar, Bağcılar İstasyonu, Siltli Kil.

To My Family

ACKNOWLEDGMENTS

I would like to express sincere appreciation to my supervisor, Prof. Dr. Erdal Çokça for his guidance, continuous understanding, trust, encouragement and support throughout this research.

I would like to acknowledge Yüksel Proje Int. Co. for providing data for the study.

Special thanks go to my father Nevzat Ustaoğlu and my mother Canan Ustaoğlu for their encouragement, valuable guidance, patience and advices.

I express my sincere thanks to my brothers Yusuf Olgun Ustaoğlu and Alperen Ahmet Can Ustaoğlu for their endless support, understanding and trust throughout my life. I also would like to thank Elif Ustaoğlu for her support.

Finally, my deepest appreciation goes to my beloved fiancé Gonca Ünal for her love and patience during my studies.

TABLE OF CONTENTS

LIST OF TABLES

TABLES

LIST OF FIGURES

FIGURES

LIST OF ABBREVIATIONS

A: Area

c: Cohesion

c': Effective Cohesion

CH: Clay with High Plasticity

CL: Clay with Low Plasticity

c_u: Undrained Shear Strength

E: Modulus of Elasticity

E': Effective Modulus of Elasticity

E_u: Undrained Modulus of Elasticity

FEM: Finite Element Method

GWL: Groundwater Level

H: Depth of Excavation

I: Moment of Inertia

I_2: Moment of Inertia about Axis 2

I_3: Moment of Inertia about Axis 3

k: Permeability Coefficient

LL: Liquid limit

MH: Silt with High Plasticity

ML: Silt with Low Plasticity

N: SPT Blow Count Number

PI: Plasticity index

PL: Plastic limit

SI: Shrinkage Index

SL: Shrinkage Limit

t: Thickness

δ_{hmax}: Maximum Lateral Displacement

ϕ: Angle of Internal Friction

ϕ': Effective Angle of Internal Friction

γ: Unit Weight of Soil

σ_n': Normal Effective Stress

σ_p': Pre-consolidation Pressure

ν: Poisson's Ratio

CHAPTER 1

INTRODUCTION

Rapid increase in urban population makes the transportation sources insufficient. Moreover, due to the lack of parking areas and lands that are used for transportation, conventional transportation methods are no longer applicable. Nowadays, with the increase in technology, application of underground transportation systems are much easier, more comfortable and safer.

Deep excavations in highly populated urban areas have been inevitable for the last decades. One of the necessity for such excavations is to prevent damage to the adjacent existing buildings. In order to provide the security for the existing buildings and excavation site, it is vital to predict possible problems. In order to estimate the wall movements and soil displacements, empirical methods and numerical analyses shall be taken into consideration.

Today, with the development in diaphragm wall technology, 40-50 m deep excavations can be performed just beside the existing structures and can be performed with minimum disturbance. Moreover, with the top-down excavation method, excavations are applicable without disturbing the life on the highly populated city centers.

Deformation or movement of walls, earth pressures, maximum moments and shear forces acting on walls are the most critical design parameters for the anchored or strutted retained deep excavations. In order to understand the behavior of wall, case studies shall be well analyzed and shall be improved.

The general act of deep excavations can be summed up as follows: When a cut is excavated, the soil alongside the supporting system behaves like a surcharge load and tends to move inward in each excavation steps; while the soil below tends to move upward.

1.1. Objective of the Study

This thesis will examine the lateral deformation behavior of diaphragm walls of a Top – Down deep excavation in Bağcılar Metro Station in İstanbul. Location of the station can be seen in Figure 1.1.

Actual diaphragm wall displacements that are measured by inclinometers will be compared with 2D and 3D FEM analysis results. 2D and 3D excavations are modeled by the finite element programs PLAXIS2D and PLAXIS3D.

Figure 1.1. Location of Bağcılar Metro Station

1.2. Scope of the Study

In the scope of this thesis, general information about deep excavations are explained in Chapter 1. Then, studies related to deep excavations are summarized in Chapter 2. In Chapter 3, information about excavation data, soil profile and instrumentation are presented. In addition, finite element analysis procedure is also mentioned in Chapter 3. Following this, comparison of inclinometer measurements and FEM calculations are shown in Chapter 4. Finally, conclusions of the study are listed in Chapter 5.

CHAPTER 2

LITERATURE REVIEW ON DEEP EXCAVATIONS

2.1. Introduction

Lateral movement of the structures is one of the major criteria that have to be taken into account for the design and application of deep excavations. In this chapter, studies about deep excavations and wall movements are examined.

2.2. Movements

The main function of excavation support systems is to resist lateral movements of the surrounding soil. Predictions of wall movements and soil displacements are the most significant factors in designing excavation support systems.

Peck (1969) states that, after investigating the lateral movements of soldier piles or vertical sheet piles, it is clear that, while excavation going on, lateral movements take place below the level of the lowest strut and even below the level of excavation itself. The magnitude of the lateral movements depends on the nature of the soil and the depth of excavation.

Mana and Clough (1981) proposed a simplified procedure for estimating wall and soil movements of braced excavation in clay. For that purpose, the authors investigated the effects of significant parameters on lateral movements by using finite element analysis and field measurements.

The results they obtained from field data can be listed as follows:

- For 11 case histories, the maximum lateral movements are divided by the excavation depth at which they were measured. This ratio is plotted versus factor of safety against basal heave (See Figure 2.1). As can be seen in the figure, there is a strong relevancy between factor of safety and movement: the movements increase rapidly below a factor of safety of 1.4-1.5. In addition, the movements are approximately constant at a value of 0.5% at higher factors of safety.
- There is an inverse linear correlation between movement and time. The rate of movement decreases rapidly as time increases (See Figure 2.2).
- The maximum settlement data are plotted versus lateral wall movements (See Figure 2.3). It can be observed that the settlements are 0.5-1.0 times the lateral wall movements. For a conservative design, the settlements would be equal to lateral wall movements.

The authors examined the effects of various factors namely, wall stiffness, strut spacing and stiffness, excavation width, preloading, depth to an underlying stiff layer, and soil stiffness and stress distribution by performing over 70 finite element analyses. To verify the finite element model and soil parameters that were considered they used the following results:

- Similar to the situation with the field results, the movements increase rapidly for the basal heave factor of safety lower than 1.5 for finite element results (See Figure 2.4).
- The maximum settlements range from 0.4-0.8 of the lateral wall movements (See
- Figure **2.5**) which is also the case with the field data. At lower factors of safety, the settlements become a larger percentage of the lateral movements.

The finite element studies' conclusions of Mana and Clough (1981) are:

- Wall bending stiffness increase or strut spacing decrease or both, cause a reduction on movements. This effect is a function of factor of safety against basal heave which is more important at lower factors of safety.
- Strut stiffness increase induces a decrease on movements. However, the effect indicates diminishing returns at very high strut stiffness values.
- As excavation depth and width to an underlying firm layer are increased, movements are increased.
- Use of preloads in the struts decreases movements. On the other hand, there is a diminishing returns effect at higher preloads.
- The soil modulus, as characterized by the modulus multiplier, dramatically affects the movements. Higher modulus values lead to smaller movements, while lower ones lead to higher movements.

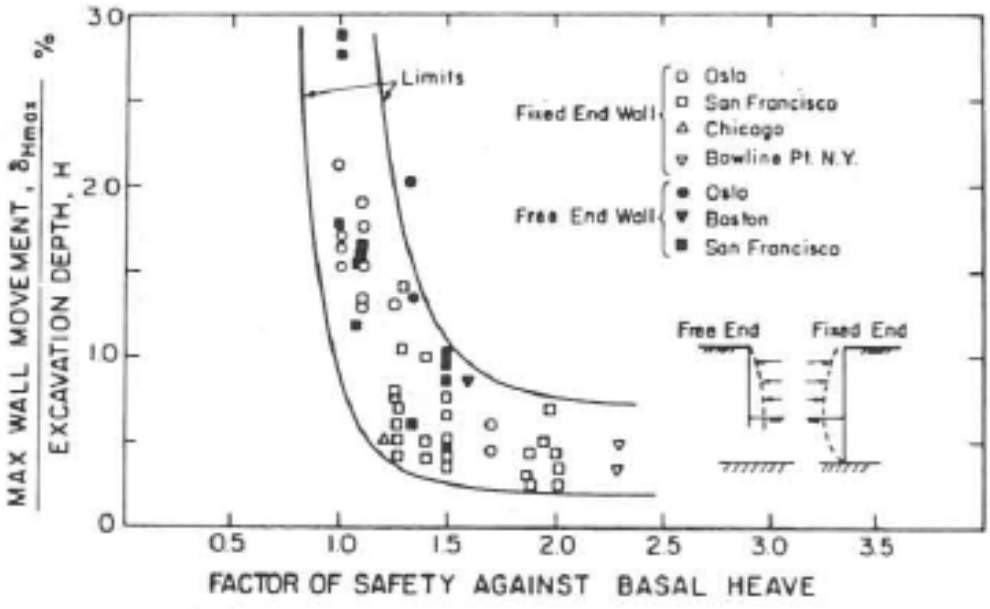

Figure 2.1. Relationship between Factor of Safety against Basal Heave and Maximum Lateral Wall Movements (Mana and Clough, 1981)

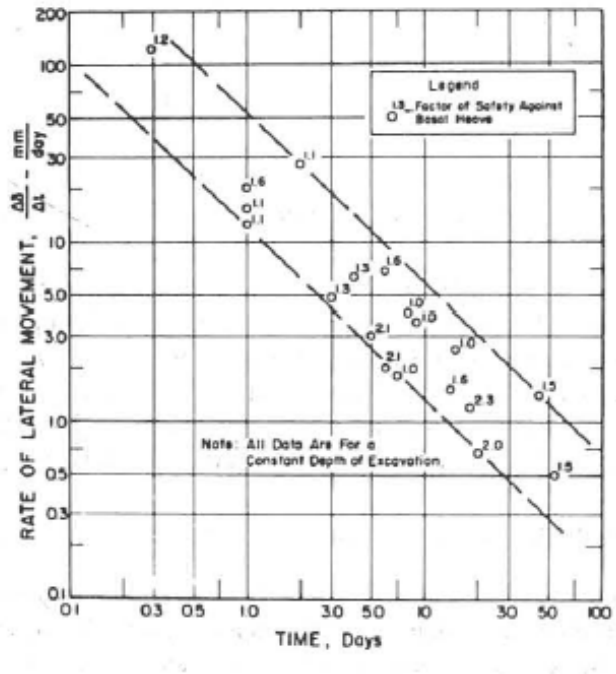

Figure 2.2. Relationship between Time and Maximum Lateral Wall Movements (Mana and Clough, 1981)

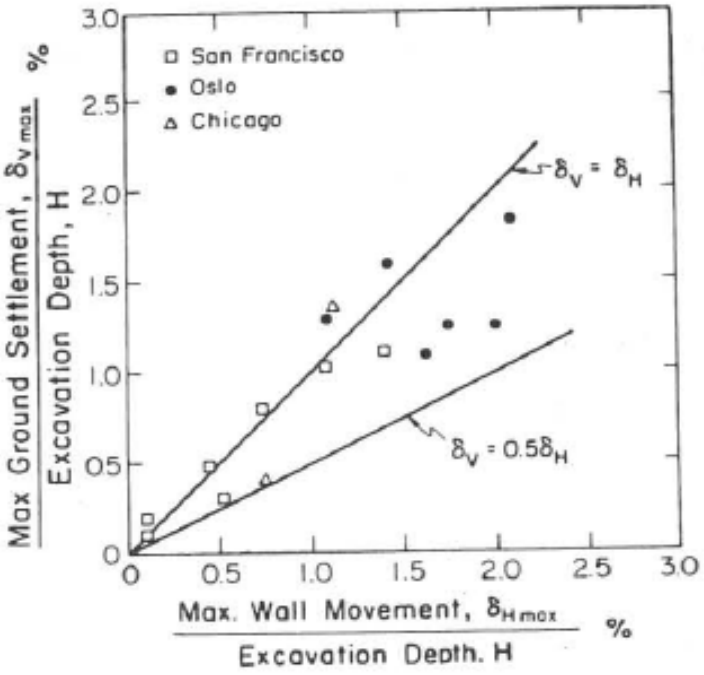

Figure 2.3. Relationship between Maximum Ground Settlements and Maximum Lateral Wall Movements (Mana and Clough, 1981)

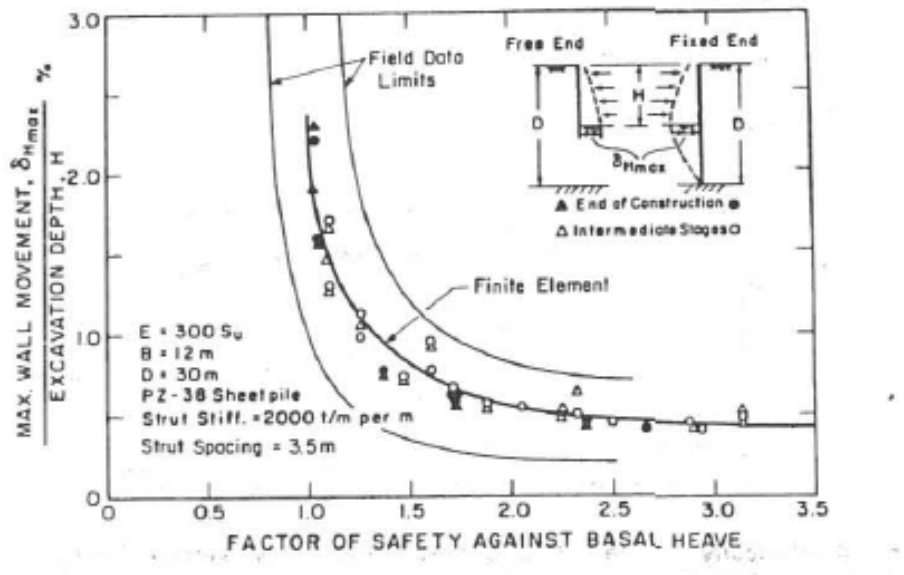

Figure 2.4. Relationship between Factor of Safety against Basal Heave and Maximum Lateral Wall Movements (Determined with Finite Element Studies) (Mana and Clough, 1981)

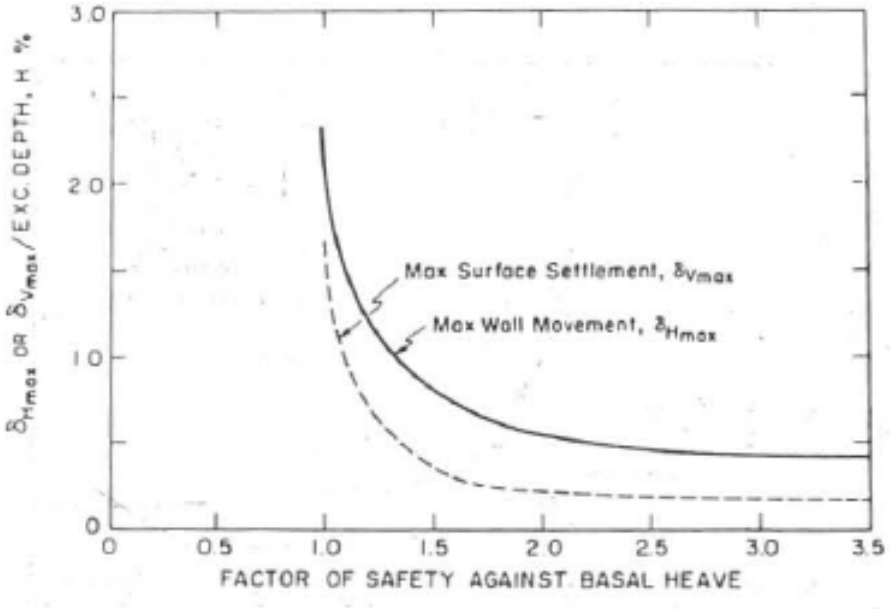

Figure 2.5. Relationship between Maximum Surface Settlements and Maximum Lateral Wall Movements (Determined with Finite Element Studies) (Mana and Clough, 1981)

Clough and O'Rourke (1990) investigated the movements of insitu walls with the help of updated existing data by considering the effects of excavation, support process and construction activities separately. The aims of the paper can be summarized in the following items:

- Update the data obtained from previous work by using the new wall systems.
- Explain ground movement patterns and examine the available methods for prediction of wall movements and settlement distributions.
- Relate the ground movement models with building damage.

According to the authors, many factors such as soil and groundwater conditions, groundwater level changes, shape and depth of excavation, wall type and stiffness, wall support conditions, construction methods of wall, surcharge loads and duration of wall exposure are responsible for the movements of insitu walls.

One principal source of wall movements is related to basic excavation and support process. In order to explore those effects, the geotechnical conditions are examined by considering different soil types. For investigating the wall movements and soil settlements in stiff clays, residual soils and sands, maximum movements and settlements are plotted versus depth of excavation (H), respectively (See Figure 2.6 and Figure 2.7). Based on the graphs, the lateral movements are mostly 0.2% of H, while the settlements show a tendency to 0.15% of H. Moreover, there is no important difference between maximum movement trends of different types of wall. The authors performed finite element analyses by considering different parameters: wall and soil stiffness, supports spacing and coefficient of lateral earth pressure. Figure 2.8 is prepared to show the estimated maximum horizontal wall movements as a function of H by using finite element analyses. In Figure 2.8, the estimated horizontal movements show a linear behavior average about 0.2% of H which is the case also in Figure 2.6. They observed that wall stiffness and strut spacing have no significant impact while soil modulus and coefficient of lateral earth pressure have important effect on movements in stiff soil.

In Figure 2.9, the wall movements or soil settlements in soft to medium clays are described in terms of the factor safety against basal heave (FS). As the FS decreases below 1.5, movements rise quickly. On the other hand, as the FS becomes over 2 and the base stability is guaranteed, maximum movements fall below 0.5%. Additionally, wall stiffness and strut spacing can have significant effect on movements especially when FS is low.

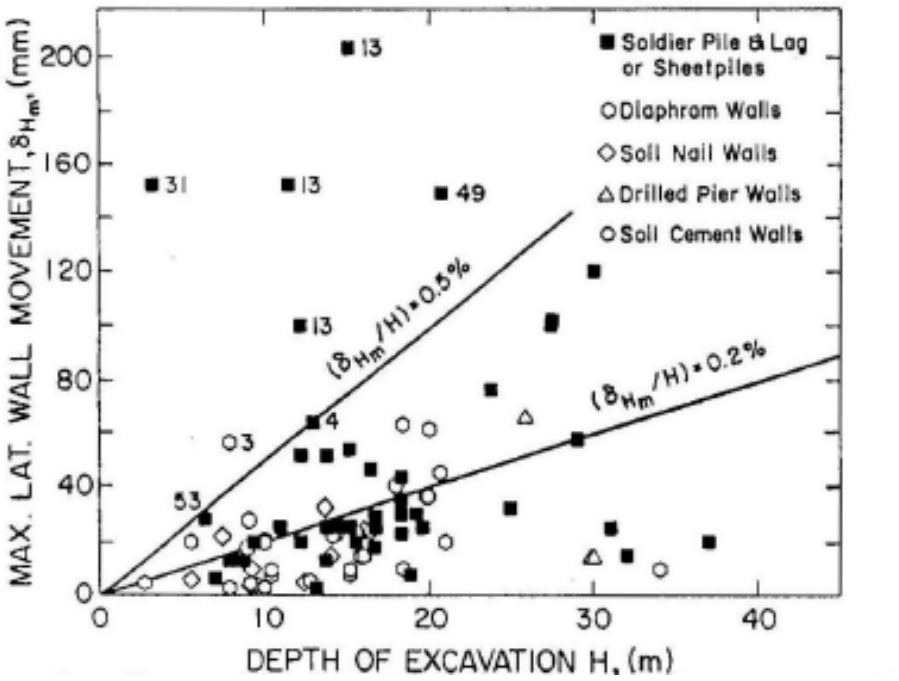

Figure 2.6. Monitored Maximum Lateral Movements for Insitu Walls in Stiff Clays, Residual Soils and Sands (Clough and O'Rourke, 1990)

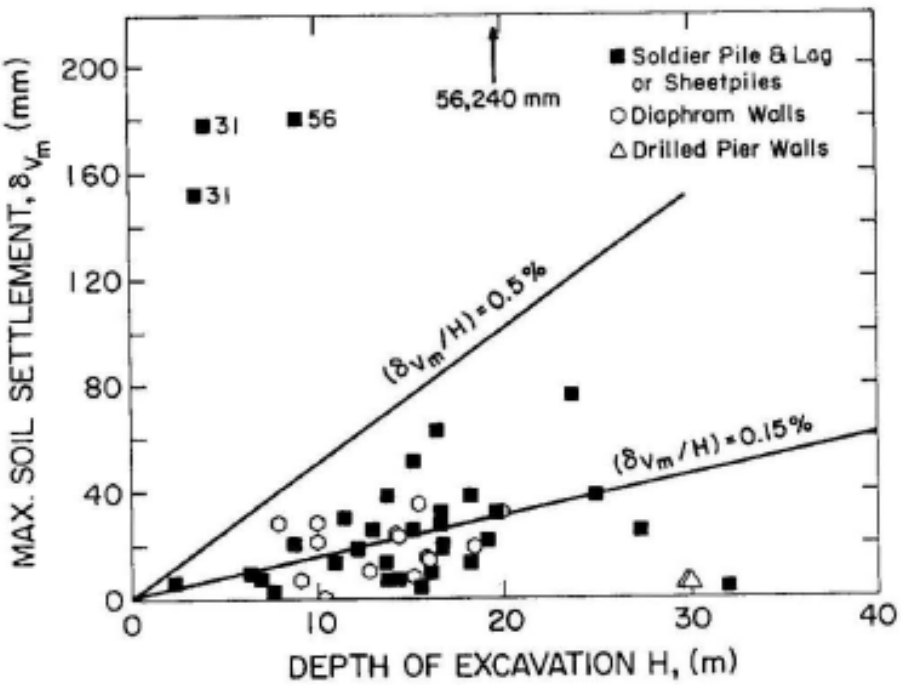

Figure 2.7. Monitored Maximum Soil Settlements in the Soil Retained by Insitu Walls (Clough and O'Rourke, 1990)

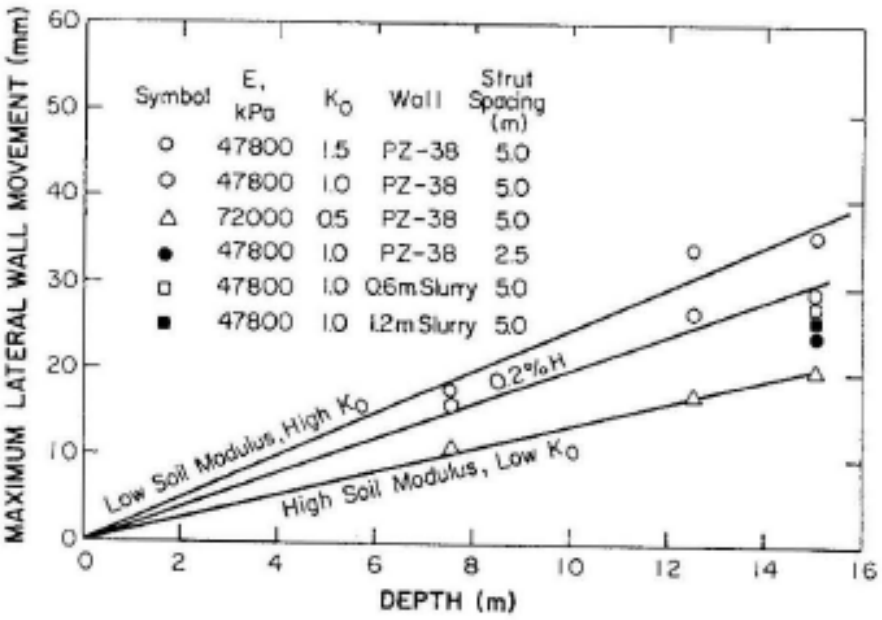

Figure 2.8. Estimated Maximum Horizontal Movements in Stiff Soil Conditions (Obtained by using Finite Element Analyses) (Clough and O'Rourke, 1990)

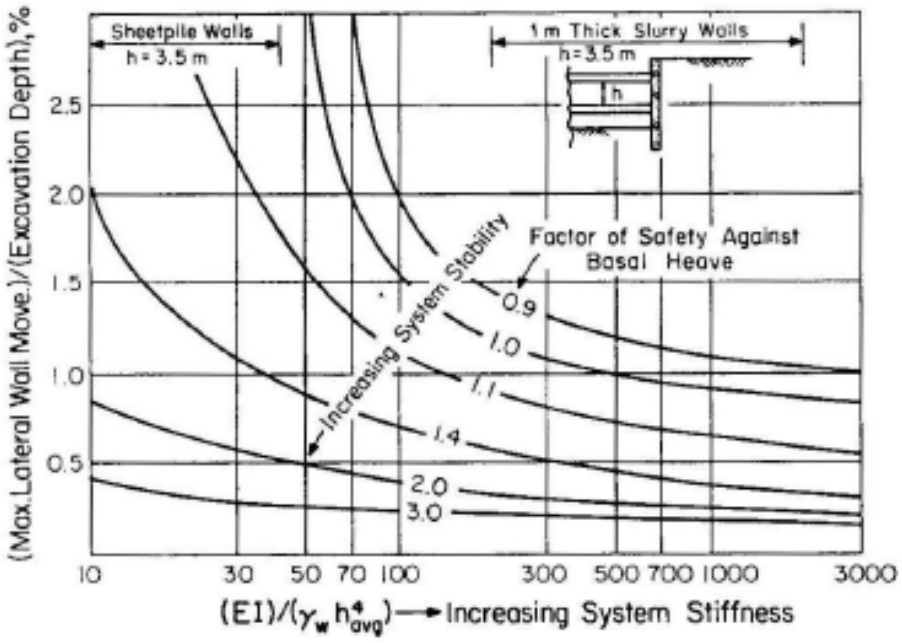

Figure 2.9. Design Curves to Acquire Maximum Horizontal Wall Movement or Soil Settlement for Soft to Medium Clays (Clough and O'Rourke, 1990)

Clough and O'Rourke (1990) presented a general pattern of wall movement and adjacent ground deformation by using inclinometer and settlement measurements for braced and tied-back excavations (See Figure 2.10). For flexible systems, the wall deforms as a cantilever and the adjacent soil settlement increases in inverse ratio to distance from excavation edge as can be seen in Figure 2.10a. When the excavation proceeds to deeper elevations, wall movement at upper levels is restrained by new support systems. This condition results as deep inward movement of the wall which is illustrated in Figure 2.10b. The combination of cantilever and deep inward behavior is represented as cumulative movement profile as shown on Figure 2.10c.

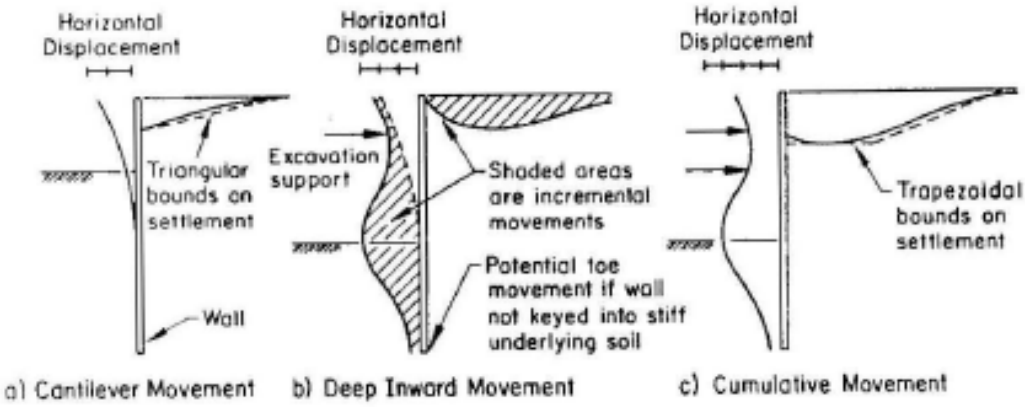

Figure 2.10. General Movement Patterns of Braced and Tied-Back Walls (Clough and O'Rourke, 1990)

Dimensionless settlement profiles are provided by using the previous researchers' data in order to be used for predicting settlement distribution near to excavations in sand, stiff to very hard clays and soft to medium clays (See Figure 2.11). In the graphs, settlement (δ_v) is divided by maximum settlement (δ_{vm}) and plotted as a function of the ratio of distance from excavation (d) to maximum excavation depth (H). From Figure 2.11a, it is easily understood that as the distance from the edge of excavation falls, settlement rises. In Figure 2.11b, the settlement decreases in roughly direct ratio to distance from the edge of cut. For both figures, a triangular bound on settlement profile observed excavations in sand and stiff to very hard clays. In Figure 2.11c, the settlement distribution is considered as a trapezoidal bound. In this bound two movement zones can be defined: the zone in which maximum settlement occurs ($0 \leq d/H \leq 0.75$) and the transition zone where settlements descend ($0.75 \leq d/H \leq 2$).

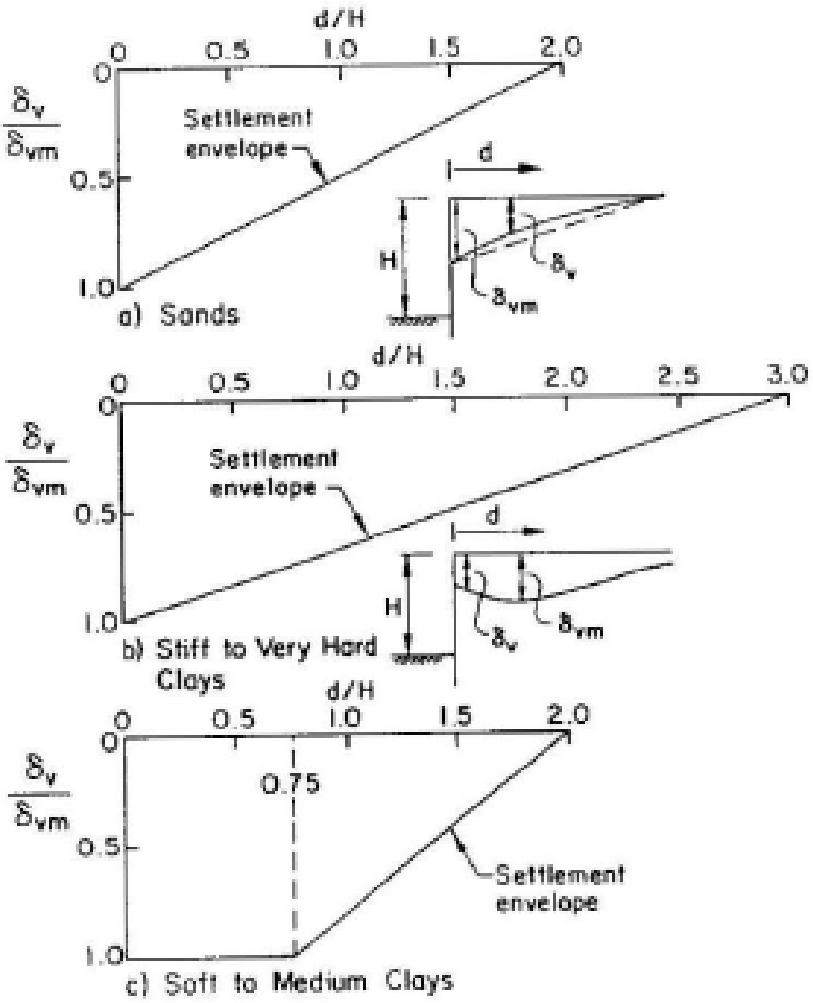

Figure 2.11. Recommended Settlement Profiles to Predict the Settlement Pattern Adjacent to Excavations in Different Soil Types (Clough and O'Rourke, 1990)

One of the significant causes of wall movements is associated with the construction of wall. Based on the authors' research, construction related factors that affect wall movements can be listed as follows:

- Wall Installation Processes: The placement of wall and the vibrations from driving process of insitu walls can generate movement.

- Construction Technique: Poor construction can cause large movements of walls. Construction quality not only depends on the experience of contractor but also the knowledge of geotechnical engineer.
- Construction and Removal of Deep Foundations: In some conditions, deep excavations are applied with existing pile removal and new deep foundation installation. This removal and installation processes can cause ground movement.
- Depth of Excavation below Support Placement: The excavation of soil below the determined location for a support can ascend wall movements.

Another important consideration for wall movements is the structural support system which can be controlled by designer. This effect is explained in terms of four factors:

- Wall Stiffness: The increase of wall stiffness results in decline of movements.
- Support Spacing and System Stiffness: System stiffness can be defined as a combination of wall flexural stiffness and support spacing. As the vertical or horizontal support spacing decreases, the support system becomes stiffer.
- Support Stiffness: The type of supports in the form of braces, tiebacks, rakers and nails has impacts on the support system to a certain extent. However, it is noted that this factor is not as significant as wall stiffness or support spacing.
- Preloading: Preloading of insitu walls mostly enhances the wall performance by taking the slack out of a support system and reducing the stress levels in soil.

Insitu wall movements are also affected by special geotechnical factors which can be listed as wall settlement, movements in the anchorage zone of an anchored wall, the use of earth berms and water movement and piozemetric pressures.

In this paper, Clough and O'Rourke (1990) concluded that:

- The wall movements are affected by mainly four factors which can be categorized as the basic excavation and support process, construction activities, support system and geotechnical considerations.
- Excavations in front of insitu walls cause vertical and horizontal movements. For examining the damage to structures, effect of each needs to be considered.
- Nature and building condition are important elements when building response to ground movements are considered.
- Insitu wall movements can be reasonably estimated as long as main reasons of displacement are regarded.

Bose and Som (1998) modeled a typical instrumented section of a metro station numerically by using finite element method. The diaphragm wall movements at various excavation stages and the corresponding ground settlements for the stratified soil under undrained conditions were examined. The objective of the study can be explained as three items:

- Investigate the basic soil-structure interaction of braced excavation in soft clay.
- Compare finite element analysis results with field measurements.
- Analyze the importance and effect of factors i.e. depth of wall penetration, excavation width and strut prestressing for such excavation.

In this research, the authors selected Metro railway in Calcutta, India which presents a proper example of braced cut in soft clay. The subsoil conditions of the excavation region show that the ground mostly included silty clay. The depths of braced cut and diaphragm wall were 13.6 m and 17 m, respectively. The width of excavation was 10 m. Before starting the digging process, 0.6 m thick diaphragm walls were constructed. Then, sequential excavation process (5 stages) and strut installation (4 levels) were implemented from top to bottom.

The two-dimensional finite element model was composed of 258 eight-noded isoparametric elements. The perpendicular boundaries were horizontally restrained, while lateral ones were both horizontally and vertically restrained. For the purpose of defining soil-wall interface, very small soil elements were used instead of slip or joint elements. Modified Cam-clay constitutive law was applied to define the soil nonlinearity. Except taking the advantage of software package CRISP, new software was developed to implement the analysis. The ground water table was taken as the same level as ground surface.

The results the authors gathered from field data and finite element analysis are:

- The diaphragm wall shows nearly an embedded cantilever type movement for the unsupported excavation stage 1 until the first strut installation. In the following excavation stages, the wall movement is restricted at strut levels. This condition forces the wall deflect mostly under the related strut level (See Figure 2.12).
- The maximum ground settlements occur at about 10 m away from the wall for each stage (Figure 2.13). In addition, it is observed that major ground settlement is limited within a distance of 3 times the depth of cut.
- The comparison of numerically predicted and measured values of maximum ground settlements indicates that finite element results underestimate the maximum ground settlements (Figure 2.14). This result could be explained by lack of construction control, problems in strut installation process and long term effects of soil creep.
- As the wall penetration in the stiffer soil layer increases, the wall deflection towards bottom decreases. On the contrary, the diaphragm wall movement remains constant above the final strut level which is 11.5 m (Figure 2.15). Moreover, rise of wall penetration depth has no significant effect on ground settlement (See Figure 2.16).

- Analysis results reveal that increase of the excavation width generates an increase both in wall deflection and ground settlements without changing the lateral force equilibrium.
- Finite element studies prove that increase in strut preload decreases the wall movement considerably at the upper portion of the wall, while no important alteration is shown at the bottom part. The ground settlement also decreases as the strut prestressing increases.

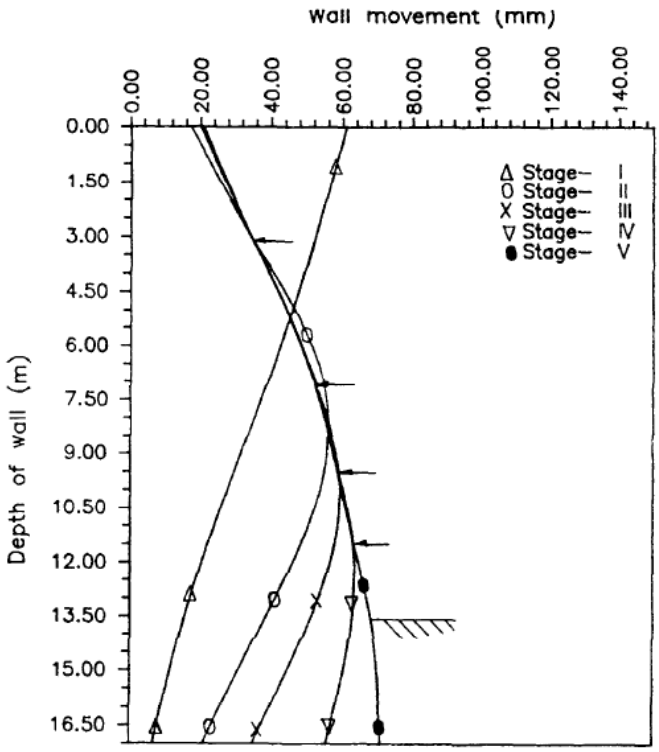

Figure 2.12. Wall Deflection at Various Excavation Stages (Bose and Som, 1998)

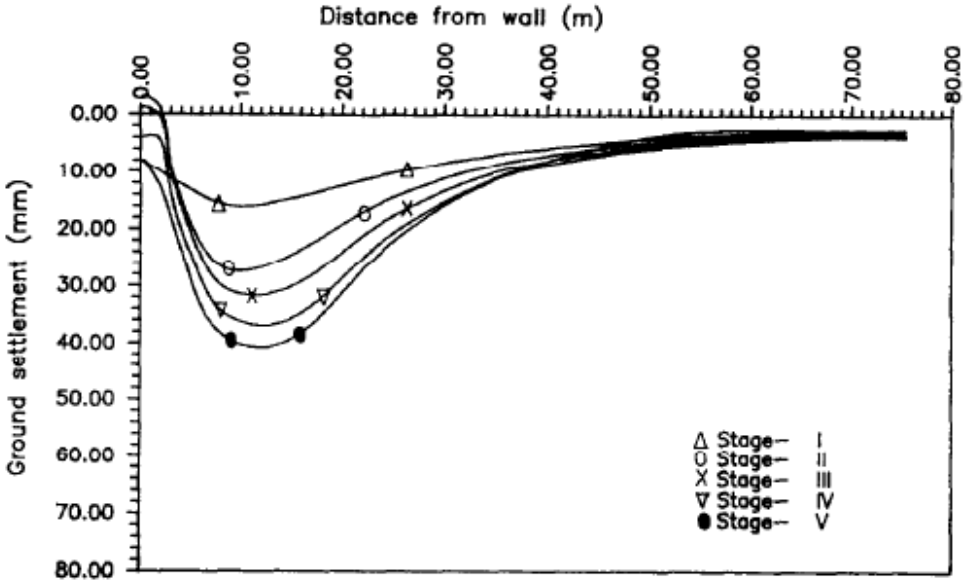

Figure 2.13. Ground Settlement at Various Excavation Stage (Bose and Som, 1998)

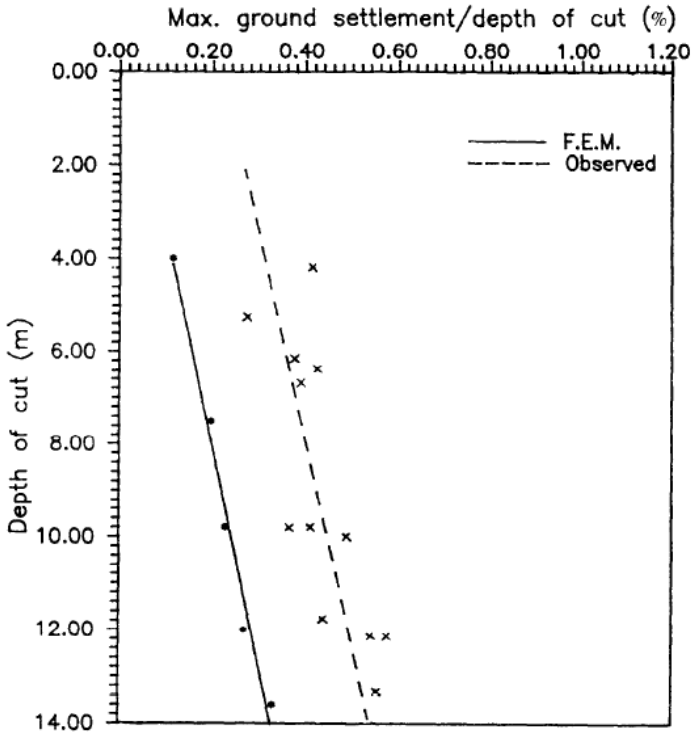

Figure 2.14. Maximum Estimated and Measured Ground Settlement vs. Depth of Cut (Bose and Som, 1998)

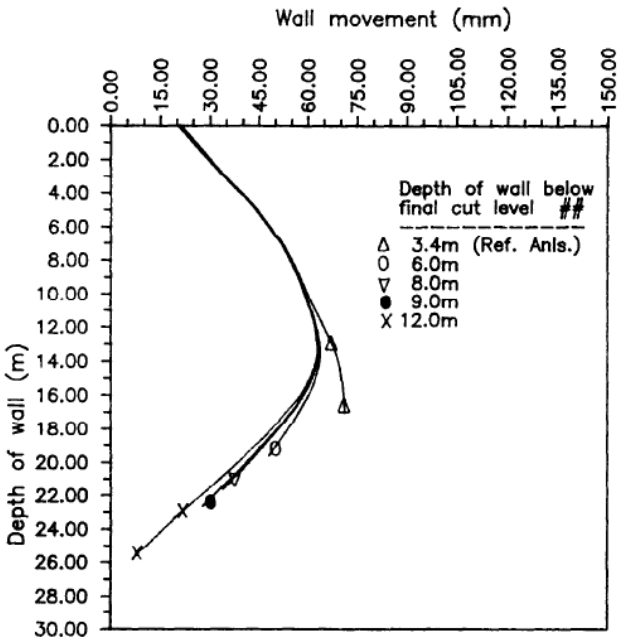

Figure 2.15. Predicted Wall Deflection Values at Final Excavation Stage for Different Wall Penetration Depths below Final Cut Level (Bose and Som, 1998)

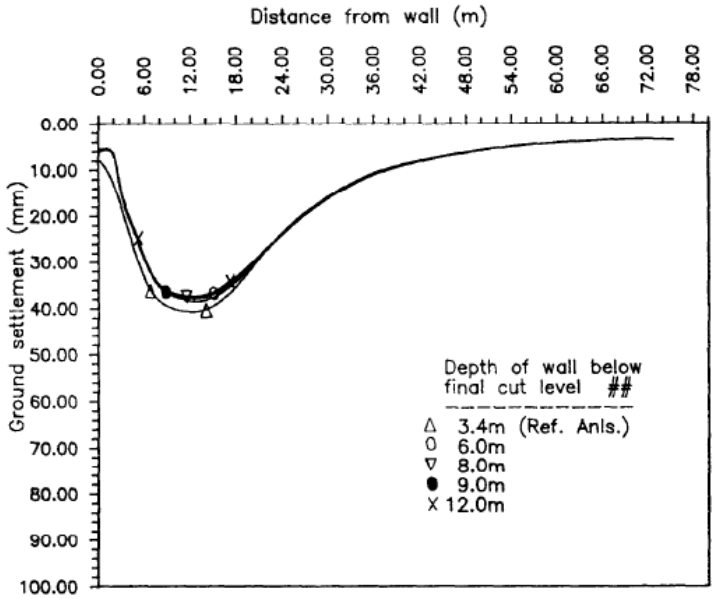

Figure 2.16. Predicted Ground Settlement Values at Final Excavation Stage for Different Wall Penetration Depths below Final Cut Level (Bose and Som, 1998)

Kung (2009) made the comparison of diaphragm wall deflection caused by excavation of the top-down method (TDM) and the bottom-up method (BUM). For that purpose, a number of excavation case histories located in Taipei silty clay were gathered and analyzed. Factors affecting wall deflection were determined and compared for each two methods. For further investigation of factors' effects, numerical studies were performed by the help of hypothetical cases. Both case histories and numerical analyses results' were used to examine the discrepancy of two methods in terms of wall deflection behavior.

Excavation is a complicated soil-structure interaction problem. Because of this reason, the factors that affect the excavation-induced wall deflection shall be well specified. These factors may be classified under three groups:

1) Inherent Factors
   - **a)** Stratigraphy: The Soil strength, the stiffness of soil and the groundwater conditions are some examples. Excavation in lower soil strength and stiffness causes larger wall deflection.
   - **b)** Site Environment: Traffic conditions and properties of adjacent buildings. High-rise buildings and heavy traffic near excavation site affect wall deflection negatively.

2) Design-Related Factors
   - **a)** Properties of Retaining System: For instance stiffness of wall, length of wall and strut stiffness. Low-stiffness wall increases wall deflection.
   - **b)** Excavation Geometry: Such as excavation depth and width. Deflection of wall is almost directly proportional to excavation depth.
   - **c)** Prestressing of Strut: The prestressing process has influence on the wall deflection. The strut prestress may decrease wall deflection.
   - **d)** Ground Improvement: Including jet grouting method, deep mixing method, and compaction grouting method. These methods may help to reduce wall deflection.

3) Construction-Related Factors

- **a)** Construction Factors: For example top-down method, bottom-up method and anchor method.
- **b)** Over-Excavation: Excessive excavation before the support installation induces greater wall deflection.
- **c)** Prior Construction: Such as trench excavation effect prior to wall construction.
- **d)** Concrete Floor Slab Construction: Thermal shrinkage of concrete slab causes a rise in wall deflection.
- **e)** Construction Sequence Duration: The duration of floor construction and/or strut installation. Longer period of these processes may cause an increase of wall deflection for excavation in clayey soil.
- **f)** Workmanship: Poor workmanship has opposite effect on wall deflection.

The author collected 26 quality excavation case histories located in Taipei, Taiwan. The cases were selected from two different zones of Taipei: Zone T2 of Tamsui River Basin and Zone K1 of Keelung River Basin. The detailed information about case histories (CH) and their excavations (Exc.) is given in Table 2.1. Triangular shaped basin of Taipei is constituted of the so-called Sungshan formation including soft to medium silty clay which is above the Chingmei gravel formation. For the numerical analyses, the groundwater table was taken 2 m below the ground surface level. Diaphragm wall was used as the support system for all cases and the number of excavation stages was different in each case. For all cases, except the first two stages, the wall deflection showed a deep-inward movement pattern that is mainly observed in braced excavations in soft to medium clay.

Table 2.1. Properties of Case Histories and Excavations (Kung, 2009)

Zones	Number of CH	Exc. Method	Range of Exc. Width (m)	Range of Final Exc. Depth (m)	Range of Wall Length (m)	Range of Wall Thickness (m)
T2	12	BUM	12.3 – 54.1	10 – 19.4	18 – 30	0.6 – 1.1
	3	TDM				
K1	8	BUM	33.4 – 70	12.6 – 23.2	22 – 50	0.6 – 1.0
	3	TDM				

When all cases are considered, the ratio of δ_{hm} (maximum lateral wall deflection)/H_0 (final excavation depth) falls in the range of (0.2-0.6) %. For Zone T2 history cases, the average δ_{hm}/H_0 ratio induced by TDM over that induced by BUM is 1.28. In the same manner, for Zone K1, average δ_{hm}/H_0 value caused by TDM/BUM is 1.29 which is scarcely equal to the result of Zone T2. According to the results from case histories, δ_{hm} value caused by BUM is smaller than the one induced by TDM, regardless of geological properties of excavation area. Since wall thickness and excavation width have significant effects on wall deflection, dissimilar cases in terms of these two factors are excluded for accurate results. In that case, the ratio of average δ_{hm}/H_0 value caused by TDM/BUM is 1.2. In addition, the ratio of H_m (depth where δ_{hm} occurs)/H_0 value is in the range of 0.8 to 1.1.

A series of parametric studies were carried out by generating two-dimensional numerical analyses of hypothetical BUM and TDM cases for further investigation of these two methods' difference with regards to wall deflection.

In the parametric studies four factors that are thought to have significant impact on wall deflection are considered:

- Excavation depth in each stage.
- Struts or floor slabs stiffness.
- Prestressing of struts.
- Duration of strut installation or construction of floor slab.

In all numerical analyses, the rate-dependent soil creep model developed by Lin and Wang (1998) and the hyperbolic model developed by Duncan and Chang (1970) were used to represent the clayey and sandy layers, respectively. For a series of hypothetical cases, 35 m deep and 0.9 m thick diaphragm wall was selected and the excavation width was taken as 40 m. In the analyses, excavation depths and strut installation or floor slab construction depths were thought as variables. For both BUM and TDM cases, the final excavation depth was assumed as 19 m. Three types of excavations were designed for BUM cases. In Type I, the strut depths were taken as same as the floor slab depths designated in TDM cases in order to compare the strut and floor slab stiffness effect. The larger excavation depths in Type II cases and the smaller excavation depths in Type III cases were preferred to search the influence of excavation depths at each stage on the wall deflection.

The following results were obtained from numerical analyses:

- The wall deflection reduces slightly as the floor slab stiffness rises. In other words, using thicker floor slab is pointless on decreasing wall deflection (See Figure 2.17).
- Irrespective of floor slab stiffness, the increase in wall deflection at each stage induced by undrained creep of clay is important and stable (See Figure 2.18).
- Increase in wall deflection due to the creep is decreased a little with increase of strut stiffness for all excavation types (See Figure 2.19).
- Decrease of prestress-induced wall deflection falls with the rise of strut stiffness for all excavation types (See Figure 2.20).

- In Figure 2.21, the calculated wall deflections of TDM and BUM cases are compared. In the calculations, the undrained creep and prestress are taken into account. In general, the wall deflection of BUM cases is smaller than that of TDM cases.
- When the thermal shrinkage of floor slab is not considered, the average ratio of wall deflection caused by the TDM to that of BUM is approximately 1.1. This value is slightly smaller than 1.2 gathered based on actual case histories collected from the Taipei Basin.

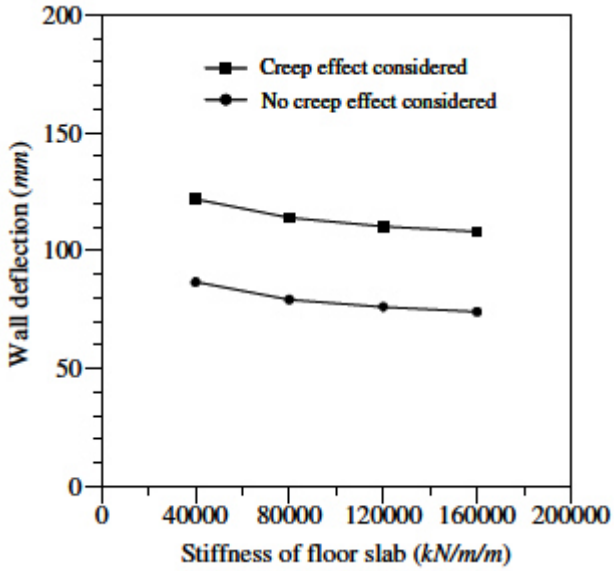

Figure 2.17. Influences of Slab Stiffness and Undrained Creep on Maximum Wall Deflection (TDM Cases) (Kung, 2009)

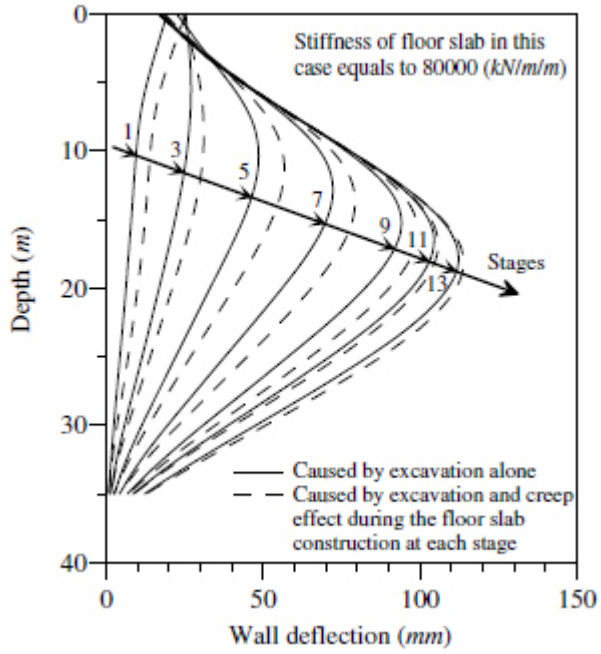

Figure 2.18. Creep Impact on Wall Deflection Caused by Floor Slab Construction (a Specific TDM Case) (Kung, 2009)

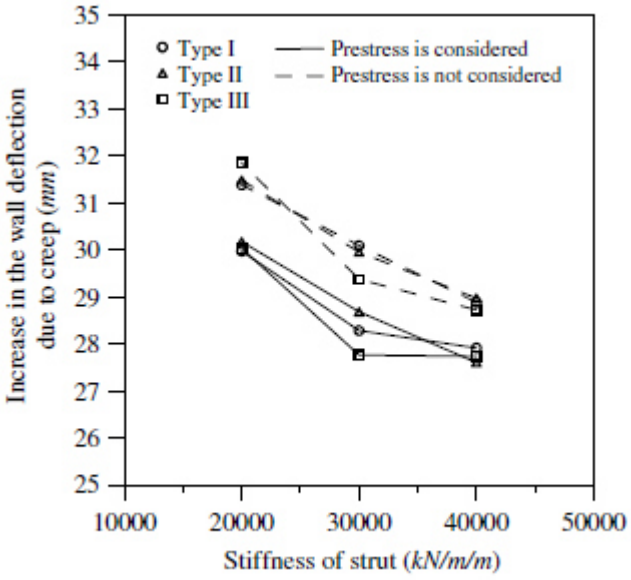

Figure 2.19. Increase of Maximum Wall Deflection Due to Creep (BUM Cases) (Kung, 2009)

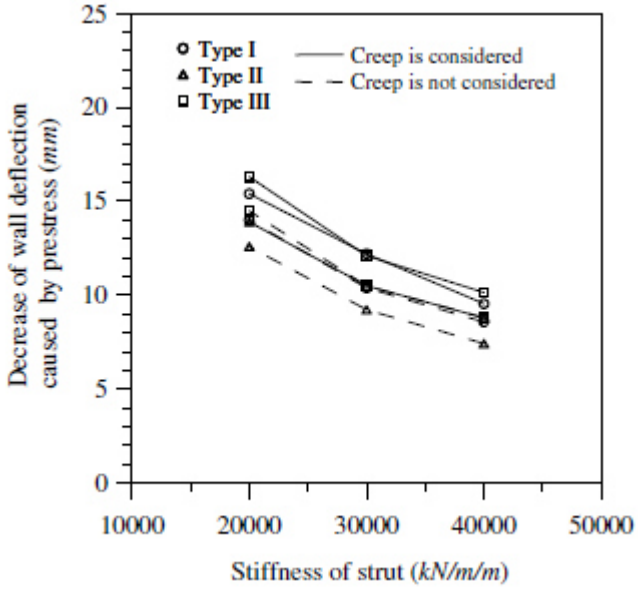

Figure 2.20. Decrease of Maximum Wall Deflection Due to Prestress (BUM Cases) (Kung, 2009)

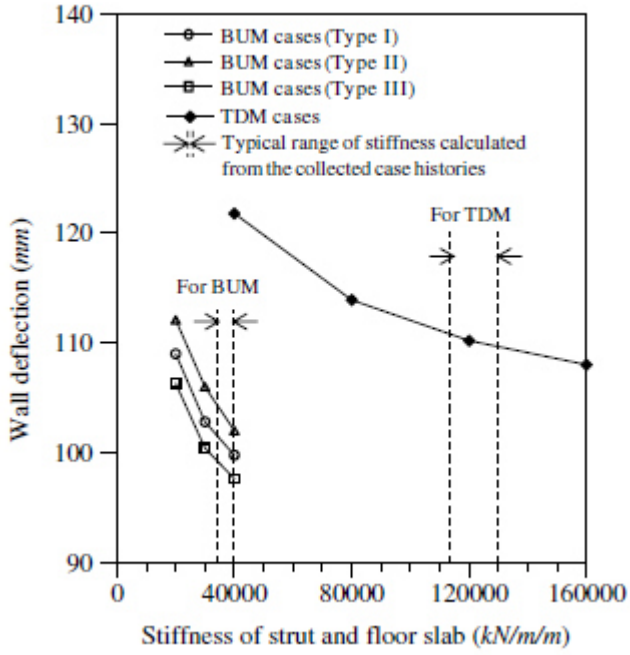

Figure 2.21. Comparison of the Maximum Wall Deflection between BUM and TDM Cases (Kung, 2009)

Tan and Li (2011) investigated a 26 m deep metro station excavation constructed by the top-down method with the use of field measurements. Some of the measured excavation related items are wall deflections, wall settlements, ground settlements and struts axial forces.

In this study, a deep excavation at East Nanjing Road Station in Downtown Shanghai, China was analyzed. The field search about subsurface conditions of excavation area show that the site is basically formed by soft clays. The excavation length is 152 m, while width is 25 m. It is surrounded by high-story buildings, other metro lines and utility pipe lines. Three reasons can be listed for the selection of top-down construction technique supported by braced concrete diaphragm walls for this deep excavation:

- Limited construction area.
- Prevention of possible unfavorable impacts of excavation on adjacent buildings and facilities.
- Continuation of commercial activities nearby station during construction.

Jet-grouting was applied to soil layers at various depths before starting the excavation. The main goals of this process are:

- Restrict wall movements during excavation by reinforcing the soil.
- Reduce possible basal heave during excavation.
- Cut off water flow seepage below the excavation surface.

The excavation was composed of three sections: south shaft, central standard segments and north shaft. The construction was started from the two end shafts toward the central one. Top-down construction sequence is listed in the following steps:

1) 1 m thick diaphragm wall construction.
2) Excavation of piles.
3) Installation of ACIP piles and interior steel columns. Implementing jet-grouting.
4) Excavation up to Level 1 and casting of ground slab.

5) Excavation and slab construction under the ground slab.

6) Excavation up to the final level and casting of base slab.

Based on the field measurement analyses, the authors deduced important results:

- The diaphragm walls display typical deep-seated inward movements (bulging profiles) during excavation.
- Case histories of excavations in soft to medium clays were used in order to understand the relationship between maximum wall deflection, δ_{hm}, excavation depth, H and maximum wall deflection location, H_m. The observed δ_{hm} values are between 0.1%H and 0.5%H (Figure 2.22a). The ratios of H_m/H tend to fall between H_m=H and H+7 m when H≤16 m, and between H_m=H-7 m and H+7 m when H>16 m (Figure 2.22b).
- There is no important post-excavation (time-dependent) wall movement occurred. Most ground settlements and wall deflections caused by stress relief during soil removal instead of creep and/or consolidation of soft clays.
- During excavation, the diaphragm walls experience serrated settlement patterns because of the wrong mobilization of soil on two sides of the walls.
- The axial forces of struts reach their maximum values in 1 to 2 weeks after being cast. The horizontal earth pressures released due to wall exposure are carried by struts and floor slabs above the excavations surfaces and deeper excavation scarcely influences the remote struts' axial forces.

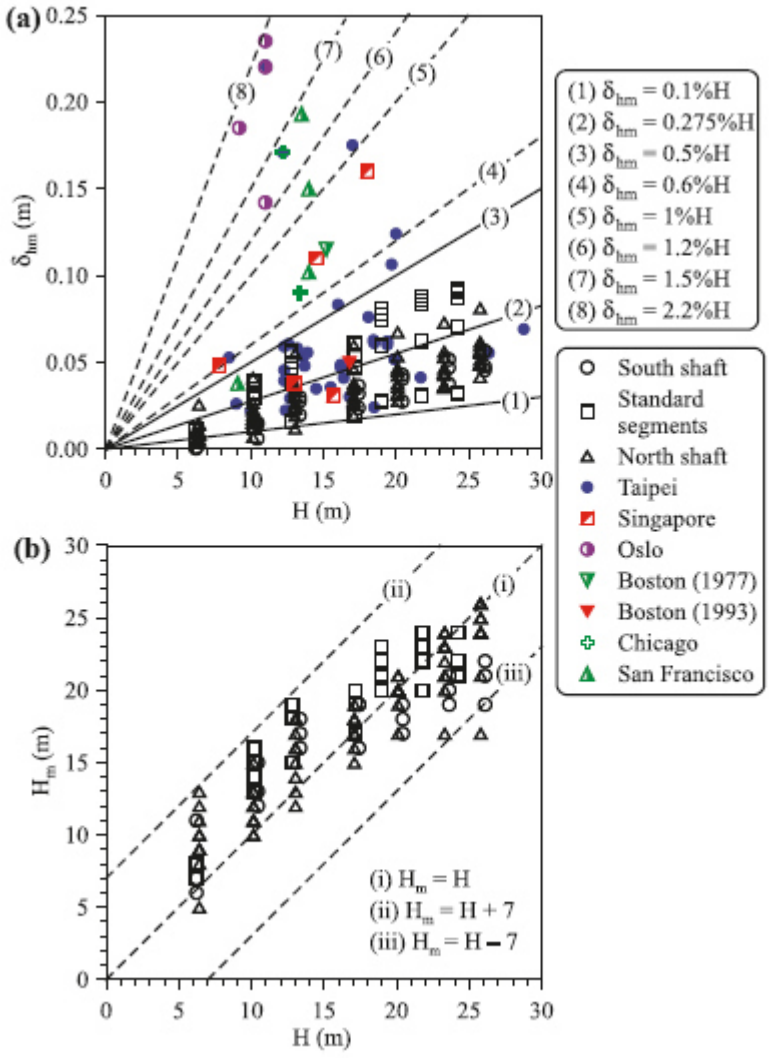

Figure 2.22. Relationships between (a) δ_{hm} and H; (b) H_m and H (Tan and Li, 2011)

Ran et al. (2011) examined the design and application of monitoring and safety evaluation system for a metro station's deep excavation. For this purpose, the authors enhanced a software platform for the analysis of data obtained from monitoring. This software system was based on the concept of dynamic construction inverse analysis. The monitoring items and instrumentation used for the related items are shown in Table 2.2. The monitoring results of deformation caused by excavation and loading in the lateral support system were reported and analyzed.

Table 2.2. Monitoring Items and Instrumentation Used (Ran et al. 2011)

Monitoring Item	Instrumentation
Horizontal displacements of diaphragm walls	Acceleration-type inclinometers
Ground soil settlements	Level sensors and Theodolite
Axial forces in the struts	Axial-force transducers and Vibration-wire stress gauges
Bottom heave within the excavation	Settlement gauges
Groundwater levels	Water-level tubes

The inspected metro station, which is an island platform, is located in the coastal plain of Qiantang River, China. Main formation of the deep excavation area includes the layers of mixed fills, silty clay, clayey silt, sandy silt and silty sand from top to bottom. The excavation length is approximately 444 m and the width is 44.5 m. Open excavation sequential operation method is used for the construction of metro station's main structure. 0.8 m thick diaphragm walls are selected as the excavation's main support system. Steel struts in four rows are constructed from top to bottom.

The horizontal displacements of diaphragm wall at different depths measured by inclinometers are demonstrated in Figure 2.23. The lateral movements of the diaphragm wall rises slowly with the increase of excavation depth. Furthermore, maximum horizontal movements' locations moved downward to the excavation face throughout the excavation process. The relationship among excavation depth (H), diaphragm wall height (Ho) and maximum horizontal displacement (δ_{hmax}) is examined and following conclusions are drawn:

- When $H/Ho < 0.5 \rightarrow \delta_{hmax}$ seems below the excavation face.
- When $H/Ho = 0.5 \rightarrow \delta_{hmax}$ normally seems at the excavation face.

Figure 2.24 is presented to show the ground surface settlements. Ground soil settlements increases gradually during excavation as the excavation depth increases. By using the measurement data of strut's axial forces, it is observed that the axial forces of steel struts transferred from the first row to the lower ones during excavation. Based on the monitoring results, the overall conclusion is that the braced excavation remained stable at different construction stages.

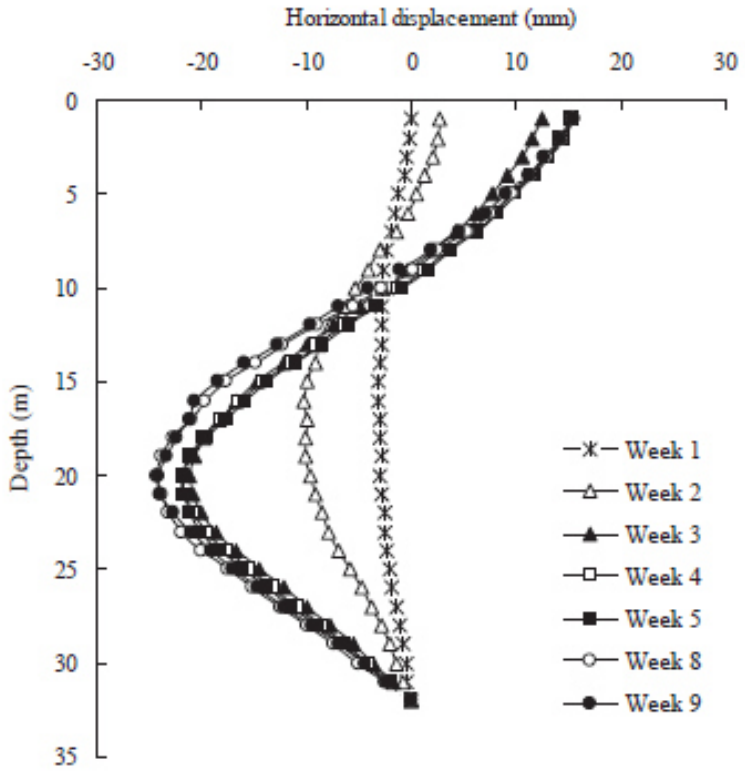

Figure 2.23. Lateral Movements of the Diaphragm Wall (Ran et al. 2011)

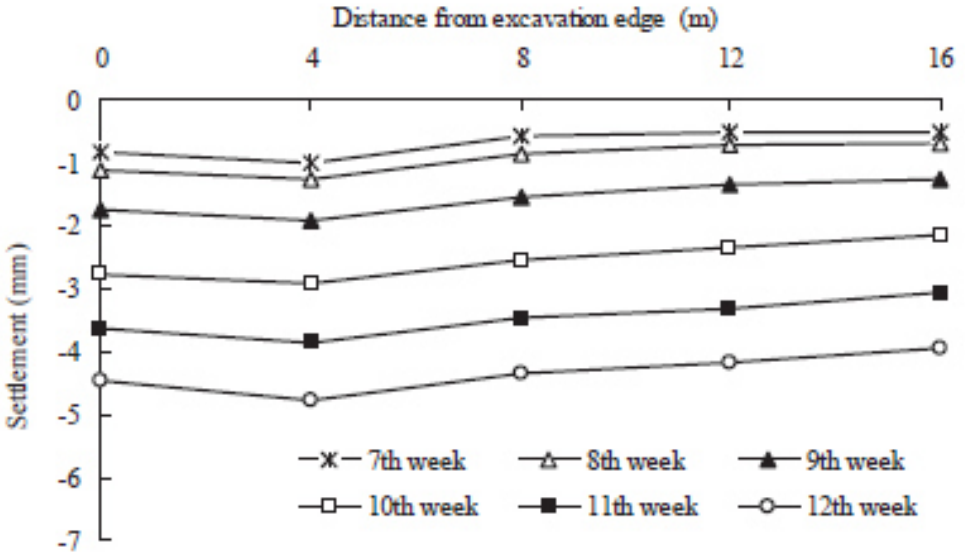

Figure 2.24. Settlement Profile of Ground Soil Induced by Excavation (Ran et al. 2011)

Qing-Yuan (2011) analyzed the basic monitoring principles, methods and monitoring program for the deformation of a metro station's deep foundation. In this research, lateral deformation of retaining piles and the axial force of steel supports were observed by using the monitoring data. The two island platform station whose deep excavation was investigated is situated near the south gate of Xi'an, China. Geological findings show that the station is located in loess area. The standard segment structure width was 20.5 m and the length was 188 m. Open-cut approach was implemented for the metro station's construction. For the support system of the standard section station, 1 m diameter bored piles and top-down constructed steel tube supports were used.

Based on the deep excavation site analysis and monitoring results, the authors have the following conclusions:

- Depth, size, formation characteristics, earth pressure and groundwater are the factors which influence the stability of deep excavation. At the beginning of the excavation, the rate of change of retaining pile deformation and axial force of

steel supports are obvious. As the excavation depth increases, this ratio begins to decrease.

- Steel support of the foundation has important impacts on deformation. When the axial force of steel supports increases, the pile deformation also increases. The removal of steel supports is the most unfavorable stage in the construction period. In order to ensure the stability of foundation, the exposure time of excavation without support shall be minimized.
- After the completion of floor construction, foundation pit curve is stabilized. The reason of this situation is that construction of the station is less affected by surrounding environment.

Lu and Tan (2012) studied the performance of top-down constructed deep metro excavation in Shanghai clay deposits. Deflections of diaphragm walls, vertical movements of steel columns and axial forces of struts constituted the scope of the investigation. When past studies are examined, few case histories and well-documented field data related to the excavation deeper than 15 m have been stated in detail. Therefore, the authors' study is important in terms of the rareness of field data and investigation about deep excavations in soft clays.

The first top-down construction stage was the implementation of 1 m thick diaphragm walls and then the load-bearing elements (cast-in-place ACIP piles). Following them, the interior H-section steel columns were constructed on deep-seated ACIP piles. After this stage, ground floors which are also used as struts were cast. As construction moved to a lower level, new steel pipes (struts) were propped. This process was repeated down to the final excavation level.

The authors presented the lateral movements of diaphragm wall at different excavation stages in Figure 2.25. In the figure, as the excavation reaches Level 2 which is 5.92 m below ground surface (BGS), upper part wall movements are restrained by ground floor and the wall starts to form deep-seated movements towards the excavation side. This kind of inward movement generates the bulging

profile. In addition, as excavation proceeds deeper, maximum wall deflections' locations move downward.

After the deep-seated wall movements towards the excavation side, the soil under the excavation may be lifted up. This condition is named as base heave. In consequence, the interior columns are also moved upwards. The uplift movements of columns increase with excavation depths. After the construction of foundation, column uplifts are decreased and stabilized. According to the authors, column uplifts (L_h) and wall movements (δ_{hm}) towards the excavations are closely related to each other. It is stated that the column uplifts fall within the boundaries between $L_h = 0.4 \times \delta_{hm}$ and $L_h = 1.3 \times \delta_{hm}$. Moreover, by using the measured axial strut forces, it is reported that most of the system loads due to the soil removal adjacent are sustained by the stiffer concrete struts and floor slabs.

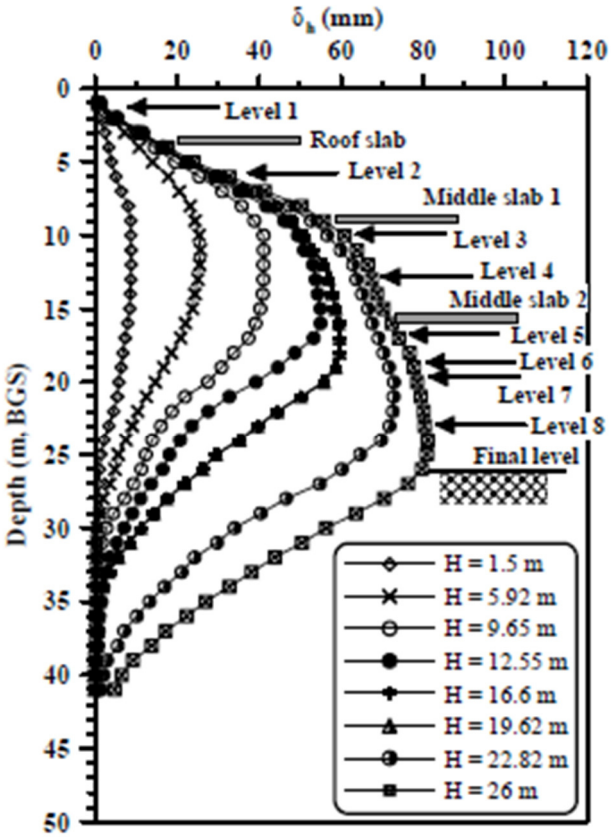

Figure 2.25. Typical Lateral Wall Movements (Lu and Tan, 2012)

Pakbaz et al. (2013) investigated the effect of five metro stations' deep excavation on lateral deformation of diaphragm walls and ground surface settlements. During the authors' research, only Kargar Square Station was under construction. Therefore, measurements of related lateral deformation and settlement data were performed for this station. The measured data were then used for the back calculation of soil parameters required for numerical method analysis. For all stations, the ground surface settlement and horizontal deformation of the diaphragm wall were estimated by taking advantage of back calculated parameters.

The observed five metro stations are located in the southern part of the Ahwaz Metro, Iran. Main geotechnical report of the project shows that the soil profiles in these locations include fine grained clay and silty layers on top and coarse grained medium to fine sand layer at the bottom. Because of the high groundwater level, the diaphragm wall method was preferred for the construction of all stations.

In order to compare the real measured data with the predicted values, a two dimensional model of diaphragm wall construction and soil excavation was implemented for the Kargar Square Station by using 2D Plaxis version 8. The geometric properties of the model are shown in Table 2.3. In the model, fine meshing pattern was selected and 15-node triangular elements were used.

Table 2.3. Geometric Properties of 2D Plaxis Model
(Pakbaz et al. 2013)

Geometric Properties	Related Values (m)
Dimension of the Model	80 x 40
Excavation Depth	17.2
Excavation Width	25.4
Excavation Length	131
Diaphragm Wall Thickness	0.8
Diaphragm Wall Depth	23

The construction stages that were considered in the numerical modeling can be listed as follows:

- Top fill soil excavation.
- Concrete guide wall construction.
- Trench excavation in the presence of bentonite slurry.
- Reinforcement installation.
- Concrete pouring process.
- Soil excavation in 10 stages and two levels of bracing systems placement.

The ground surface settlements and lateral deformations of the top of the wall were monitored and measured at different points at various distances from the wall. Monitoring results indicate that the surface settlement values for points located at a farther distance from the longitudinal wall are smaller than those closer to the longitudinal wall. In addition, the settlement magnitudes at points which are closer to the end of the cross wall are similar to those of points away from the end of the cross wall. This condition proves that three dimensional effects on the surface settlement along the longitudinal axis are unimportant. In other words, the plain strain assumption in the modeling is acceptable which means that using two-dimensional model is valid and enough in the analysis. This consequence is also correct for the horizontal deformations of the wall.

Figure 2.26 represents the 2D Plaxis model predictions for the ground surface settlement by the side of the wall and the lateral deformation of the wall at various excavation stages of the Kargar Square Station. In Figure 2.26b, it is read that the diaphragm wall has a cantilever-type deflection at excavation stages 2-4. For this case, the spandrel type of settlement, in which maximum surface settlement occurs very close to the wall, is observed (Figure 2.26a). Conversely, maximum lateral wall deflection occurs at deeper levels for the stages 5-10 by comparison with the stages 2-4 (Figure 2.26b). In the same manner, a concave type of settlement, in which maximum surface settlement occurs at a distance farther from the wall, is produced (Figure 2.26a).

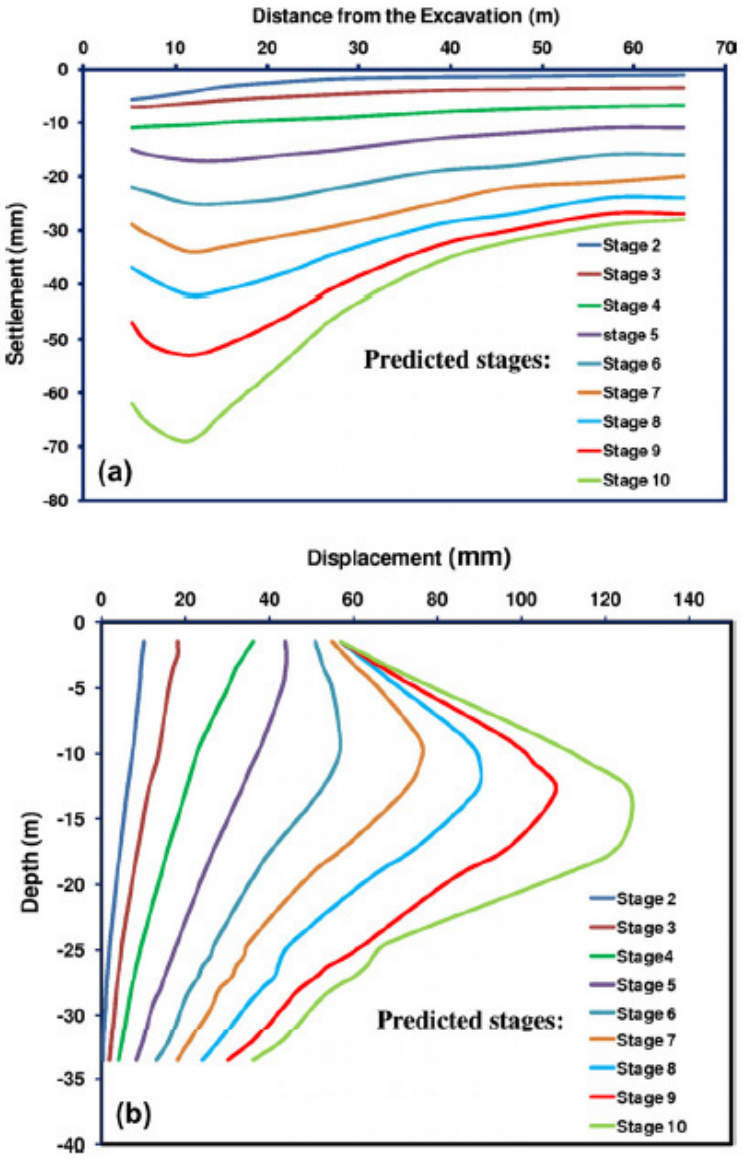

Figure 2.26. Predicted Ground Surface Settlement (a) Lateral Wall Deformation (b) at Various Excavation Stages in Kargar Square Station (Pakbaz et al. 2013)

The authors compared the measured data at the Kargar Square Station with the estimated values of the lateral wall deformations and ground surface settlements in Figure 2.27 and Figure 2.28, respectively. In both figures, it can be easily seen that the model predictions are higher than the actual measured data. This conclusion could be clarified by the lack of reliance on laboratorial soil parameters.

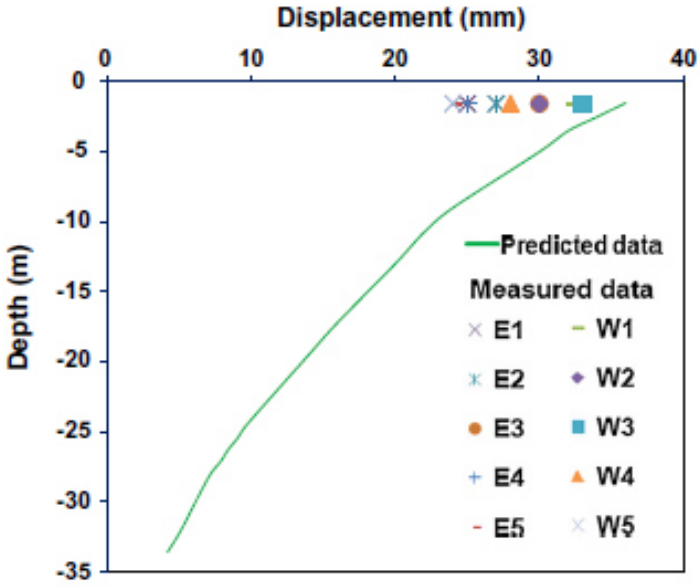

Figure 2.27. Maximum Measured and Numerical Estimation of Lateral Wall Deformation at Different Points (E1...E5, W1...W5)
(Pakbaz et al. 2013)

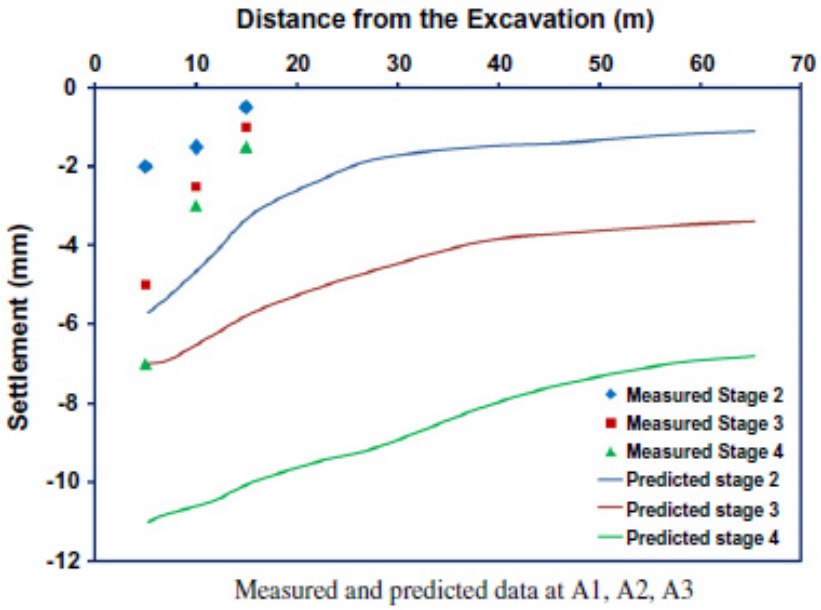

Figure 2.28. Measured Ground Settlements at Different Distances (A1=5m, A2=10m, A3=15m) from the Wall with Related Predicted Values
(Pakbaz et al. 2013)

Enhanced predictions of model parameters were obtained by using the back analysis method. With the help of back analysis method and available measured data, soil parameters namely Young's Modulus and shear strength parameters were determined. The back analysis method is an iterative procedure in which involved factors are changed to make the obtained results same as the measured values. In Figure 2.29, for the Kargar Square Station, predicted ground surface settlements and diaphragm wall displacements at the final stage of excavation with and without back calculated soil parameters are compared. Deformations without back calculated soil parameters are higher than the back calculated ones.

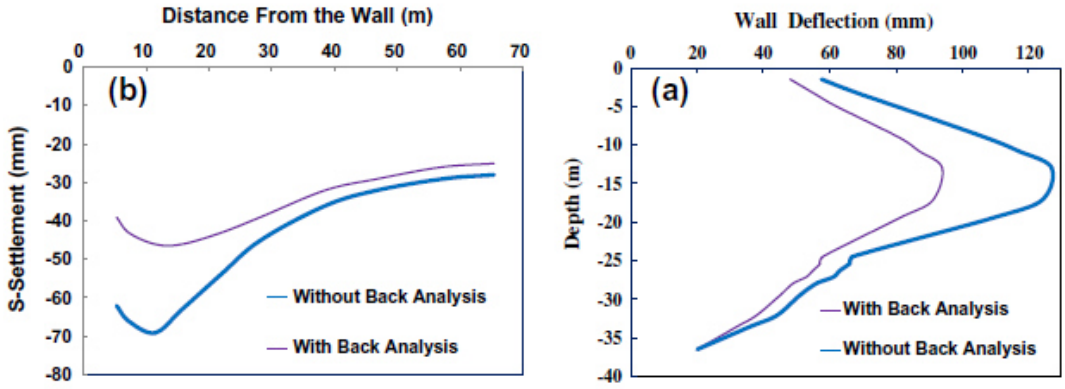

Figure 2.29. Comparison of Predicted Ground Settlements and Wall Deformations with and without Back Calculated Soil Parameters in Kargar Square Station (Pakbaz et al. 2013)

The maximum diaphragm wall movements (δ_{hm}) and the maximum ground settlements (δ_{vm}) of all five Ahwaz stations were estimated by using back calculated parameters. According to obtained results, following items were concluded:

- δ_{hm} values lies between 0.5% H_e and 0.7% H_e where H_e is depth of excavation.
- The depth at which δ_{hm} occurs is shallower than H_e.
- δ_{vm}/H_e ratio is in the range of (0.25 - 0.35).
- δ_{vm} predictions fall in regions I and II of Peck diagram.

- δ_{vm} estimates are between 0.5 δ_{hm} and 0.6 δ_{hm}. This condition revealed that the maximum ground surface settlements are generally smaller than the maximum lateral wall deflections in soft soils.

Jin, Zhao and Liu (2014) suggested a construction method for the supporting system of deep foundation of metro station's covered excavation in order to make construction easier and faster.

In this research, the covered excavation construction of Zha Nongkou Station in Hangzhou, China was explained. The geological conditions indicate that the excavation area mainly consists of silt and the stability is bad. The station length is approximately 181 m, excavation width is 22.5 m and the maximum digging depth is 17.5 m. The station is a two-layer double-column, three-span in-situ concrete frame structure. The covered excavation construction was applied for the middle of station and the open construction was implemented for the rest. The underground retaining wall of station is 37.5 m long and 0.8 m thick. Five steel pipe support and steel lattice column were preferred as inner support system.

The implementation of proposed method is summarized as follows:

1) The Top-Down Method and Construction

- Construction of Support Column: After finishing the construction of underground continuous wall, ten steel lattice columns in two rows are constructed. Bored piles are present under steel lattice column.
- Construction of Reinforced Concrete Beam and Slab: Reinforced concrete beam and slab structure basically consists of the upper concrete slab and beams. The top of steel lattice columns inserted into the main sub-beams and stiffeners were welded.

2) Installation of Steel Shotcrete and Steel Tie Rod

- Installation Process: Erecting steel shotcrete and welding steel tie rod that under the reinforced concrete structure shall be nearly combined in terms of the order and rate of earthwork excavation. From top to bottom the construction is a continuous and cyclic process, in which the earthwork is first excavated, then the support is erected, following the corresponding steel shotcrete is erected and finally the steel tie rod is welded for each layer.

According to the authors, the deformation of foundation area was under the safe limit with the application of the proposed method. It was concluded that the method needs to be more used for the construction of metro stations to ensure the safety of foundation area and continuity of traffic flow.

2.3. Conclusion

The findings about wall displacements mentioned in literature review will be compared with this study's results obtained from inclinometers and FEM analysis. One of the most significant findings is the maximum lateral wall displacement over excavation depth ratio value (Clough and O'Rourke, 1990). Moreover, case studies prepared by Kung (2009) and Ran et al. (2011) will be compared with the excavation analyzed in thesis study.

CHAPTER 3

ANALYSIS OF DATA FROM BAĞCILAR STATION EXCAVATION

3.1. General

In the scope of thesis, Bağcılar Station excavation in İstanbul is investigated. The station is on Otogar – Bağcılar rail transit line. The line is 21.7 km long with the extensions and consists of 16 stations. The construction of Bağcılar Station was completed in 2013. Figure 3.1 shows the entrance of the station.

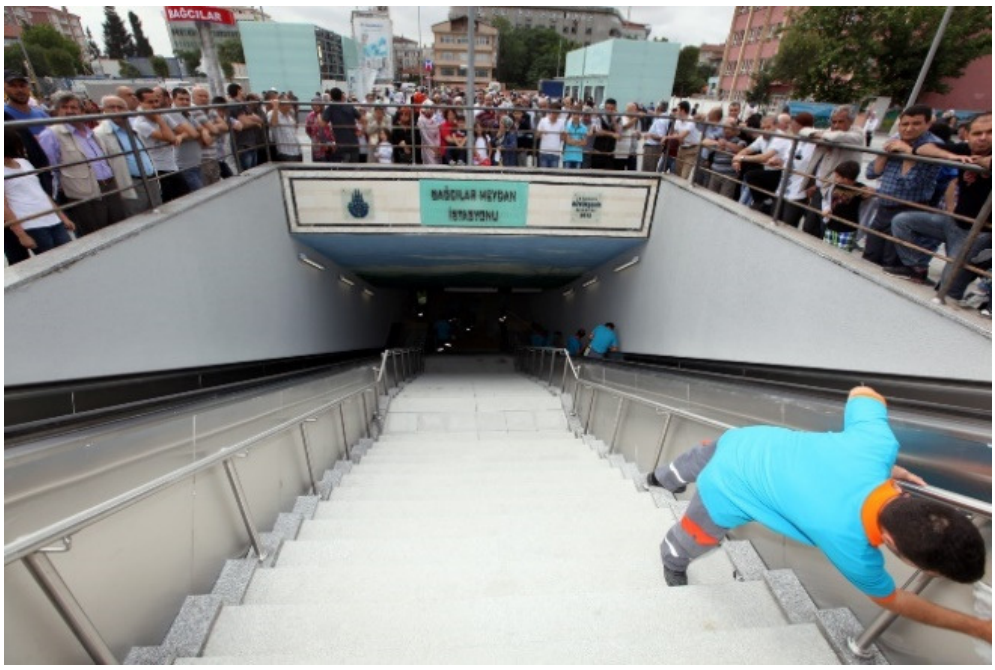

Figure 3.1. Bağcılar Station (source: http://www.ibb.gov.tr/tr-TR/HaberResim/21234/IMG_5286.jpg) [Last accessed on 28.04.2015]

Since the Bağcılar Station is located in crowded part of İstanbul, in order to use the roads and the social areas in very short time again and not to harm surrounding buildings and hinder the life excessively; Top – Down construction method was selected. In the Top – Down excavation system, firstly, the diaphragm walls were produced, which are both retaining structure and the outer walls of the station; then starting from the top slab, slab production went on. In addition to diaphragm walls, due to the large openings between the outer walls, two steel and concrete composite columns were used in the middle of the openings.

The excavation pit was about 132 m x 31 m in plan view and the deepest point of excavation was at the 54 m depth. The diaphragm wall thickness is 1.5 m and the embedded length is 8 m. The diaphragm columns are composite columns (steel and concrete) above the bottom slab and the dimensions are 0.8 m x 2.8 m. Moreover, the embedded parts of diaphragm columns are composed of concrete and the dimensions are 1.2 m x 2.8 m. The embedded length of diaphragm columns is 18 m. The thickness of bottom slab is 1.5 m. Other slabs' thicknesses vary from 0.6 m to 0.7 m. In addition, because of the larger floor height and excessive moments and shear forces, struts are used only between bottom slab and the slab above it. The diameter of the strut is 1200 mm and the wall thickness is 25 mm. The horizontal spacing of struts is 3.5 m.

In the following figures (Figure 3.2 - Figure 3.10), photographs from the excavation field; longitudinal section, cross section, plan view and the excavation stages are demonstrated.

Figure 3.2. Bağcılar Station Diaphragm Wall Equipment

Figure 3.3. Bağcılar Station Excavation Field

Figure 3.4. Bağcılar Station Diaphragm Wall Reinforcements

Figure 3.5. Inside View of Bağcılar Station during Construction

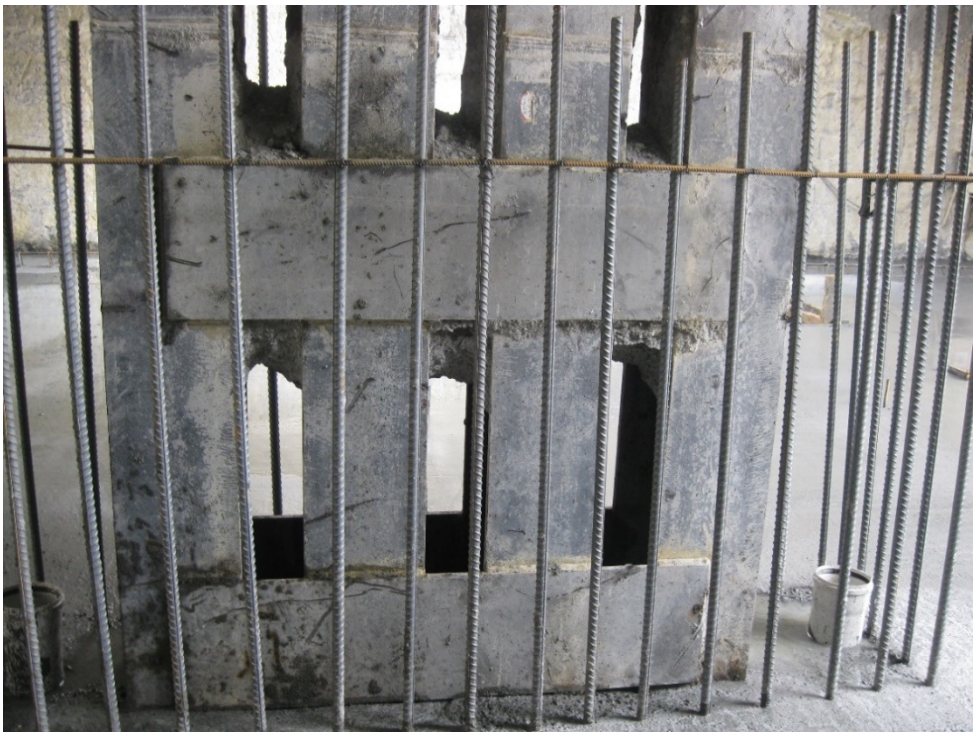

Figure 3.6. Bağcılar Station Steel-Concrete Composite Column

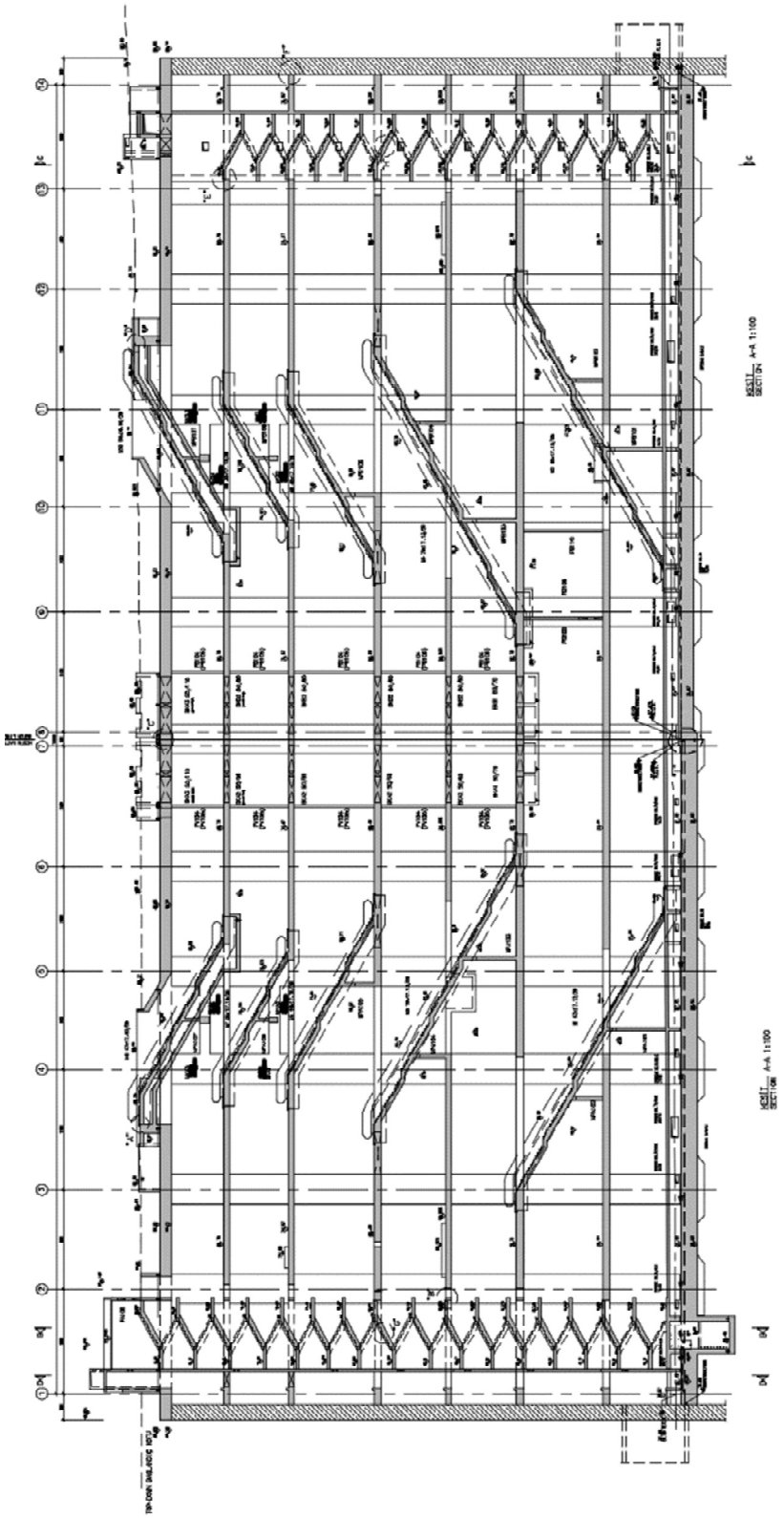

Figure 3.7. Bağcılar Station Longitudinal Section

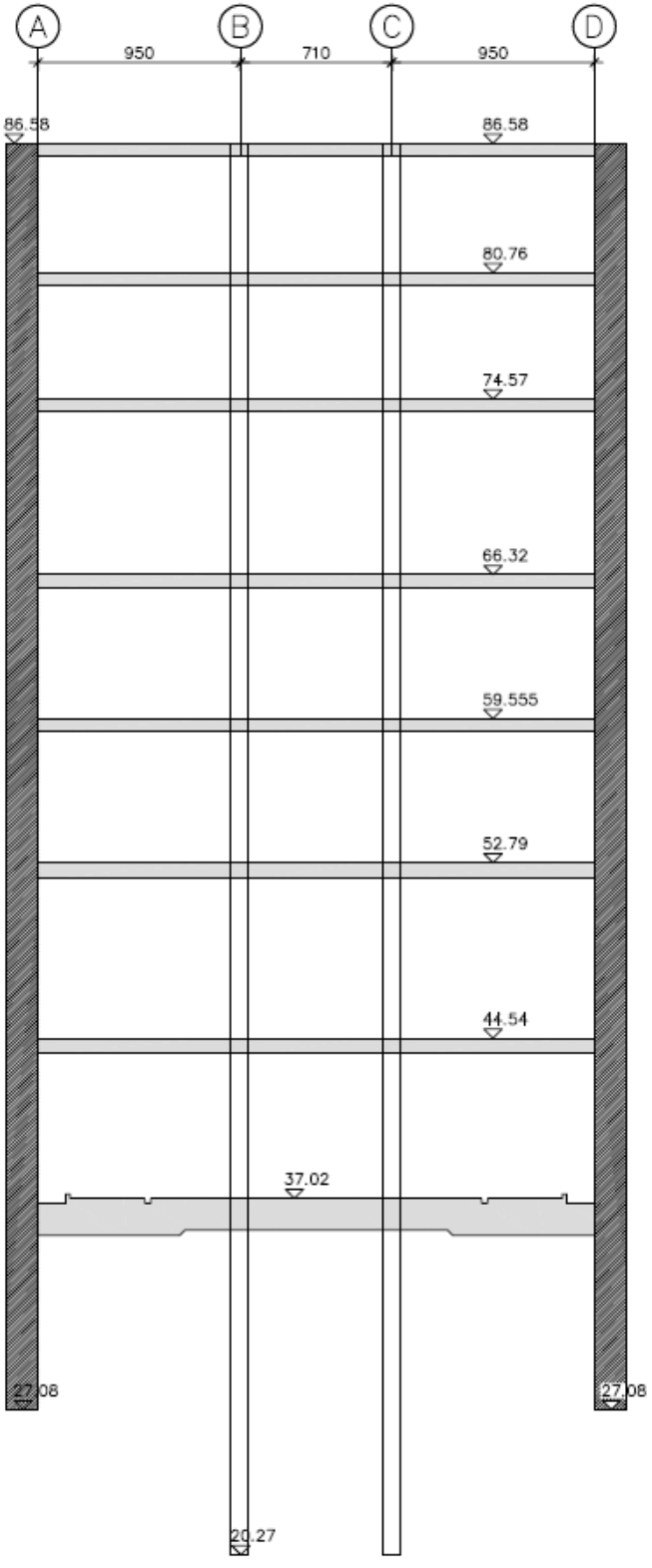

Figure 3.8. Cross Section of Bağcılar Station Excavation

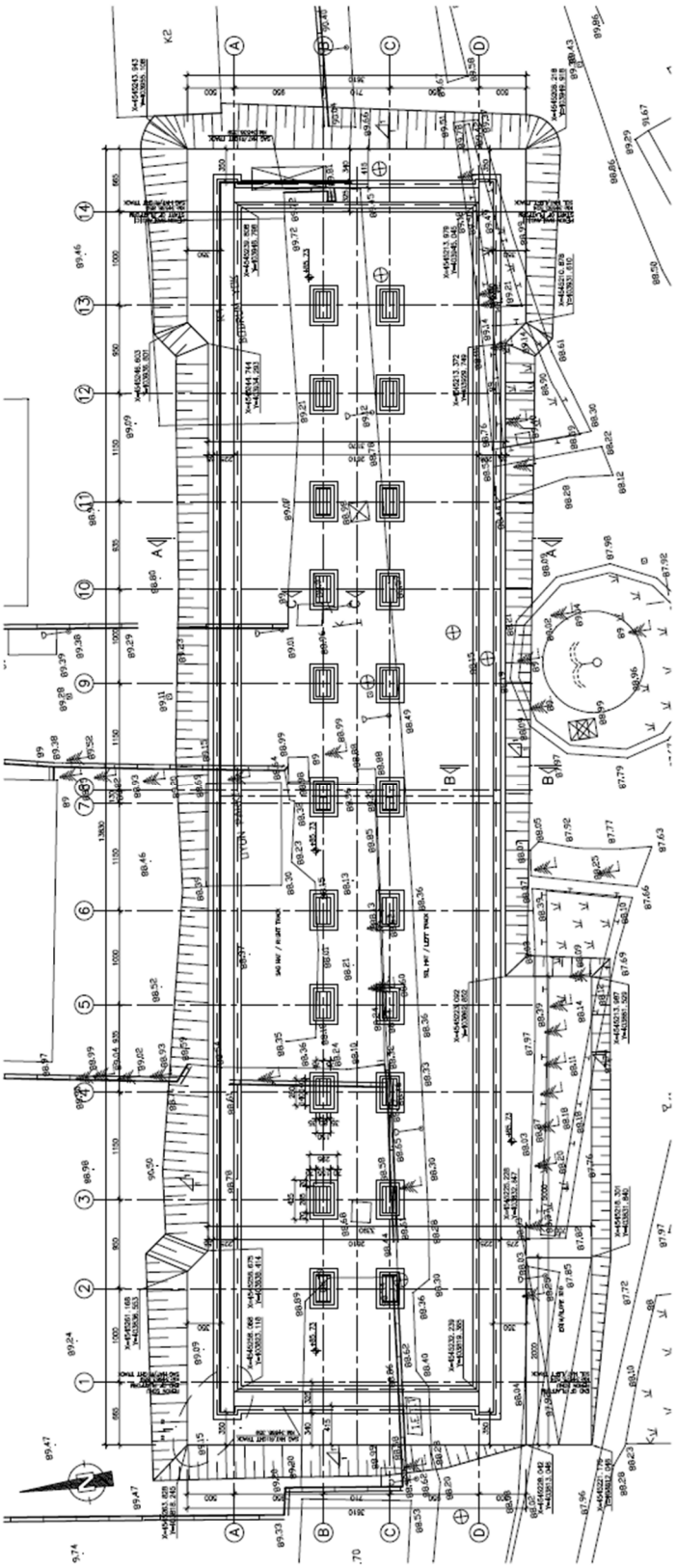

Figure 3.9. Plan View of Bağcılar Station Excavation

3.2. Excavation Stages

The Bağcılar Metro Station construction was performed by Top-Down excavation method and completed in 10 excavation stages. In the first stage, 2.5 m of surface excavation was completed in order to place the diaphragm walls and diaphragm columns to the desired locations. Moreover, in the first stage, construction of diaphragm walls and diaphragm columns are completed. For the stages in which slab production takes place, excavations were performed up to 15 cm below the slabs. In the second stage, after the completion of excavation, top slab was produced. In the following stages, slabs at the elevations of 80.76 m, 74.57 m, 66.32 m, 59.55 m, 52.79 m and 44.54 m were produced. In the ninth stage, excavation was performed up to 140 cm below the location of struts. Moreover, in the ninth stage, struts were installed. Finally, in the tenth excavation stage, bottom slab was produced and the construction was finished.

The explanations above can be seen schematically in Figure 3.10 which shows the excavation stages in cross section of the station.

The construction progression dates can be seen in Appendix A.

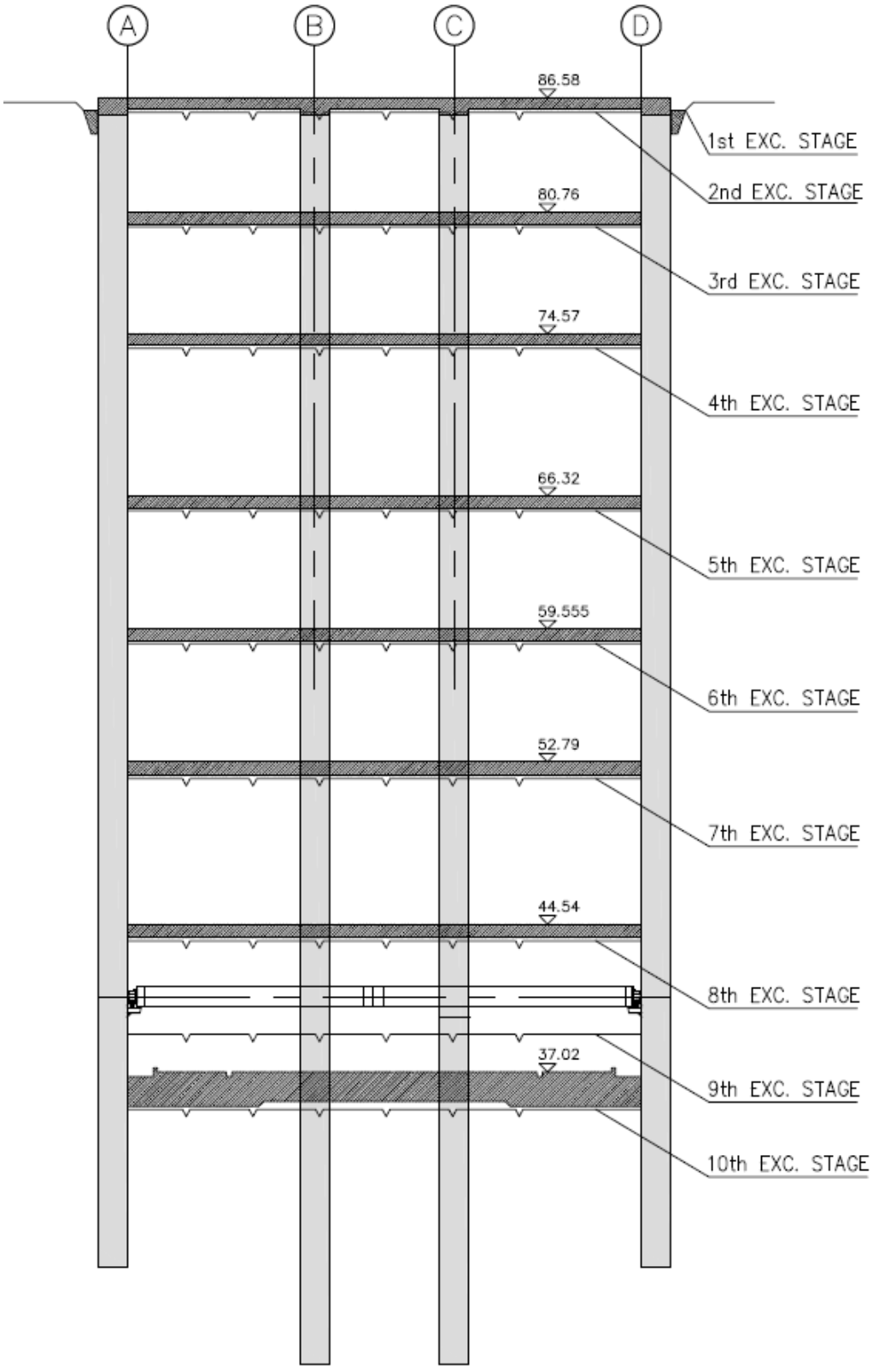

Figure 3.10. Excavation Stages of Bağcılar Station

3.3. Determination of Soil Profile

3.3.1. General Information

The Bağcılar Station, which is in the scope of Otogar – Bağcılar Light Rail System Project, has 31m x 132m dimensions on plan view with the maximum excavation depth of 54m. In order to determine soil and groundwater conditions; borehole drillings, piezometer measurements and laboratory tests were performed.

3.3.2. Soil Investigation Tests

In this thesis, following site investigation test results were used in order to determine the soil parameters;

- Borehole drillings YS01, YS02, YS03, YS04, YS05, YS06 and laboratory tests (Performed in August 2006).
- 10 piezometer borehole measurements which were located around YS02, YS03 and YS04 boreholes.
- Borehole drilling YS03 A which was located closer to YS03.

3.3.3. Soil Profile

3.3.3.1. Soil Index Properties

The soil formation observed in the project site is called Güngören formation and it consists of green and brown silty clay. Boreholes YS02 and YS04 were placed near to the short edges of the excavation. In addition, boreholes YS03 and YS03 A were placed in the middle of the excavation area. All the samples, which were taken from the boreholes YS02, YS03, YS03 A and YS04, were subjected to the soil classification tests in order to determine the index properties. In order to assess the behavior of the soil in excavation site, classification test results were investigated. Summary of the test results are presented in Appendix B.

As it can be clearly seen from the results, dominant soil type is silty clay, which has fine grained material in an interval of 70-90%.

After placing the plasticity index and liquid limit values to the plasticity chart (Figure 3.11), it can be seen that, the soil includes mostly clay with low plasticity (CL), silt with high plasticity (MH) and sand layer.

Hydrometer test, which was performed on the clay with low plasticity (CL), shows that fine grained soil contains considerable amount of silt. Average plasticity index and average liquid limit values of the soil texture CL is presented below:

Liquid Limit LL = 42 %

Plasticity Index PI = 20 %

Average plasticity index and average liquid limit values of the soil texture silt with high plasticity (MH) is presented below:

Liquid Limit LL = 60 %

Plasticity Index PI = 26 %

In the borehole drillings, sand layers were also observed and classified as silty sand (SC).

According to the results, the soil profile dominantly includes silty clay. The soil profile also includes little amount of sand layers. Since the clayey formation is dominant, PI value for clay with low plasticity (CL) is used in calculations which is 20 %.

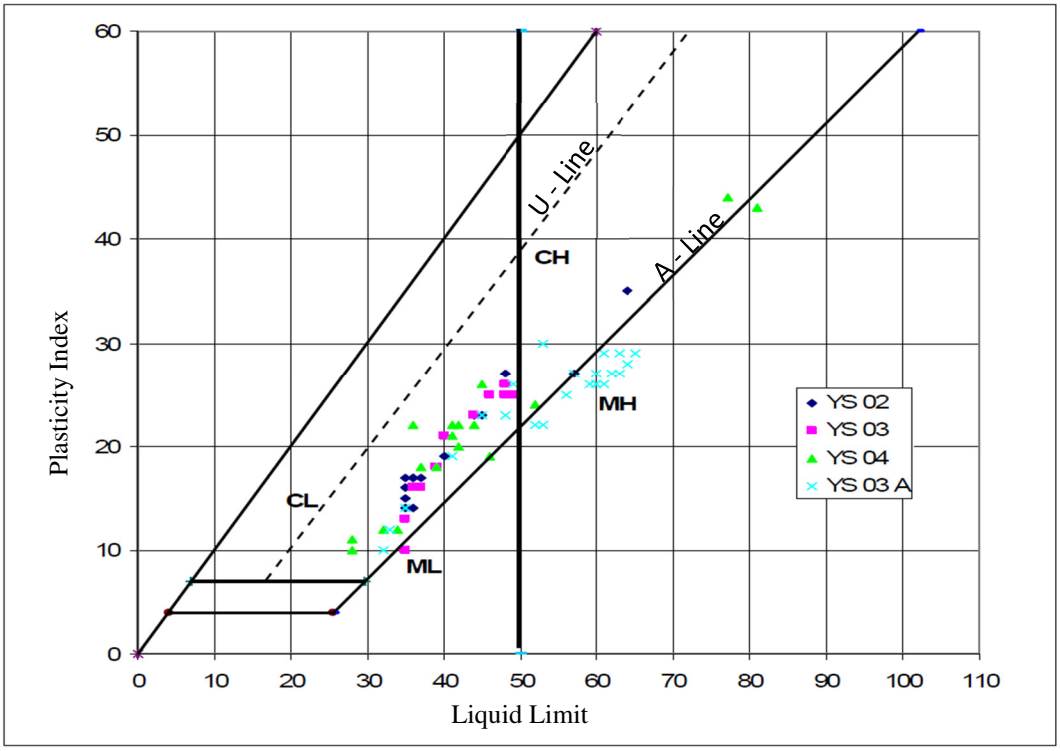

Figure 3.11. Plasticity Chart (Yüksel Proje Uluslararası A.Ş., 2007)

3.3.3.2. Strength and Deformation Characteristics of the Soil

In order to determine the strength parameters of the soil, standard penetration tests were performed. For the purpose of calculating the soil strength parameters, number of blows required to drive the sampler 30 cm through the soil, which is called as N value. N values of boreholes YS01, 02, 03, 03 A, 04, 05 and 06 are listed below with the depths. As it can be seen from the Figure 3.12, N values increases with the depth. Average N values are shown in Figure 3.12 and listed below:

00-10 m ⟶ N=20

10-20 m ⟶ N=30

20-30 m ⟶ N=35

30-50 m ⟶ N=45

50-70 m ⟶ N=60

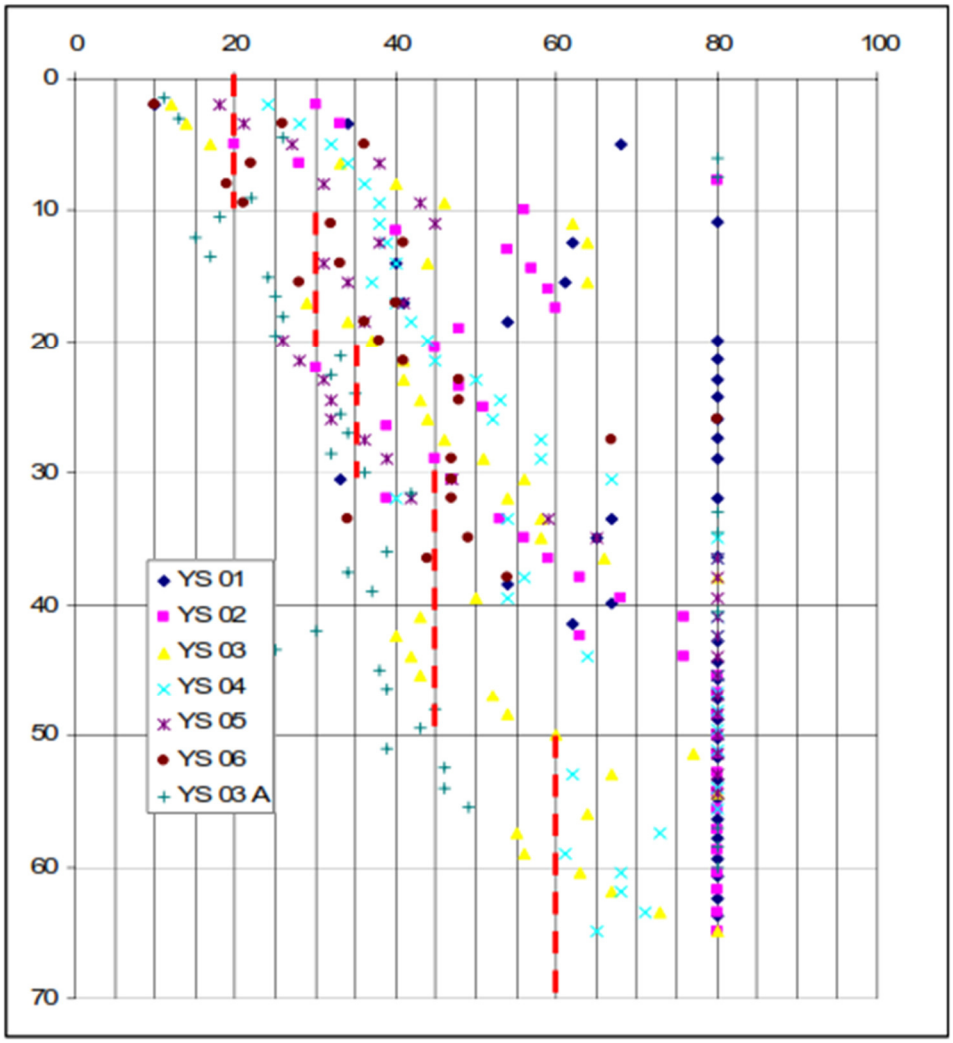

Figure 3.12. SPT N Values vs Depth (Yüksel Proje Uluslararası A.Ş., 2007)

According to the SPT N values, undrained shear strength parameter of the soil is calculated by using the correlations recommended by Stroud (1974) considering Plasticity Index (PI).

$c_u = f_1 N$ (PI = 20 $\longrightarrow$ f_1= 5.3)

00 - 10 m c_u= 100 kPa

10 - 20 m c_u= 160 kPa

20 - 30 m c_u= 185 kPa

30 - 50 m c_u= 240 kPa

> 50 m c_u= 320 kPa

Undrained Modulus of Elasticity in cohesive soil is calculated as below:

$E_u = 500 – 1500\ c_u$ (Bowles, 1988)

In this project, E_u is selected as 500 c_u. E_u values are listed below:

00 - 10 m E_u= 50000 kPa

10 - 20 m E_u= 80000 kPa

20 - 30 m E_u= 92500 kPa

30 - 50 m E_u= 120000 kPa

> 50 m E_u= 160000 kPa

In order to determine the long term soil parameters, effective angle of internal friction (ϕ'), which is related to plasticity index, was used as recommended by Bowles (1988) and ϕ' is selected as 26°.

For the effective cohesion value, the method recommended by Mesri and Abdel-Ghaffar (1993) is taken into consideration. The equation is presented below:

$$c' = \sigma_p' \, (1 - m) \tan \phi' \, (\sigma_p'/\sigma_n')^{-m}$$

where , σ_p' = pre consolidation pressure

σ_n' = normal effective stress

m = coefficient depends on plasticity index

For the Plasticity Index (PI) = 20 %, m value can be selected between 0.64 and 0.87. The m value is preferred as the average value m = 0.75. For the first 30 m depth, over consolidation ratio is determined as 1.5, for the depths larger than 30 m, over consolidation ratio is determined as 1.0. The c' values, calculated according to formula recommended by Mesri and Abdel-Ghaffar (1993), are listed below:

00-10 m c'= 13 kPa

10-20 m c'= 34 kPa

20-30 m c'= 47 kPa

30-50 m c'= 60 kPa

>50 m c'= 84 kPa

After evaluating the above results, in order to be on the safe side, c' values are rounded and/or decreased. The selected values for c' are listed below:

00-10 m c'= 15 kPa

10-20 m c'= 25 kPa

20-30 m c'= 35 kPa

30-50 m c'= 50 kPa

>50 m c'= 50 kPa

Unit weight values are determined with the help of Table 3.1 which was prepared by Carter and Bentley, 1991.

Table 3.1. Typical Ground Parameters (Carter and Bentley, 1991)

Type of Material	Bulk Unit Weight γ (kN/m³)		Saturated Bulk Unit Weight γ_s (kN/m³)		Effective Stress ϕ' (degrees)		Total Stress Cohesion c_u (kN/m²)
	Loose	Dense	Loose	Dense	Loose	Dense	
Gravel	16,0	18	20	21	35	40	
Well graded sand & gravel	19,0	21	21,5	23	35	40	
Coarse or medium sand	16,5	18,5	20	21,5	35	40	
Well graded sand	18,0	21	20,5	22,5	35	40	
Fine or silty sand	17,0	19	20	21,5	30	35	
Rock fill & quarry waste	15,0	17,5	19,5	21	40	45	
Brick hardcore	13,0	17,5	16,5	19	40	45	
Slag fill	12,0	15	18	20	30	35	
Ash fill	6,5	10	13	15	35	40	
Top soil	16,0	19	20	21	25		
River mud	14,5	17,5	19	20	5 - 10		
Silt	18		18		25		
Peat	12		12		15		
Very soft clay	16		16		*		< 20
Soft clay	17		17		*		20 - 40
Soft to firm clay	17,5		17,5		*		40 - 50
Firm clay	18		18		*		50 - 75
Firm to stiff clay	18,5		18,5		*		75 - 100
Stiff clay	19		19		*		100 - 150
Very stiff clay or hard clay	20 - 21		20 - 21		*		> 150

Long term modulus of elasticity is calculated from the method recommended by Hemsley (2000). The equation is presented below:

$$E' = 0.80\ E_u$$

E' values are listed below:

00-10 m E'= 40,000 kPa

10-20 m E'= 64,000 kPa

20-30 m E'= 74,500 kPa

30-50 m E'= 96,000 kPa

>50 m E'= 128,000 kPa

3.3.3.3. Groundwater Conditions and Soil Permeability Properties

In order to investigate the groundwater conditions, 10 piezometer wells were installed on site. Groundwater levels measured from the piezometer wells are summarized in Table 3.2. Change in hydrostatic pressures created by the water levels versus depth is indicated in Figure 3.13. As it can be seen from the Figure 3.13, measured water levels show signs of groundwater table. Especially measurements from the piezometer no YS03 indicate the water table is at 10 m depth. Although a static water table is not expected in clayey and silty textures, due to the possibility of water in sand and silt layers and in order to be on the safe side, water table is assumed at 10 m depth from the ground surface.

Table 3.2. Groundwater Levels (GWL) measured in piezometers.
(Yüksel Proje Uluslararası A.Ş., 2007)

Piezometer no	Depth (m)	GWL (m)
YS - 02	20.0	5.57
YS - 02	38.5	18.6
YS - 02	62.0	30.25
YS -03	15.0	11.13
YS - 03 A	36.5	16.05
YS - 03	62.5	17.5
YS -03	71.5	35.4
YS - 04	9.0	6.55
YS - 04	13.5	4.36
YS - 04	62.0	26.37

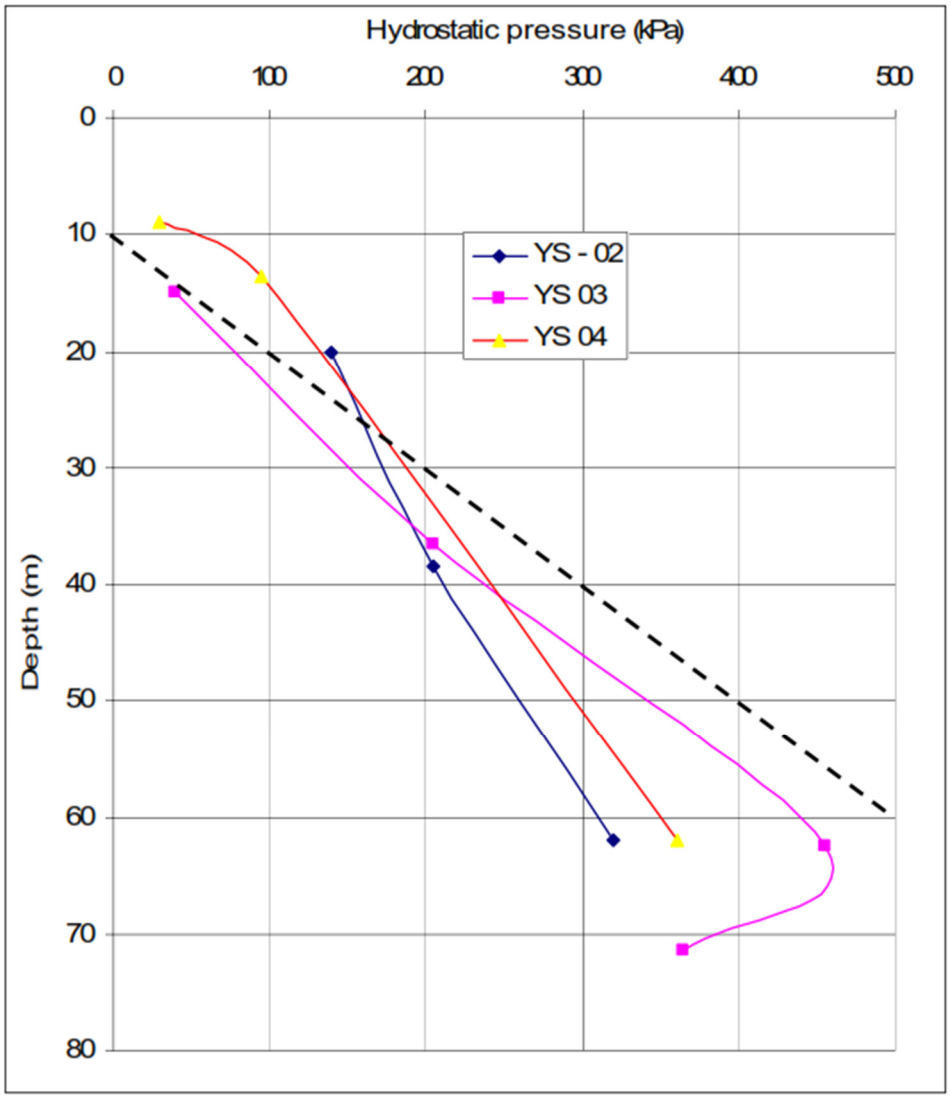

Figure 3.13. Hydrostatic Pressure Distribution

(Yüksel Proje Uluslararası A.Ş., 2007)

In order to determine the permeability of the soil, rising head permeability test was performed and results are presented in Table 3.3. During the test, all the piezometer wells were discharged by bailer buckets and change in water levels were measured for 6 hours. Permeability coefficients calculated from the measurements are presented in Figure 3.14. Average permeability coefficient is determined as, k =3.3 x 10 -8 m/s.

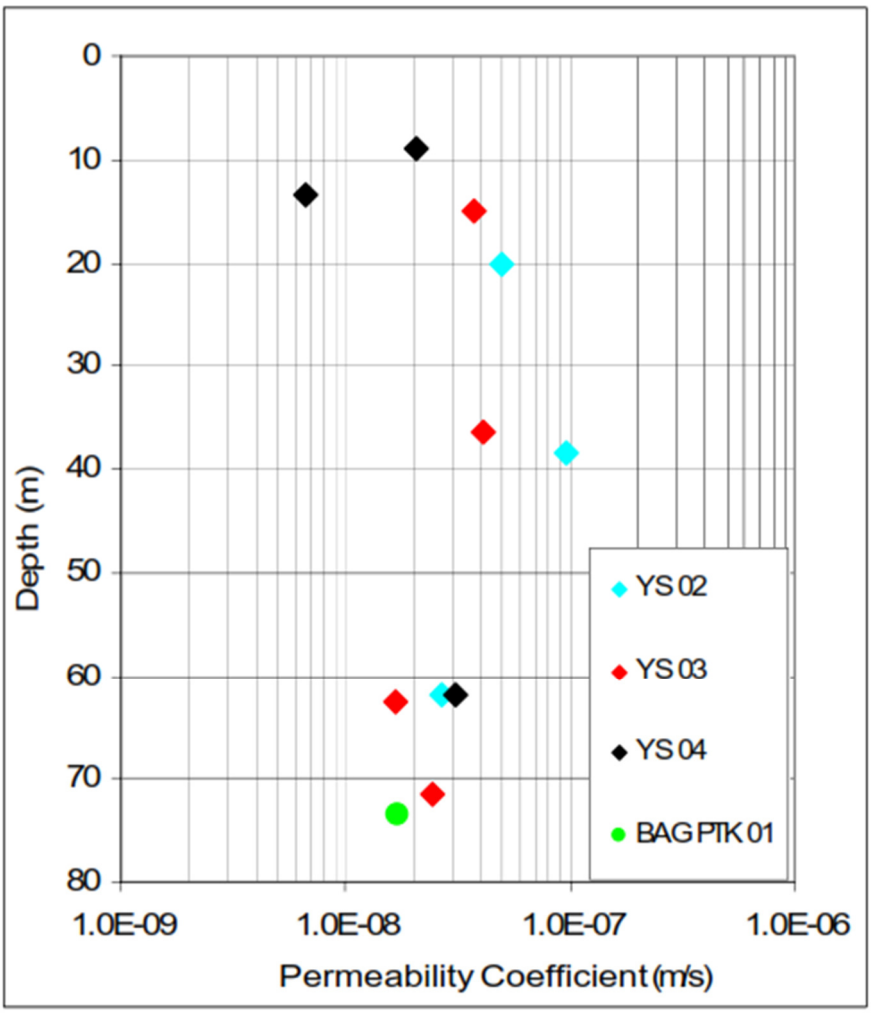

Figure 3.14. Permeability Coefficient vs Depth

(Yüksel Proje Uluslararası A.Ş., 2007)

Table 3.3. Rising Head Permeability Test Results

(Yüksel Proje Uluslararası A.Ş., 2007)

	Piezometer no	GWL (m)	Filter beginning (m)	Filter end (m)	Average Test Depth (m)	Filter Length (m)	Well Dia. (m)	F	Water Level at the Beginning (m)	Water Level after 6 Hours (m)	Permeability Coefficient (m/s)
YS 02	YS - 02 B	5.57	19.00	21.00	20.00	2.00	0.1	3.40	15.50	11.80	5.0E-08
	YS - 02 A	18.60	37.00	40.00	38.50	3.00	0.1	4.60	34.50	23.25	9.7E-08
	YS - 02	30.25	59.00	65.00	62.00	6.00	0.1	7.87	58.75	46.30	2.7E-08
YS 03	YS -03 B	11.13	14.00	16.00	15.00	2.00	0.1	3.40	13.50	12.80	3.7E-08
	YS - 03 A	16.05	35.00	38.00	36.50	3.00	0.1	4.60	32.10	25.60	4.1E-08
	YS - 03	17.50	60.00	65.00	62.50	5.00	0.1	6.82	59.50	48.30	1.7E-08
	YS -03 C	35.40	68.00	75.00	71.50	7.00	0.1	8.90	68.80	53.70	2.5E-08
YS 04	YS - 04 A	6.55	8.00	10.00	9.00	2.00	0.1	3.40	8.80	8.40	2.1E-08
	YS - 04 B	4.36	12.00	15.00	13.50	3.00	0.1	4.60	12.50	11.85	6.6E-09
	YS - 04	26.37	59.00	65.00	62.00	6.00	0.1	7.87	58.00	42.60	3.1E-08
pumping	BAG PTK 01	51.88	67.00	80.00	73.50	13.00	0.3	18.30	76.00	62.00	1.7E-08

$$F = \frac{2\pi L}{\ln((L/D) + \sqrt{(1+(L/D)^2}} \qquad k = \frac{A}{F(t_2 - t_1)} \ln \frac{H2}{H1}$$

3.3.4. Results

According to the investigations Groundwater Level is selected at the 10 m depth.

Short Term Strength Parameters are listed below;

00-10 m	c_u= 100 kPa	E_u=50,000 kPa
10-20 m	c_u= 160 kPa	E_u=80,000 kPa
20-30 m	c_u= 185 kPa	E_u=92,500 kPa
30-50 m	c_u= 240 kPa	E_u=120,000 kPa
>50 m	c_u= 320 kPa	E_u=160,000 kPa

Long term strength parameters are listed below;

00-10 m	c'=15 kPa	ϕ'=26º	E'=40,000 kPa
10-20 m	c'= 25 kPa	ϕ'= 26º.	E'=64,000 kPa
20-30 m	c'= 35 kPa	ϕ'= 26º	E'=74,000 kPa
30-50 m	c'= 50 kPa	ϕ'= 26º	E'=96,000 kPa
>50 m	c'= 50 kPa	ϕ'= 26º	E'=128,000 kPa

Idealized soil profile can be seen below from Figure 3.15.

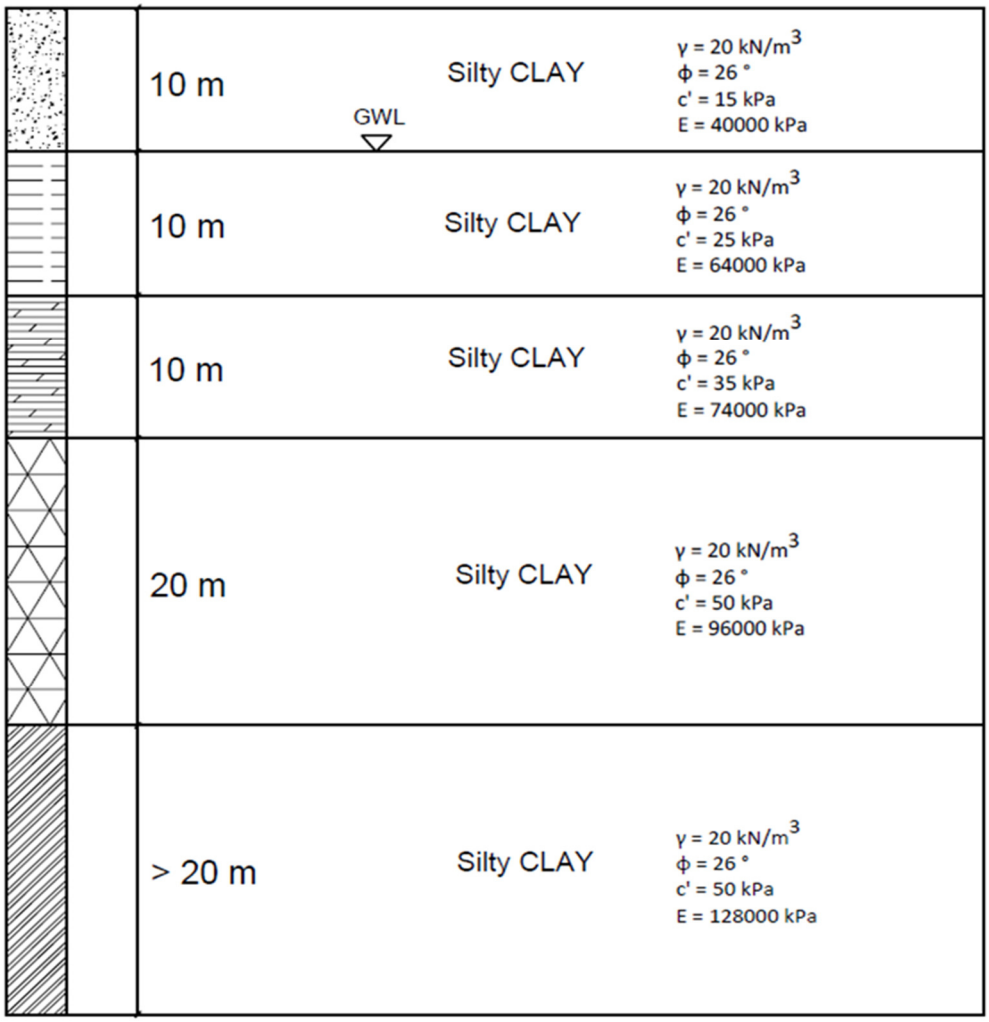

Figure 3.15. Idealized Soil Profile

3.4. Instrumentation and Monitoring

Inclinometers were used in order to monitor the displacements at each stage during the excavation. 8 inclinometers were placed behind diaphragm walls. The inclinometers give results up to 65 m depth. For the comparison of results with FEM models, 3 of the inclinometer readings are taken into account. Inclinometer 1 (BAG INK 01), Inclinometer 2 (BAG INK 02) and Inclinometer 3 (BAG INK 03) are the chosen inclinometers. The reason of selecting these 3 inclinometers is their position. 2D models are constructed in order to determine the displacements of short edge, a point on the long edge which is closer to the corner and a point at the middle of the long edge. Location of the inclinometers can be seen from the Figure 3.16. As can be seen from the inclinometer measurements in Appendix C, displacement measurements are given for two axes, namely north and east. For the diaphragm walls, which are located in the long edge, displacement measurements of the north direction is used. On the other hand, for the diaphragm walls, which are located in the short edge, displacement measurements of the east direction is used.

Figure 3.16. Location of Inclinometers

(source: Bağcılar Station Contractor Documents)

3.5. Finite Element Analysis

For the 2D finite element analysis PLAXIS 2D software is used. PLAXIS 2D is a program, which uses finite element method, developed for the analysis of deformation and stability for two-dimensional analysis in geotechnical engineering. (PLAXIS 2D User Manual)

For the 2D analysis, 3 models, which are assumed plane strain, are constructed. The reason of using plane strain models is the geometry of the excavation. Excavation is in a rectangular shape, so a uniform cross section can be assumed for the modelling. Plane strain models assume uniform cross section, uniform loading and zero deformation in the alignment which is perpendicular to the cross section.

In order to model the soil, 15 nodded triangular elements are used. The boundary conditions for the finite element mesh allow vertical movements at the sides and full fixity at the base. In the modeling, fine meshing is selected because of obtaining more accurate results.

In the analysis model, top slab and bottom slab are connected to diaphragm walls with fixed support while other slabs connected to diaphragm walls with hinged support. Typical 2D finite element meshes used in the analysis is shown in Figure 3.17. In addition, total displacement behavior of 2D analysis is indicated in Figure 3.18.

In the analysis, Hardening Soil model, which is an advanced model for the simulation of soil behavior, is used. Hardening Soil model is an elastoplastic type of hyperbolic model, formulated in the framework of shear hardening plasticity. Hardening Soil model is a second order model which can simulate the behavior of sands, gravel, clays and silts. The difference between Mohr – Coulomb model and Hardening Soil model is that, Mohr – Coulomb model is a linear model, which can be used as a first approximation of soil behavior. Mohr – Coulomb model uses a constant soil stiffness so this model can only be used for a first approximation. (PLAXIS 2D User Manual)

In the Hardening Soil model, unit weight (γ), internal friction angle (ϕ), cohesion (c), modulus of elasticity (E) and Poisson's Ratio (ν) are considered as the necessary input data.

Excavation is modeled in 10 stages and PLAXIS 2D lists the results for each stage.

Input data of the structural elements used in modelling are tabulated in Table 3.4. In this table, EA and EI values for diaphragm columns are divided by the distance between columns which is 11 m in average.

Table 3.4. Input Data of the Structural Elements for Plaxis2D

Element	**EA (kN/m)**	**EI (kNm^2/m)**
Diaphragm Wall	4.8×10^7	9.0×10^6
Diaphragm Column (Steel)	1.4×10^6	4.2×10^4
Diaphragm Column (Concrete)	8.7×10^6	1.1×10^6
Slab (t = 60 cm)	1.7×10^7	5.1×10^5
Slab (t = 70 cm)	2.0×10^7	8.2×10^5
Slab (t = 150 cm)	4.3×10^7	8.0×10^6
Strut (D1200 / 25 mm)	1.9×10^7	-

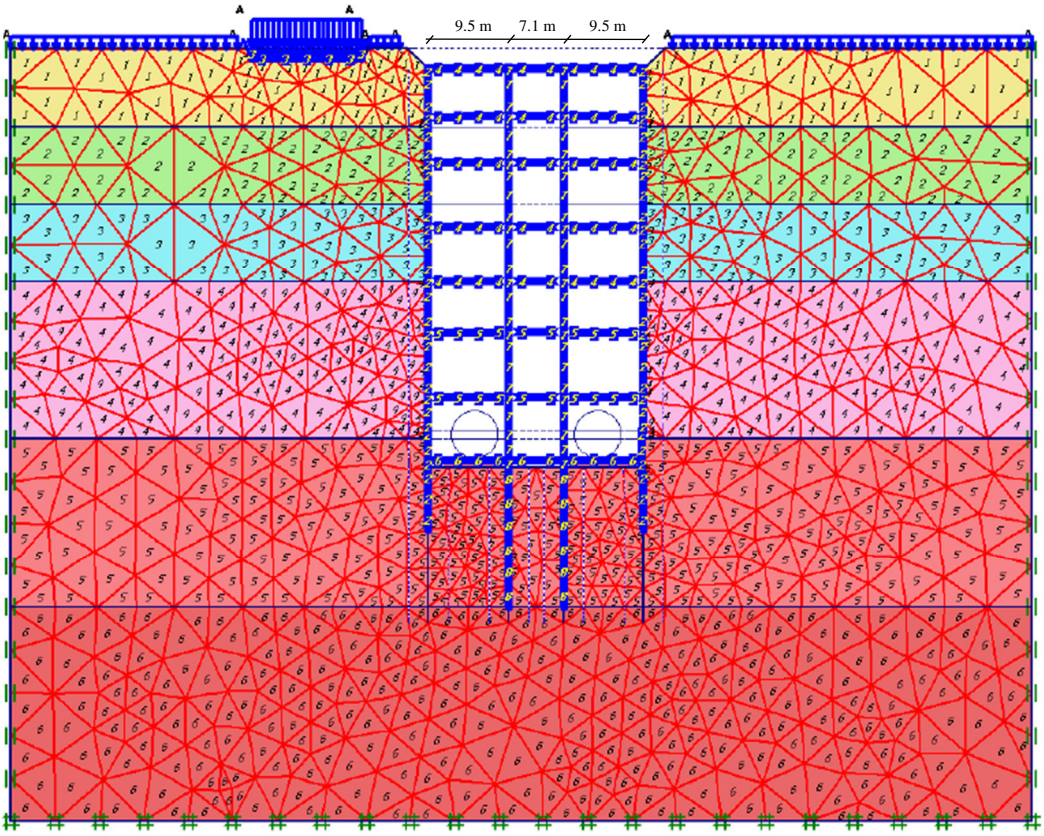

Figure 3.17. Typical 2D Analysis Mesh

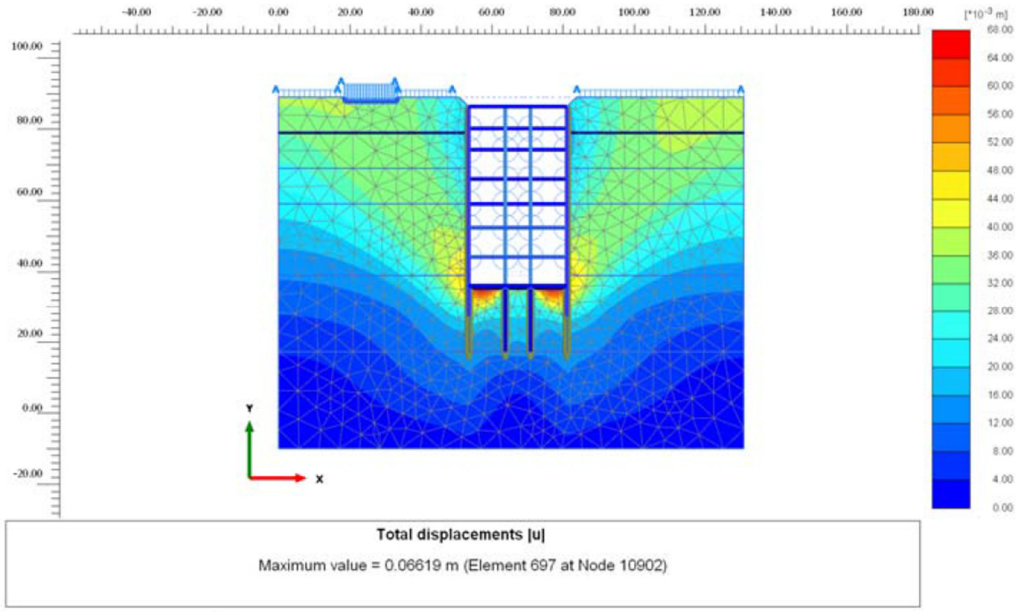

Figure 3.18. 2D Analysis Total Displacement Behavior

For the 3D finite element analysis, PLAXIS 3D software is used. PLAXIS 3D is a program, which uses finite element method, developed for the analysis of deformation and stability for three-dimensional analysis in geotechnical engineering. (PLAXIS 3D User Manual)

For the 3D analysis, one model including all the soil properties, loads, existing surcharge loads was constructed. In the analysis model, top slab and bottom slab are connected to diaphragm walls with fixed support while other slabs connected to diaphragm walls with hinged support.

In the analysis, Hardening Soil model, which is an advanced model for the simulation of soil behavior, is used. In the Hardening Soil model, unit weight (γ), internal friction angle (ϕ), cohesion (c), modulus of elasticity (E) and Poisson's Ratio (ν) are considered as the necessary input data.

Excavation is modeled in 10 stages and PLAXIS 3D lists the results for each stage. Input data of the structural elements used in modelling are tabulated in Table 3.5, Table 3.6 and Table 3.7.

Table 3.5. Input Data of the Structural Elements for Plaxis3D (Plate Elements)

Element	**t (m)**	**E (kN/m^2)**
Diaphragm Wall	1.5	32.0×10^6
Slab (t = 60cm)	0.6	28.6×10^6
Slab (t = 70cm)	0.7	28.6×10^6
Slab (t = 150cm)	1.5	28.6×10^6

Table 3.6. Input Data of the Structural Elements for Plaxis3D (Beam Elements)

Element	**A (m^2)**	**E (kN/m^2)**	**I_3 (m^4)**	**I_2 (m^4)**
Diaphragm Column (Steel)	0.08	200×10^6	2.3×10^{-3}	0.02
Diaphragm Column (Concrete)	3.36	28.6×10^6	2.19	0.40

Table 3.7. Input Data of the Structural Elements for Plaxis3D (Anchor Element)

Element	**EA (kN)**
Strut (D1200 / 25 mm)	1.9×10^7

In Figure 3.19, different soil layers defined in the 3D model is shown. Moreover, the inner structure modeled in PLAXIS 3D is presented in Figure 3.20.

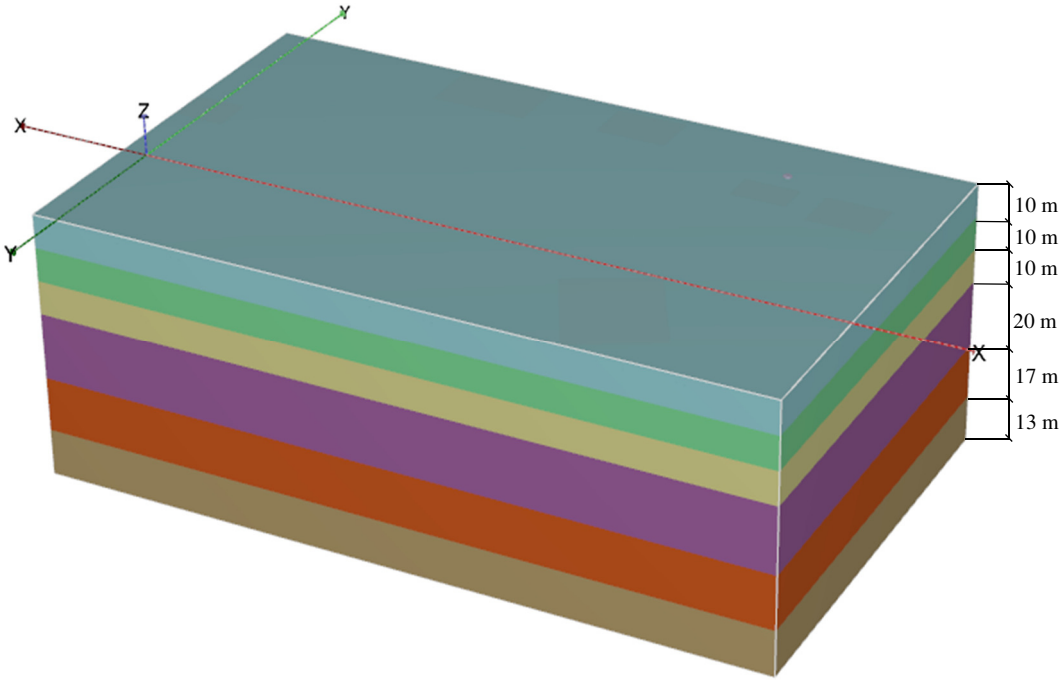

Figure 3.19. Soil Layers

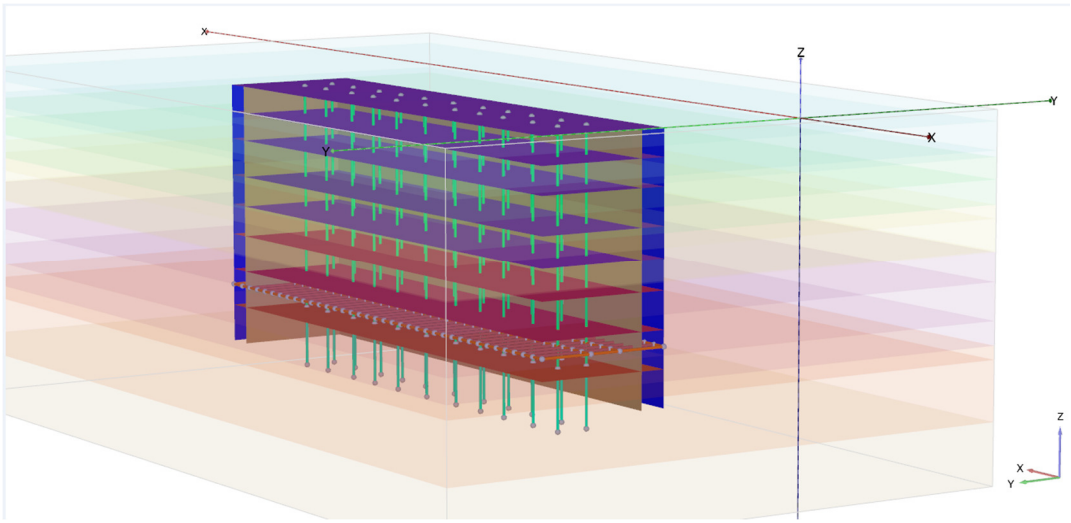

Figure 3.20. Inner Structure

In the modeling, 15 kN/m^2 surcharge load is assigned on top of the station because of the live load around the station. Moreover, additional surcharge loads are applied due to the existing buildings. For these additional surcharge loads, 12.5 kN/m^2 per storey is applied. Figure 3.21 shows the additional surcharge loads of existing buildings.

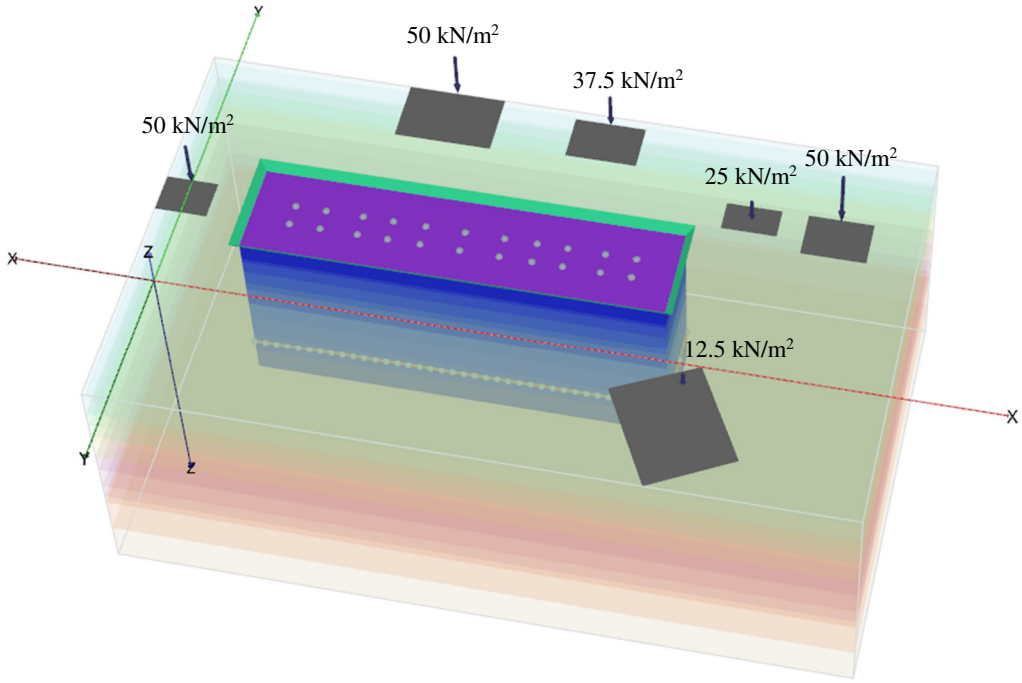

Figure 3.21. Surcharge Loads of Existing Buildings

Finite element meshing of 3D model is presented in Figure 3.22.

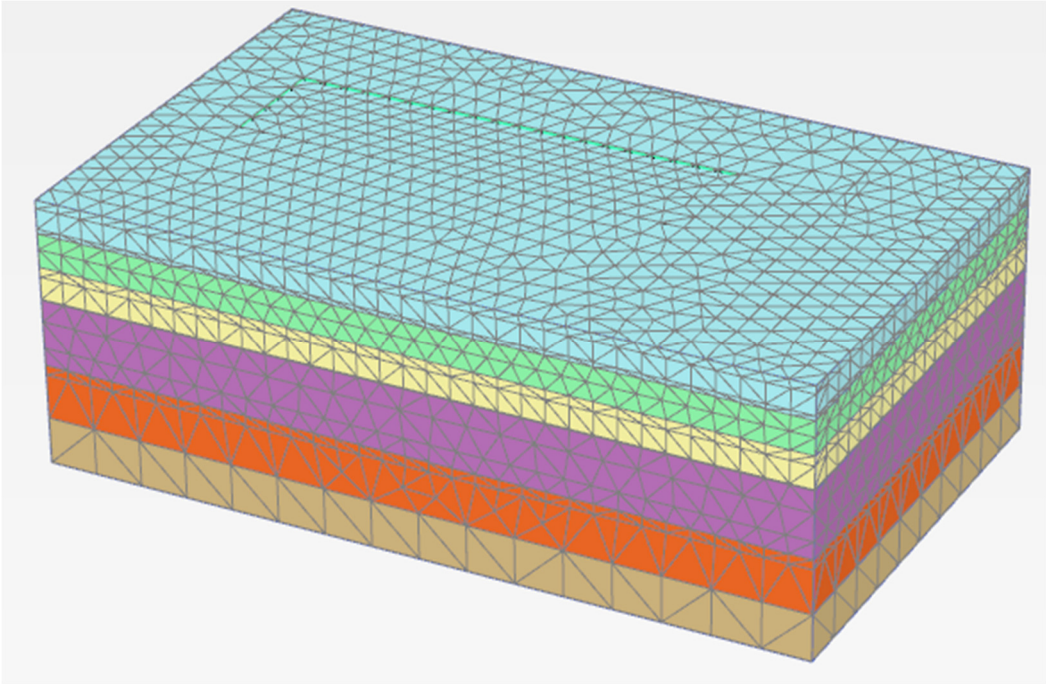

Figure 3.22. Finite Element Meshing

The displacement behavior of diaphragm walls can be seen in Figure 3.23. It is clear that displacement of walls is getting smaller as getting closer to the corners. On the other hand, displacement of walls is getting larger as getting closer to the middle of the structure.

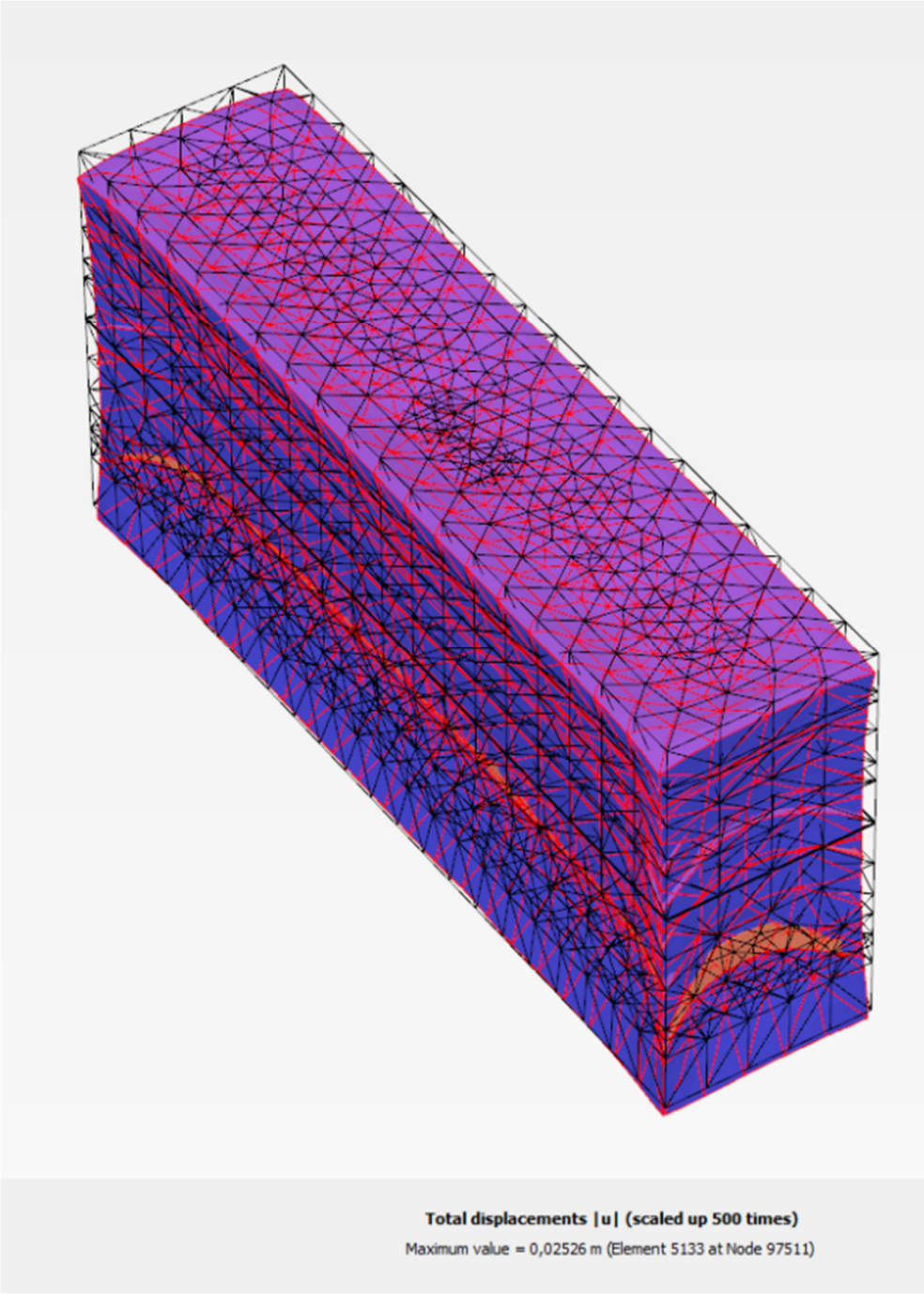

Figure 3.23. Displacement Behavior of Diaphragm Walls

In Figure 3.24, total displacement behavior obtained from 3D analysis is shown. At the bottom, displacement jumps can be seen due to the embedded parts of diaphragm columns. In addition, it is observed that larger displacements occur below the bottom slab and below the existing buildings.

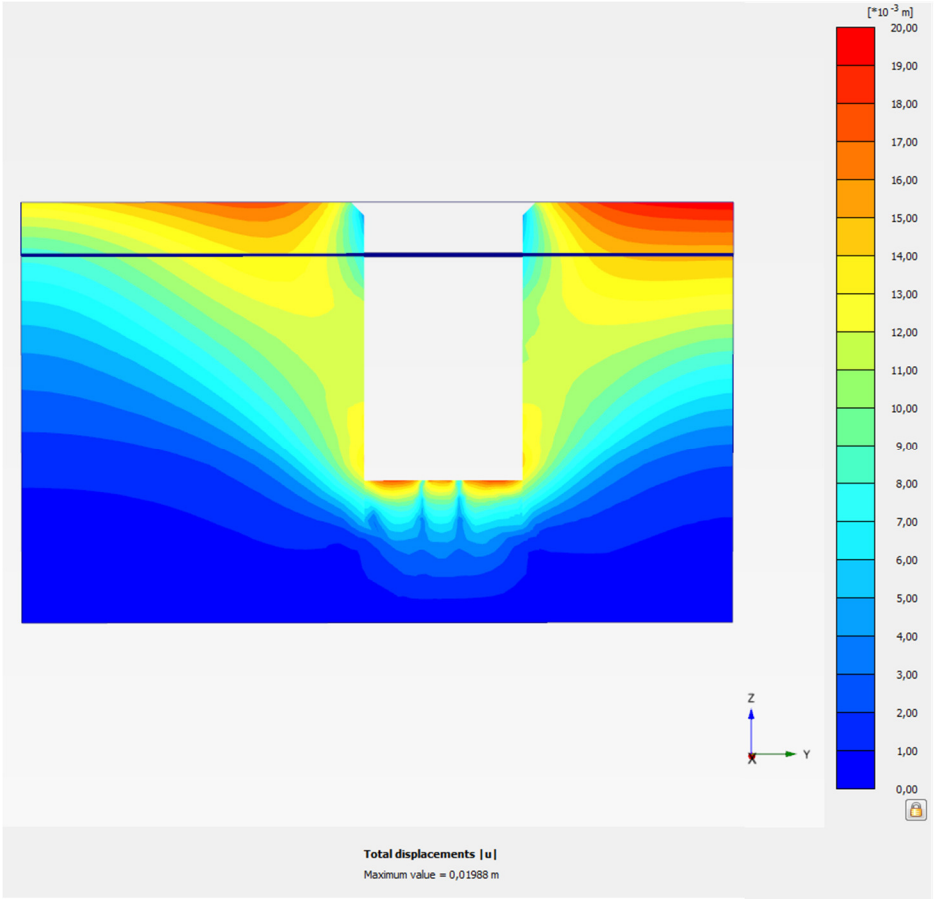

Figure 3.24. 3D Analysis Total Displacement Behavior

In Figure 3.25, total displacement vectors can be seen. It is clear that soil below the excavation tends to move upwards while soil alongside the excavation tends to move inwards.

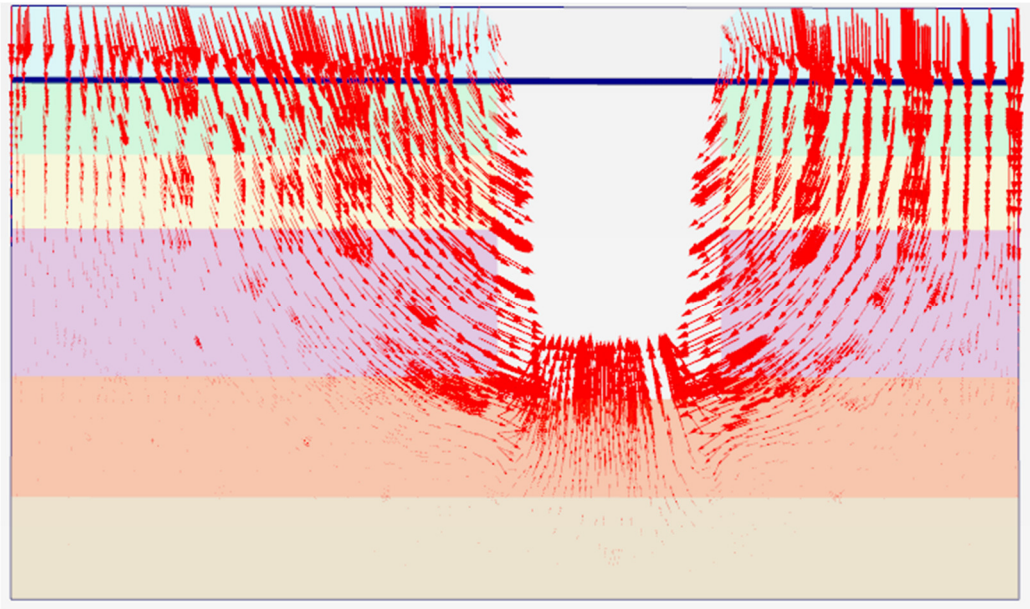

Figure 3.25. Total Displacement Vectors

In the modeling, K_0 (at rest) condition is selected for the initial condition.

In Figure 3.26 and Figure 3.27, water pressures at initial and final stages are presented. In both stages, water pressure values are same. Moreover, observed water pressure values in FEM analysis are similar with the theoretical hydrostatic water pressure values. Figure 3.28 shows the groundwater flow. It is obvious that groundwater flow does not occur.

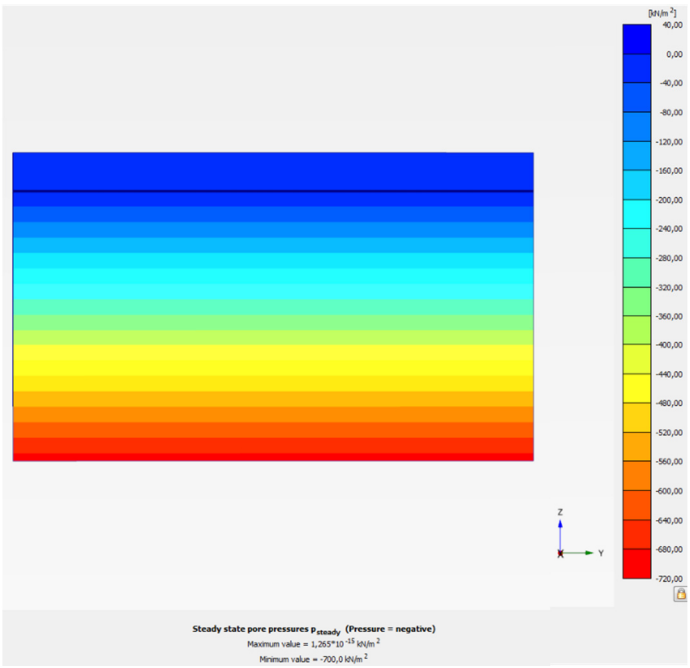

Figure 3.26. Water Pressures at the Initial Phase

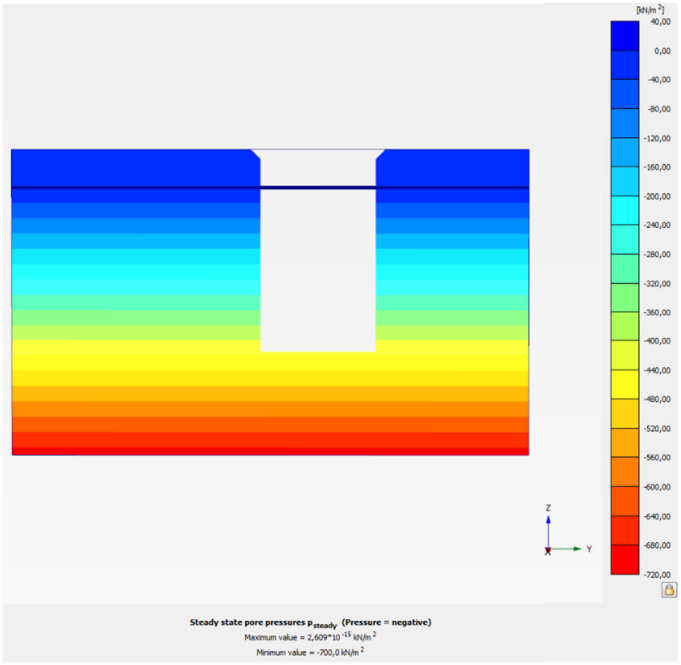

Figure 3.27. Water Pressures at the Final Phase

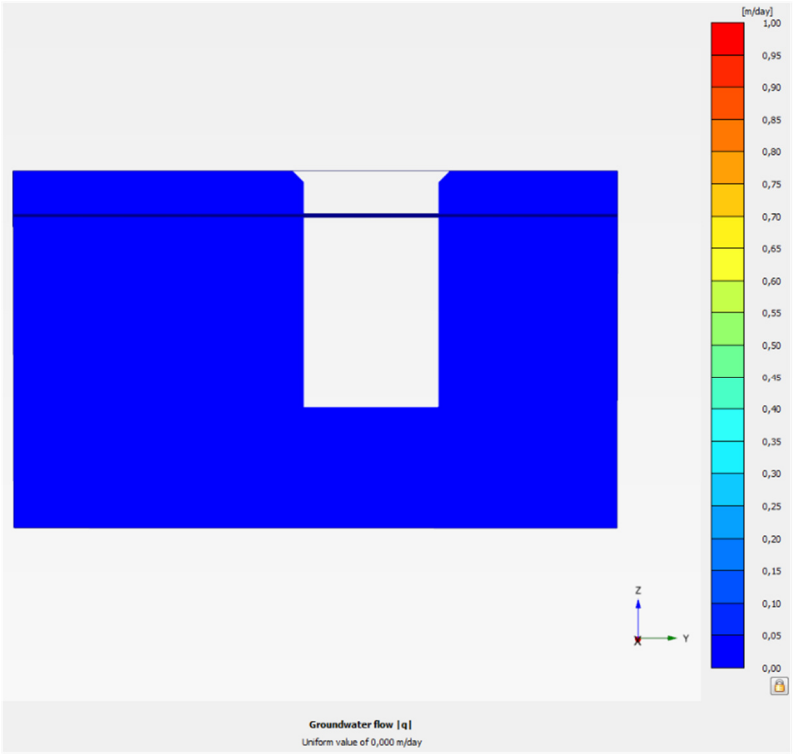

Figure 3.28. Groundwater Flow

CHAPTER 4

RESULTS AND COMPARISONS

4.1. Results

As it can be clearly seen from the Figure 3.15, soil profile at the excavation site consists of silty clay layers, moreover groundwater table takes place at 10 m depth from the ground surface. Deepest point of excavation is at the 54 m depth and the excavation pit is about 132 m x 31 m in plan view.

After the final excavation stage, maximum lateral displacements observed in Inclinometer 1, maximum lateral displacements calculated in 2D and 3D FEM analysis are listed below in Table 4.1:

Table 4.1. Maximum Lateral Displacements for Inclinometer Region 1

Inclinometer 1 Region	
Result Type	Maximum Lateral Displacement, δhmax (m)
Inclinometer	0,012
3D FEM	0,012
2D FEM	0,050

(δ_{hmax}/H) values for inclinometer reading and FEM results are listed below:

For Inclinometer 1: (δ_{hmax}/H) = (0,012/54) = 0.02%

For 3D FEM Result: (δ_{hmax}/H) = (0,012/54) = 0.02%

For 2D FEM Result: (δ_{hmax}/H) = (0,050/54) = 0.10%

After the final excavation stage, maximum lateral displacements observed in Inclinometer 2, maximum lateral displacements calculated in 2D and 3D FEM analysis are listed below in Table 4.2:

Table 4.2. Maximum Lateral Displacements for Inclinometer Region 2

Inclinometer 2 Region	
Result Type	**Maximum Lateral Displacement, δhmax (m)**
Inclinometer	0,013
3D FEM	0,017
2D FEM	0,050

(δ_{hmax}/H) values for inclinometer reading and FEM results are listed below:

For Inclinometer 2: (δ_{hmax}/H) = (0,013/54) = 0.02%

For 3D FEM Result: (δ_{hmax}/H) = (0,017/54) = 0.03%

For 2D FEM Result: (δ_{hmax}/H) = (0,050/54) = 0.10%

After the final excavation stage, maximum lateral displacements observed in Inclinometer 3, maximum lateral displacements calculated in 2D and 3D FEM analysis are listed below in Table 4.3:

Table 4.3. Maximum Lateral Displacements for Inclinometer Region 3

Inclinometer 3 Region	
Result Type	**Maximum Lateral Displacement, δhmax (m)**
Inclinometer	0,015
3D FEM	0,015
2D FEM	0,051

(δ_{hmax}/H) values for inclinometer reading and FEM results are listed below:

For Inclinometer 3: (δ_{hmax}/H) = (0,015/54) = 0.03%

For 3D FEM Result: (δ_{hmax}/H) = (0,015/54) = 0.03%

For 2D FEM Result: (δ_{hmax}/H) = (0,051/54) = 0.10%

Clough and O'Rourke (1990) conclude that, maximum lateral displacements are mostly 0.2% of H. Excavation depth H, for the studied excavation is 54 m.

The (δ_{hmax}/H) values for the excavation in all of the inclinometer regions are much smaller than the expectations of Clough and O'Rourke (1990). But in Figure 2.6, 0.02% and 0.10% values are also represented for diaphragm walls. Moreover, predictions concluded by Clough and O'Rourke are not for Top-Down excavations. Clough and O'Rourke also reveals that, decrease in spacing of supporting elements decrease the lateral wall deflection. Since the analyzed excavation is a Top-Down excavation and supports are mainly the slabs, no support spacing occurs, slabs create continuous supporting. In addition to slabs continuous support, the slabs also increase the total system stiffness. As Clough and O'Rourke emphasize, increase in total system stiffness, decrease the lateral movements. The authors also discover that, wall stiffness decreases the lateral displacements. The conventional Bottom-Up method uses the retaining structures only for excavation stages that means the retaining structures are temporary. Because of that reason the wall thickness and stiffness are relatively smaller than the wall thickness and stiffness used in Top-Down method. Hence, for a Top – Down excavation, it is expected to see smaller displacements than Clough and O'Rourke's suggestions.

Kung (2009) also pointed out that, the lateral movements are nearly the 0.2% of H. Kung's study is prepared for top-down excavations but also for the less stiff systems. In the Kung's study, wall thickness is 1.1 m, while the studied excavation in this thesis has 1.5 m wall thickness. Therefore, it is expected to get smaller displacement values than Kung's predictions.

In the study of Ran et al. (2011), a metro excavation in China in silty clay was inspected. Depth of excavation is approximately 35 m, and the diaphragm thickness is 0.8 m. The maximum displacement of that excavation is 0.025 m and the maximum lateral displacement over the excavation depth value is 0.07%. The 0.07% value is closer to the excavation studied in this thesis. The closer results explain the effect of wall stiffness, the depth of excavation and the excavation method.

For all the inclinometer regions, 2D FEM analyses give higher lateral displacement results as expected. Since the sizing of diaphragm walls and slabs are performed according to 2D FEM analysis results and the lateral displacements for 2D results are acceptable; the smaller lateral displacements for Inclinometers and 3D FEM results are inevitable. Moreover, for the designer's point of view, it is much safer to design with smaller displacements.

In addition to lateral displacements, as it can be clearly observed from the Figure 3.18 and Figure 3.24, total displacement results of 2D FEM analysis are approximately 3 times larger than the 3D FEM analysis.

4.2. Comparisons

For all the inclinometer regions, inclinometer readings, 2D FEM analysis displacement results and 3D FEM analysis displacement results are indicated in graphics. As stated before, excavation was completed in 10 stages and graphics are prepared for all the excavation stages.

In Figure 4.1, Figure 4.2 and Figure 4.3, lateral displacements of 3D FEM analysis, 2D FEM analysis and inclinometer measurements are compared for final excavation stage. As can be seen from the figures, it is obvious that displacement pattern of 3D and 2D analysis are similar. Moreover, results obtained from 3D analysis are approximately same as inclinometer measurements. On the other hand, 2D analysis results are between 3 and 4 times larger than inclinometer measurements. The reason for that is the plain strain modeling of 2D analysis. In plain strain models, uniform loading, uniform ground conditions and zero displacements in the side which is perpendicular to model are assumed. In addition, the structure is also assumed as uniform and the discontinuities are ignored.

Comparison graphics of excavation stages 1 to 9 for all the inclinometer regions can be seen in Appendix D. In the first stages, inclinometer readings are not consistent, in other words measurements show variety. The reason for this fluctuation is the continuation of construction and the very small displacement values in first stages.

Moreover, starting from the first excavation stage displacement pattern of 3D and 2D analysis are similar.

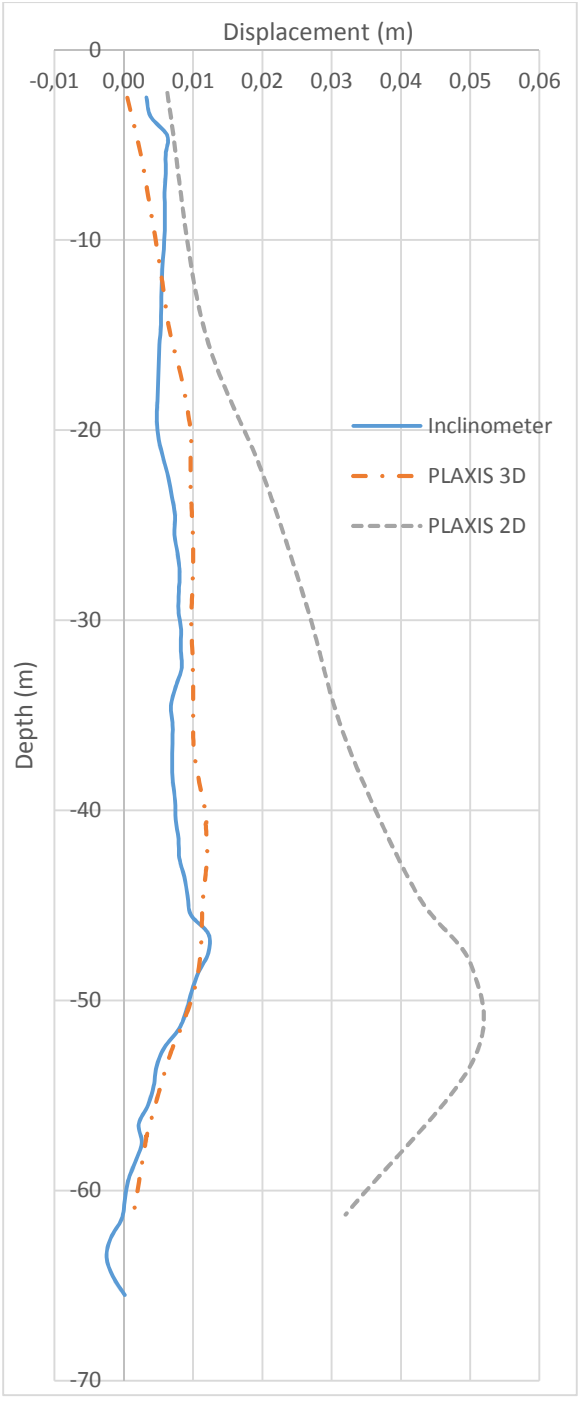

Figure 4.1. Comparison of Displacements for Final Stage (Inclinometer 1)

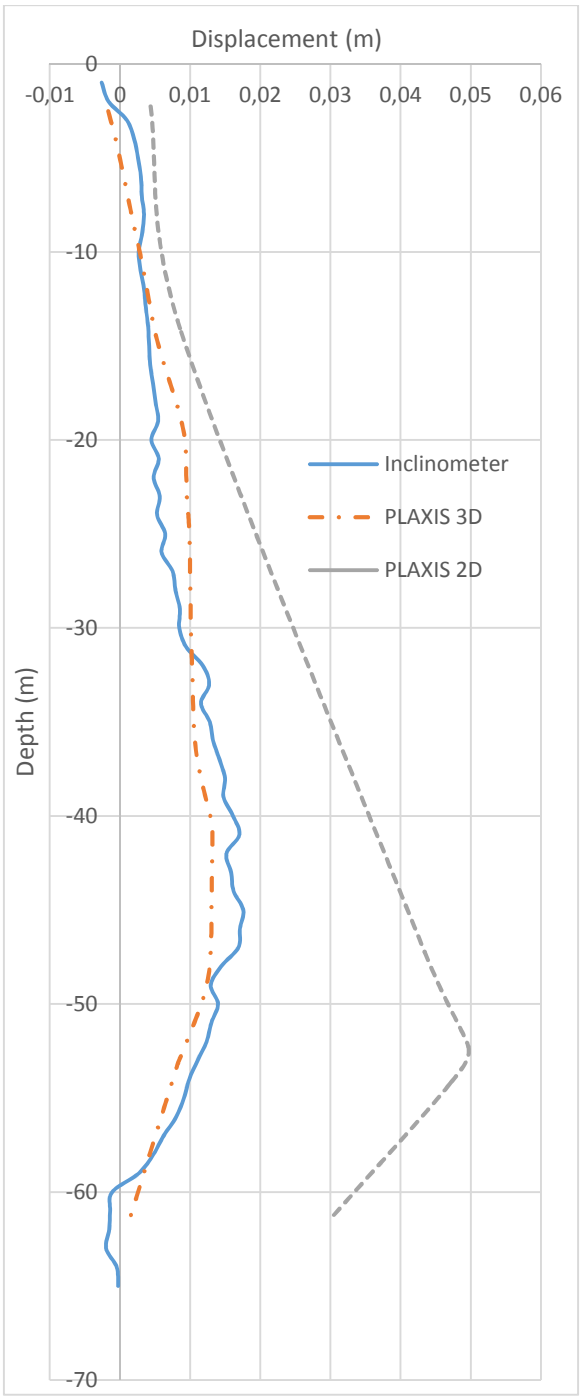

Figure 4.2. Comparison of Displacements for Final Stage (Inclinometer 2)

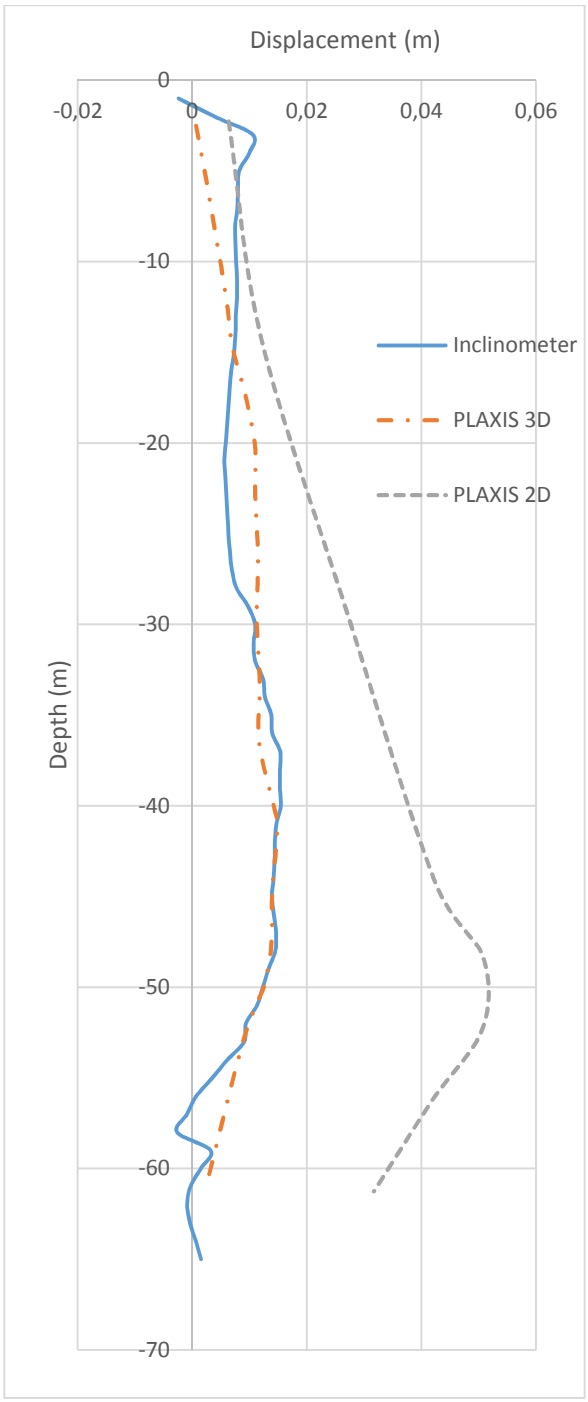

Figure 4.3. Comparison of Displacements for Final Stage (Inclinometer 3)

Summaries of the maximum lateral displacements for all inclinometer regions are tabulated below in Table 4.4, Table 4.5 and Table 4.6.

Table 4.4. Maximum Lateral Displacements Measured in Different Excavation Stages for Inclinometer 1 Region

	Maximum Lateral Wall Displacements (m)		
Stage	Inclinometer Reading	PLAXIS3D	PLAXIS2D
1	0,004	0,001	0,000
2	0,003	0,002	0,001
3	0,003	0,005	0,005
4	0,005	0,009	0,014
5	0,008	0,009	0,020
6	0,006	0,009	0,028
7	0,006	0,011	0,038
8	0,007	0,012	0,039
9	0,011	0,012	0,050
10	0,012	0,012	0,050

Table 4.5. Maximum Lateral Displacements Measured in Different Excavation Stages for Inclinometer 2 Region

	Maximum Lateral Wall Displacements (m)		
Stage	Inclinometer Reading	PLAXIS3D	PLAXIS2D
1	0,004	0,001	0,000
2	0,003	0,002	0,001
3	0,004	0,005	0,004
4	0,005	0,010	0,013
5	0,005	0,010	0,020
6	0,009	0,010	0,027
7	0,009	0,013	0,038
8	0,012	0,013	0,039
9	0,016	0,013	0,049
10	0,017	0,013	0,050

Table 4.6. Maximum Lateral Displacements Measured in Different Excavation Stages for Inclinometer 3 Region

	Maximum Lateral Wall Displacements (m)		
Stage	Inclinometer Reading	PLAXIS3D	PLAXIS2D
1	0,006	0,001	0,000
2	0,007	0,003	0,001
3	0,007	0,005	0,005
4	0,010	0,010	0,014
5	0,009	0,011	0,020
6	0,013	0,011	0,028
7	0,013	0,014	0,039
8	0,014	0,015	0,040
9	0,013	0,015	0,050
10	0,015	0,015	0,051

In Appendix E, displacement versus depth graphs are prepared for 3 inclinometers separately. In the graphs, inclinometer readings are shown for all stages.

4.2.1. Summary of Comparisons

As it can be clearly seen from the graphics, 2D FEM analysis results are on the safe side and that results are approximately between three and four times larger than the real displacements. Table 4.7, Table 4.8 and Table 4.9 show the ratio of maximum lateral displacements obtained from FEM analysis to maximum lateral displacements measured in inclinometers for each stage.

Table 4.7. FEM Results / Inclinometer Measurements for Inclinometer 1 Region

	Inclinometer 1 Region									
	Stage 1	Stage 2	Stage 3	Stage 4	Stage 5	Stage 6	Stage 7	Stage 8	Stage 9	Stage 10
2D FEM Results / Inclinometer Measurements	0,00	0,50	1,59	2,69	2,47	4,26	6,71	5,59	4,72	4,11
3D FEM Results / Inclinometer Measurements	0,26	0,86	1,60	1,73	1,11	1,44	1,95	1,67	1,13	0,98

Table 4.8. FEM Results / Inclinometer Measurements for Inclinometer 2 Region

	Inclinometer 2 Region									
	Stage 1	Stage 2	Stage 3	Stage 4	Stage 5	Stage 6	Stage 7	Stage 8	Stage 9	Stage 10
2D FEM Results / Inclinometer Measurements	0,03	0,39	1,05	2,40	3,84	3,14	4,09	3,19	3,09	2,92
3D FEM Results / Inclinometer Measurements	0,23	0,70	1,18	1,75	1,94	1,19	1,39	1,08	0,83	0,77

Table 4.9. FEM Results / Inclinometer Measurements for Inclinometer 3 Region

	Inclinometer 3 Region									
	Stage 1	Stage 2	Stage 3	Stage 4	Stage 5	Stage 6	Stage 7	Stage 8	Stage 9	Stage 10
2D FEM Results / Inclinometer Measurements	0,02	0,18	0,64	1,37	2,24	2,19	2,95	2,94	3,83	3,28
3D FEM Results / Inclinometer Measurements	0,16	0,37	0,71	1,01	1,18	0,88	1,09	1,09	1,13	0,95

As results indicate, actual displacements (inclinometer readings) are smaller in inclinometer 1, which was located in the middle of the short edge of the excavation; and larger in inclinometer 3, which was located in the middle of the long edge of the excavation. Actual displacements in Inclinometer 2 is in between the results of Inclinometer 1 and Inclinometer 3. Actual displacements show that, in the short edge of a rectangular excavation, smaller displacements occur, moreover in the middle of the long edges larger displacements occur and as getting closer to the corners, displacements are getting smaller.

According to the results of 2D FEM analysis results, it is obvious that, displacements values are not far from each other. Moreover, the results for each of the 3 models, displacement values are very close. Since, the only difference in 2D models is the surcharge loads, it is obvious that, little differences in surcharge loads of the existing structures do not affect excavation so much.

3D FEM analysis results also show that, displacements in the short edge of the excavation are smaller than the displacements measured in the long edge of the excavation.

CHAPTER 5

CONCLUSION

As a result of the comparison of inclinometer measurements, 2D FEM analysis and 3D FEM analysis of Bağcılar Metro Station, following results are obtained:

1. 2D Analysis are on the very safe side. Lateral displacements of 2D analysis are between 3 and 4 times larger than the field measurements and 3D FEM analysis results.
2. As Table 4.7, Table 4.8 and Table 4.9 indicate, field measurements (inclinometer readings) and 3D FEM analysis results are very close to each other.
3. 2D FEM analysis displacements and 3D FEM analysis displacements have same displacement pattern.
4. For deep excavations, it is safer to design according to 2D FEM analysis. 3D FEM analysis results are very close to real values. If the designs are performed according to 3D FEM analysis, results or inputs of the models shall be multiplied by a factor of safety between 3 and 4.

5. Displacements in the short edge of a rectangular excavation are smaller than the displacements in the long edge of the excavation. In the corners, displacement values are getting smaller.

6. Studies that prepared according to Bottom - Up method do not represent the displacement ratios of the Top - Down excavations. Due to the stiffer supporting elements, ratio of lateral displacements to the excavation depth is smaller than expected in literature review.

7. Total displacement values of 2D FEM analysis are approximately 3 times greater than total displacement values of 3D FEM analysis.

REFERENCES

Bose, S.K., and Som, N.N., "Parametric Study of a Braced Cut by Finite Element Method", *Computers and Geotechnics*, Vol. 22, No. 2, pp. 91-107, 1998.

Bowles, J.E., Foundation Analysis and Design, McGraw-Hill Book Company, New York, 1988.

Carter, M., and Bentley, S.P., Correlations of Soil Properties, Pentech, 1991.

Clough, G.W., and O'Rourke, T.D., "Construction Induced Movements of Insitu Walls", *Design and Performance of Earth Retaining Structures*, ASCE, pp. 439-470, 1990.

Duncan, J.M., and Chang, C.Y., "Nonlinear Analysis of Stress and Strain in Soils", *Journal of the Soil Mechanics and Foundations Division*, Vol. 96, No. 5, pp. 1629-1653, 1970.

Hemsley, J.A., Design Applications of Raft Foundations, Thomas Telford Publishing, London, 2000.

Jin, B., Zhao, H., and Liu, Y., "A Practical Method for the Construction of the Supporting System of Covered Excavation of Metro Station", *Key Engineering Materials*, Vol. 574, pp. 151-161, 2014.

Kung, G.T.C., "Comparison of excavation-induced wall deflection using top-down and bottom-up construction methods in Taipei silty clay", *Computers and Geotechnics*, Vol. 36, pp. 373–385, 2009.

Lin, H.D., and Wang, C.C., "Stress-Strain-Time Function of Clay", *Journal of Geotechnical and Geoenvironmental Engineering*, Vol. 124, No. 4, pp. 289–296, 1998.

Lu, Y., and Tan, Y., "Top-down Excavation of a Metro Station in Soft Clay", *Advanced Materials Research*, Vols. 368-373, pp. 2866-2869, 2012.

Mana, I.A., and Clough, G.W., "Predictions of movements for braced cuts in clay", *Journal of the Geotechnical Engineering Division*, ASCE, Vol. 107, No. GT6, pp. 759-777, 1981.

Mesri, G., and Abdel-Ghaffar, M.E.M., "Cohesion Intercept in Effective Stress-Stability Analysis", *Journal of the Geotechnical Engineering Division*, ASCE Vol.119, No.8, 1993.

Pakbaz, S., Imanzadeh, S., and Bagherinia, K.H., "Characteristics of diaphragm wall lateral deformations and ground surface settlements: Case study in Iran-Ahwaz metro", *Tunnelling and Underground Space Technology*, Vol. 35, pp. 109–121, 2013.

Peck, R.B., "Deep Excavations and Tunneling in Soft Ground", *Proceedings, Seventh I.C.S.M.F.E.,* State of Art Volume, Mexico, pp. 225-290, 1969.

PLAXIS 2D Reference Manual, Retrieved from http://www.plaxis.nl/files/files/2D-2-Reference.pdf, 2015. [Last accessed on 28.04.2015]

PLAXIS 3D Reference Manual, Retrieved from http://www.plaxis.nl/files/files/3D-2-Reference.pdf, 2015. [Last accessed on 28.04.2015]

Qing – Yuan, L., "Monitoring of Deformation Laws of Deep Excavation in Metro Station", *Applied Mechanics and Materials*, Vols. 99-100, pp. 1141-1145, 2011.

Ran, L., Ye, W., and Zhu, H., "Long - Term Monitoring and Safety Evaluation of a Metro Station during Deep Excavation", *Twelfth East Asia-Pacific Conference on Structural Engineering and Construction*, 2011.

Stroud, M.A., "The Standard Penetration Test in Sensitive Clays and Soft Rocks", *Proceedings, European Symposium on Penetration Testing*, Vol. 2.2, Stockholm, Sweden, pp. 367-375, 1974.

Tan, Y., and Li, M., “Measured Performance of a 26 m Deep Top-Down Excavation in Downtown Shanghai”, *Canadian Geotechnical Journal*, Vol. 48, No. 5, pp. 704-719, 2011.

Yüksel Proje Uluslararası A.Ş., “Bağcılar İstasyonu Zemin Koşulları Değerlendirme Raporu”, 2007.

APPENDIX A

CONSTRUCTION PROGRESSION DATES

Table below (Table A.1) shows the inclinometer reading dates of each excavation stages.

Table A.1. Excavation Stages and Inclinometer Reading Dates

Excavation Stage	Inclinometer Reading Date
1	13.04.12
2	02.05.12
3	18.05.12
4	08.06.12
5	26.06.12
6	24.07.12
7	28.08.12
8	09.10.12
9	20.11.12
10	22.12.12

The figure below (Figure A.1) shows the progress of construction. In this figure, the dates above the slabs show the completion time of each piece.

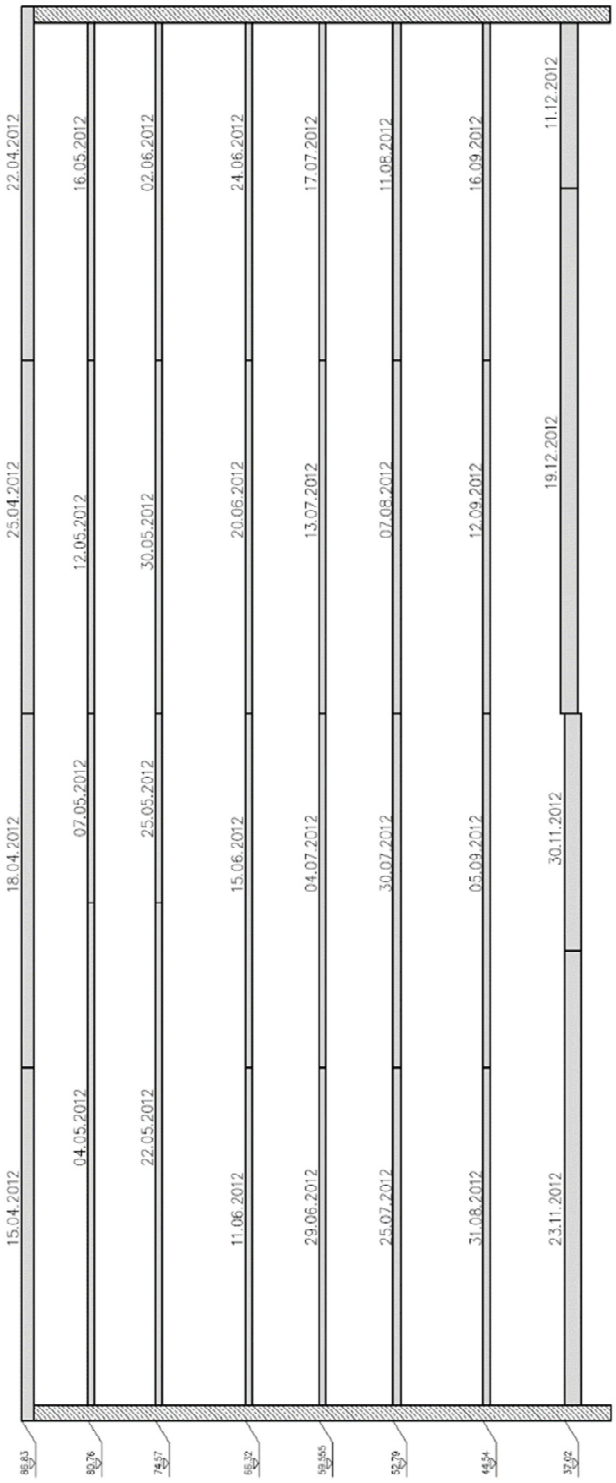

Figure A.1. Progression Dates of Construction

APPENDIX B

SOIL INVESTIGATION TEST RESULTS

The following tables (Table B.1 to Table B.4) that indicate the soil investigation test results were taken from the report of Yüksel Proje Uluslararası A.Ş., 2007.

Table B.1. Soil Investigation Test Results of Borehole YS 02

Borehole No	Depth (m)	LL	PL	PI	+No 4	-No 200	Soil Class
YS 02	6.00 – 6.45	36	19	17	0	95	CL
YS 02	9.00 – 9.45	35	18	17	5	85	CL
YS 02	11.00 – 11.45	36	19	17	16	50	CL
YS 02	19.50 – 19.95	35	20	15	0	93	CL
YS 02	21.00 – 21.45	37	20	17	0	93	CL
YS 02	24.00 – 24.05	35	19	16	2	80	CL
YS 02	28.50 – 28.95	40	19	21	0	86	CL
YS 02	32.50 – 33.00	64	29	35			CH - MH
YS 02	37.50 – 37.95	57	30	27			CH - MH
YS 02	39.00 – 39.45	45	22	23	0	90	CL
YS 02	43.50 – 43.75	35	21	14	0	19	CL
YS 02	48.00 – 48.05	36	22	14	0	93	CL
YS 02	49.50 – 49.95				2	62	
YS 02	54.00 – 54.25	44	21	23	0	83	CL
YS 02	58.50 – 58.70	48	21	27	0	98	CL
YS 02	61.50 – 61.75	40	21	19	41	51	CL
YS 02	63.00 – 63.40				0	57	

Table B.2. Soil Investigation Test Results of Borehole YS 03

Borehole No	Depth (m)	LL	PL	PI	+No 4	-No 200	Soil Class
YS 03	3.00 – 3.45	36	20	16	0	98	CL
YS 03	6.00 – 6.45	35	25	10	2	68	CL
YS 03	16.50 – 16.95	48	22	26	0	90	CL
YS 03	19.50 – 19.95	48	23	25	0	87	CL
YS 03	25.50 – 25.95	35	22	13	1	34	SC
YS 03	30.00 – 30.45	40	19	21	0	85	CL
YS 03	36.00 – 36.45	39	21	18	0	80	CL
YS 03	42.00 – 42.45	44	21	23	3	90	CL
YS 03	45.00 – 45.45	49	24	25			CL
YS 03	52.50 – 52.95	37	21	16	0	75	CL
YS 03	60.00 – 60.45	46	21	25	0	34	SC

Table B.3. Soil Investigation Test Results of Borehole YS 04

Borehole No	Depth (m)	LL	PL	PI	+No 4	-No 200	Soil Class
YS 04	6.00 – 6.45	46	27	19	5	77	CL
YS 04	12.00 – 12.45	28	17	11	0	9	SP-SM
YS 04	19.50 – 19.45	34	22	12	0	75	CL
YS 04	21.00 – 21.45	42	20	22	0	90	CL
YS 04	25.50 – 25.95	41	19	22	0	36	SC
YS 04	30.00 – 30.45	45	19	26	0	91	CL
YS 04	31.50 – 31.95	81	38	43			MH-CH
YS 04	33.00 – 33.45	32	20	12	2	75	CL
YS 04	40.50 – 40.95	39	21	18	0	50	CL
YS 04	42.00 – 42.10	42	22	20	0	87	CL
YS 04	43.50 – 43.95	52	28	24			CH
YS 04	46.50 – 46.75	77	33	44			CH
YS 04	48.00 – 48.10	44	22	22	0	66	CL
YS 04	52.50 – 52.95	37	19	18	1	83	CL
YS 04	57.00 – 57.45	36	14	22	0	72	CL
YS 04	58.50 – 58.95	41	20	21	0	85	CL
YS 04	63.00 – 63.45		NP		0	98	ML
YS 04	64.50 – 64.90	28	18	10	0	80	CL

Table B.4. Soil Investigation Test Results of Borehole YS 03 A

Borehole No	Depth (m)	LL	PL	PI	+No 4	-No 200	Soil Class
YS 03 A	1.50 – 1.95	49	23	26			CL
YS 03 A	4.50 – 4.95	35	21	14	0	54	CL
YS 03 A	3.00 – 3.45	53	23	30			CH
YS 03 A	6.00 – 6.35	32	22	10	0	38	CL
YS 03 A	9.00 – 9.45	33	21	12	0	52	CL-ML
YS 03 A	10.50 – 10.95	48	25	23			CL
YS 03 A	12.00 – 12.45	41	22	19			CL
YS 03 A	13.50 – 13.95	45	22	23			CL
YS 03 A	15.00 – 15.45	24				18	SM
YS 03 A	16.50 – 16.95	23			0	10	SM
YS 03 A	18.00 – 18.95	21			0	6	SM
YS 03 A	19.50 – 19.95	22			0	14	SM
YS 03 A	21.00 – 21.45	63	34	29			MH
YS 03 A	22.50 – 22.95	60	34	26			MH
YS 03 A	24.00 – 24.45	53	31	22			MH
YS 03 A	25.50 – 25.95	60	34	26			MH
YS 03 A	27.00 – 27.45	61	35	26			MH
YS 03 A	28.50 – 28.95	52	30	22			MH
YS 03 A	30.00 – 30.45	56	31	25			MH
YS 03 A	31.00 – 31.45	57	30	27			MH
YS 03 A	34.50 – 34.52	60	33	27			MH
YS 03 A	37.50 – 37.95	64	36	28			MH
YS 03 A	42.00 – 42.95	62	35	27			MH
YS 03 A	45.00 – 45.45	59	33	26			MH
YS 03 A	46.50 – 46.95	61	32	29			MH
YS 03 A	48.00 – 48.45	65	36	29			MH
YS 03 A	49.50 – 49.95	60	33	27			MH
YS 03 A	51.00 – 51.45	63	36	27			MH
YS 03 A	52.50 – 52.95	25					SM
YS 03 A	55.00 – 55.45	24					SM
YS 03 A	58.00 – 58.24	23					SM
YS 03 A	60.00 – 60.37	24					SM

APPENDIX C

TYPICAL INCLINOMETER READING DATA

The data in the following pages is a typical inclinometer measurement result and it was taken from the Bağcılar Station contractor documents.

Site : BAGCILAR Casing : BINK-2

Measur. Nr. : 054 Measur. Date : 22/12/2012

Place : BAGCILAR ISTASYONU

Displacement from measur. Nr. 000 - From bottom

Metres	Incr. Displ. EAST Dir [mm]	Incr. Displ. NORTH Dir [mm]	Cumul. Displ. EAST Dir [mm]	Cumul. Displ. NORTH Dir [mm]	Cumul. Val. Displacem. [mm]	Cumul. Val. Azimuth [degr.]
1,0	-0,05	0,83	11,15	4,15	11,90	20,42
2,0	0,53	2,62	11,20	3,32	11,68	16,53
3,0	0,05	1,02	10,67	0,70	10,70	3,75
4,0	0,00	0,45	10,62	-0,32	10,63	358,25
5,0	-0,05	0,42	10,62	-0,77	10,65	355,83
6,0	-0,08	0,10	10,67	-1,20	10,74	353,59
7,0	-0,05	0,48	10,75	-1,30	10,83	353,10
8,0	0,07	-0,17	10,80	-1,77	10,94	350,67
9,0	-0,20	-0,50	10,72	-1,60	10,84	351,52
10,0	-0,12	0,28	10,92	-1,10	10,98	354,25
11,0	0,20	0,70	11,05	-1,37	11,14	352,91
12,0	-0,15	0,25	10,85	-2,07	11,05	349,17
13,0	0,02	0,33	11,00	-2,32	11,24	348,07
14,0	0,07	0,03	10,97	-2,65	11,29	346,43
15,0	-0,03	0,18	10,90	-2,67	11,22	346,21
16,0	0,00	0,37	10,93	-2,85	11,29	345,38
17,0	-0,23	0,37	10,93	-3,22	11,39	343,55
18,0	-0,58	0,52	11,15	-3,60	11,72	342,11
19,0	-2,13	-0,95	11,73	-4,12	12,43	340,62
20,0	1,42	1,05	13,85	-3,17	14,21	347,09
21,0	-0,32	-0,73	12,43	-4,22	13,12	341,22
22,0	0,15	0,88	12,75	-3,50	13,22	344,65
23,0	0,65	-0,38	12,60	-4,37	13,34	340,85
24,0	2,05	1,15	11,95	-4,00	12,60	341,49
25,0	0,05	-0,60	9,90	-5,15	11,16	332,52
26,0	0,20	1,47	9,85	-4,55	10,85	335,21
27,0	0,38	0,40	9,65	-6,02	11,38	328,02
28,0	0,45	0,62	9,27	-6,42	11,28	325,29

Site : BAGCILAR Casing : BINK-2

Measur. Nr. : 054 Measur. Date : 22/12/2012

Place : BAGCILAR ISTASYONU

Displacement from measur. Nr. 000 - From bottom

Metres	Incr. Displ. EAST Dir [mm]	Incr. Displ. NORTH Dir [mm]	Cumul. Displ. EAST Dir [mm]	Cumul. Displ. NORTH Dir [mm]	Cumul. Val. Displacem. [mm]	Cumul. Val. Azimuth [degr.]
29,0	0,03	-0,08	8,82	-7,05	11,30	321,38
30,0	0,57	0,95	8,80	-6,97	11,23	321,60
31,0	-0,12	2,38	8,22	-7,92	11,42	316,06
32,0	-0,22	0,77	8,35	-10,30	13,26	309,03
33,0	-0,47	-1,18	8,57	-11,07	14,01	307,75
34,0	0,48	1,33	9,05	-9,90	13,41	312,43
35,0	0,48	0,47	8,57	-11,22	14,13	307,38
36,0	0,03	1,12	8,10	-11,70	14,23	304,70
37,0	-0,15	0,77	8,07	-12,82	15,16	302,20
38,0	-0,05	-0,20	8,22	-13,60	15,89	301,16
39,0	0,13	1,43	8,27	-13,40	15,75	301,70
40,0	0,47	0,90	8,15	-14,82	16,92	298,80
41,0	0,42	-1,85	7,67	-15,72	17,50	296,02
42,0	0,30	0,85	7,25	-13,87	15,65	297,59
43,0	0,57	0,50	6,95	-14,73	16,28	295,27
44,0	-0,50	1,38	6,37	-15,23	16,51	292,72
45,0	0,73	-0,48	6,87	-16,60	17,97	292,50
46,0	0,65	0,10	6,15	-16,13	17,26	290,88
47,0	-0,85	-2,45	5,50	-16,23	17,13	288,73
48,0	1,40	-1,48	6,35	-13,78	15,17	294,75
49,0	-0,35	1,03	4,95	-12,30	13,26	291,92
50,0	1,13	-0,95	5,30	-13,33	14,34	291,69
51,0	-0,43	-0,67	4,17	-12,38	13,06	288,64
52,0	1,13	-1,28	4,60	-11,70	12,57	291,46
53,0	1,23	-1,05	3,47	-10,43	10,99	288,43
54,0	0,07	-0,75	2,25	-9,37	9,64	283,50
55,0	-0,45	-1,00	2,17	-8,63	8,90	284,15
56,0	0,57	-1,78	2,62	-7,63	8,06	289,00

Site : BAGCILAR Casing : BINK-2

Measur. Nr. : 054 Measur. Date : 22/12/2012

Place : BAGCILAR ISTASYONU

Displacement from measur. Nr. 000 - From bottom

Metres	Incr. Displ. EAST Dir [mm]	Incr. Displ. NORTH Dir [mm]	Cumul. Displ. EAST Dir [mm]	Cumul. Displ. NORTH Dir [mm]	Cumul. Val. Displacem. [mm]	Cumul. Val. Azimuth [degr.]
57,0	2,58	-1,38	2,05	-5,85	6,20	289,31
58,0	0,50	-1,98	-0,53	-4,47	4,51	263,31
59,0	0,92	-3,80	-1,03	-2,50	2,70	247,71
60,0	-0,60	-0,22	-1,95	1,30	2,34	146,31
61,0	0,30	-0,13	-1,35	1,52	2,04	131,52
62,0	0,97	-0,45	-1,65	1,65	2,33	135,00
63,0	-1,35	1,57	-2,63	2,10	3,36	141,34
64,0	-1,33	0,25	-1,28	0,53	1,38	157,62
65,0	0,05	0,28	0,05	0,28	0,28	79,69

APPENDIX D

COMPARISON GRAPHICS

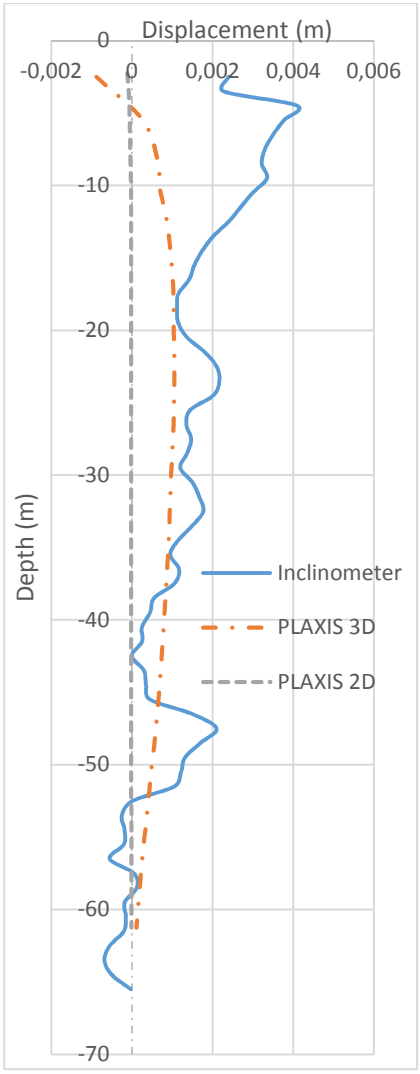

Figure D.1. Comparison of Displacements for Excavation Stage 1 (Inclinometer 1 Region)

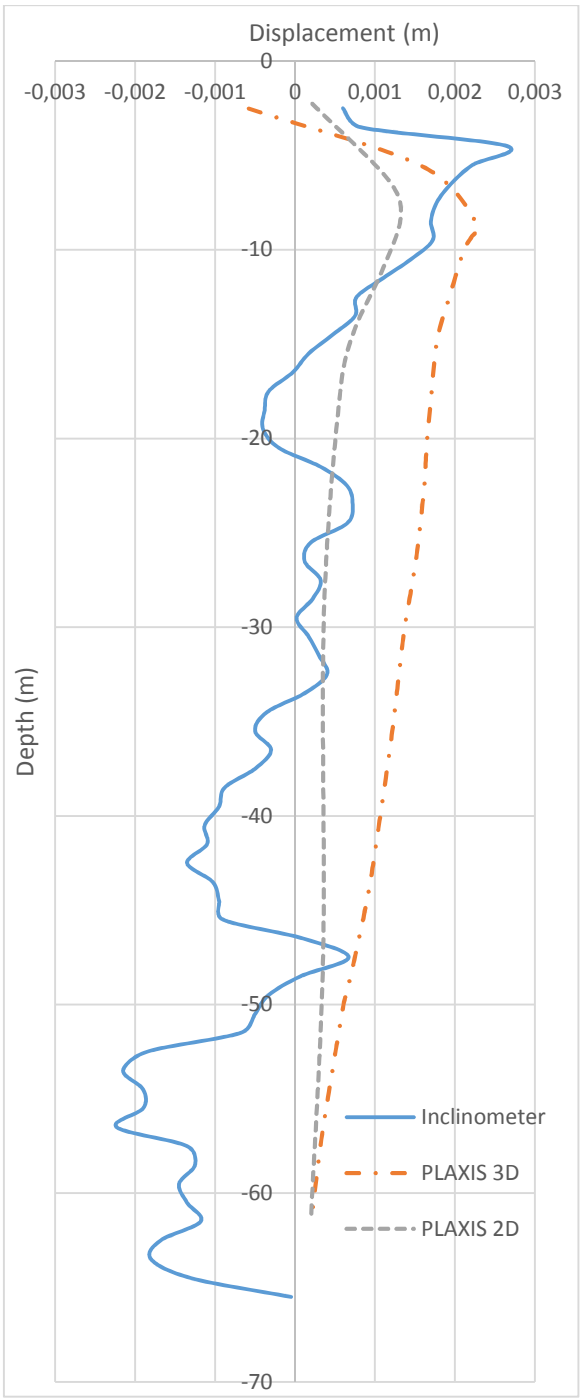

Figure D.2. Comparison of Displacements for Excavation Stage 2 (Inclinometer 1 Region)

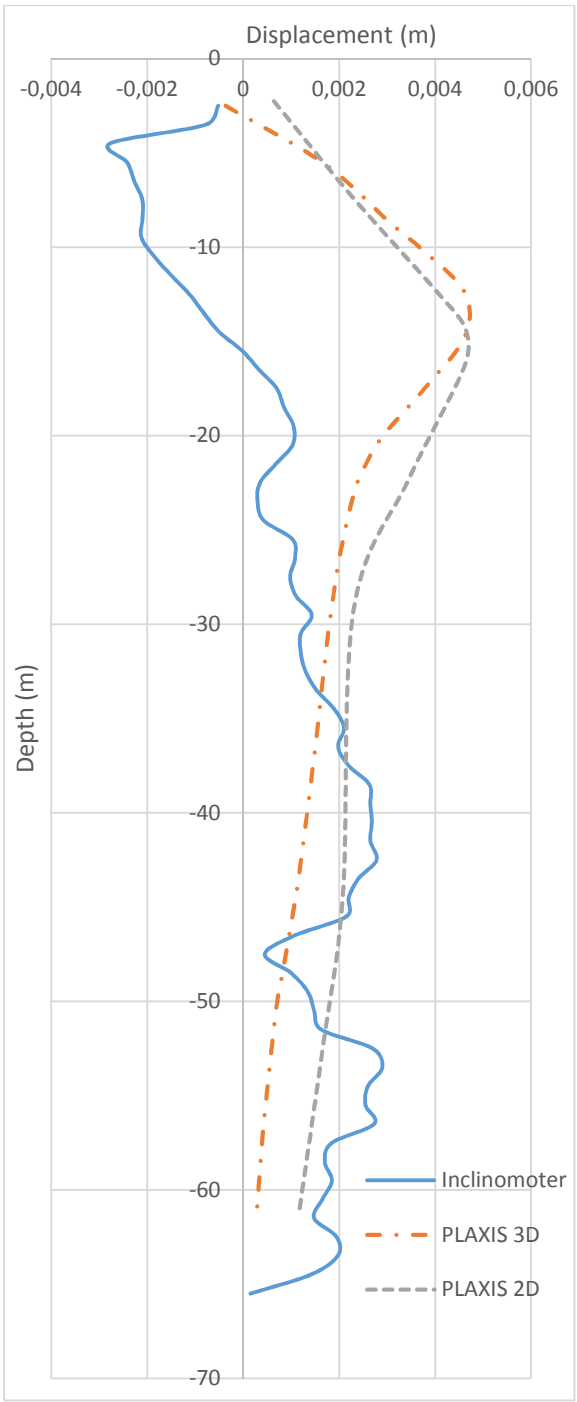

Figure D.3. Comparison of Displacements for Excavation Stage 3 (Inclinometer 1 Region)

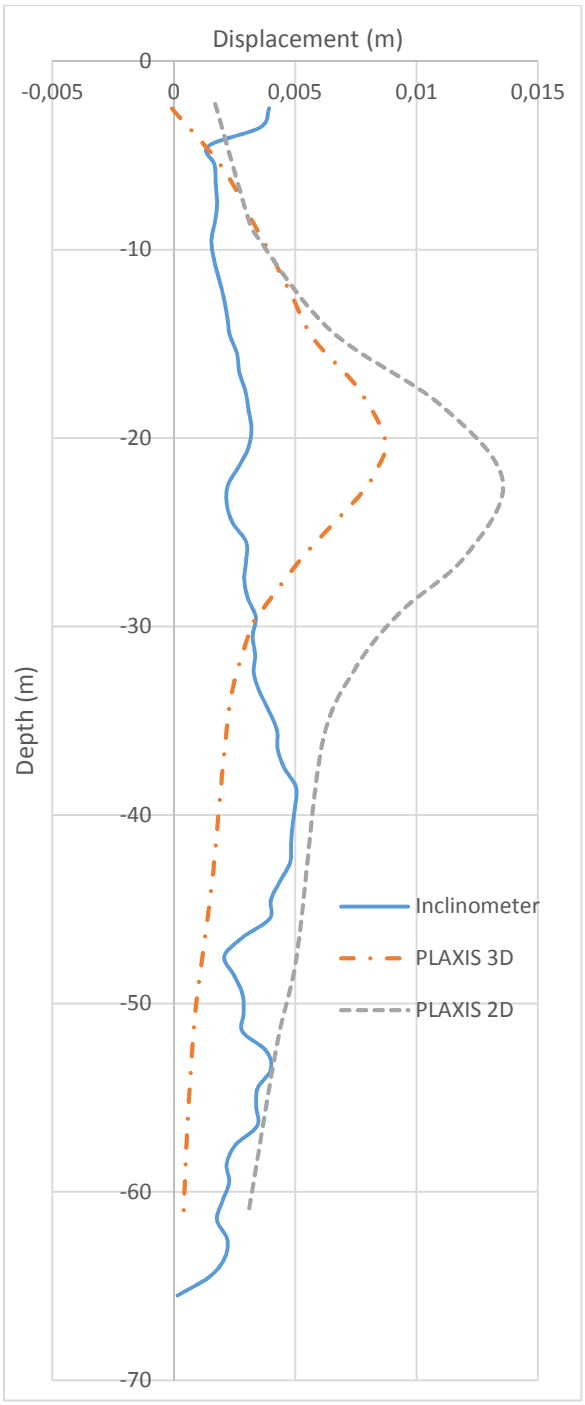

Figure D.4. Comparison of Displacements for Excavation Stage 4 (Inclinometer 1 Region)

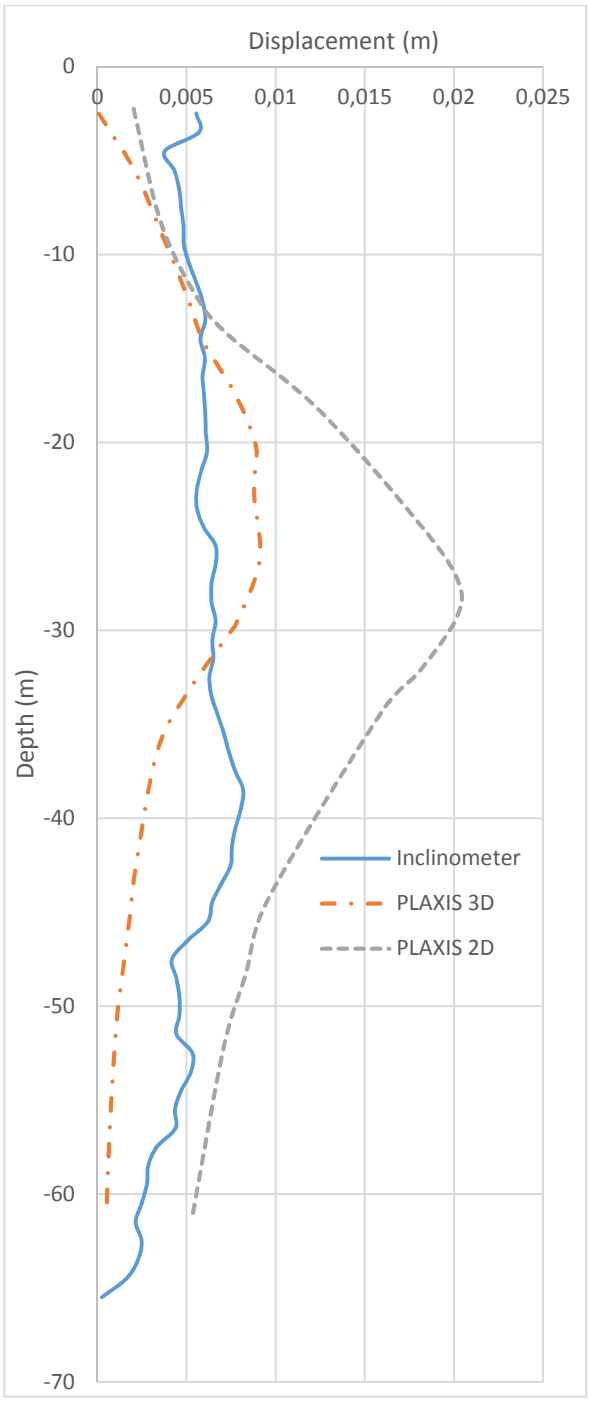

Figure D.5. Comparison of Displacements for Excavation Stage 5 (Inclinometer 1 Region)

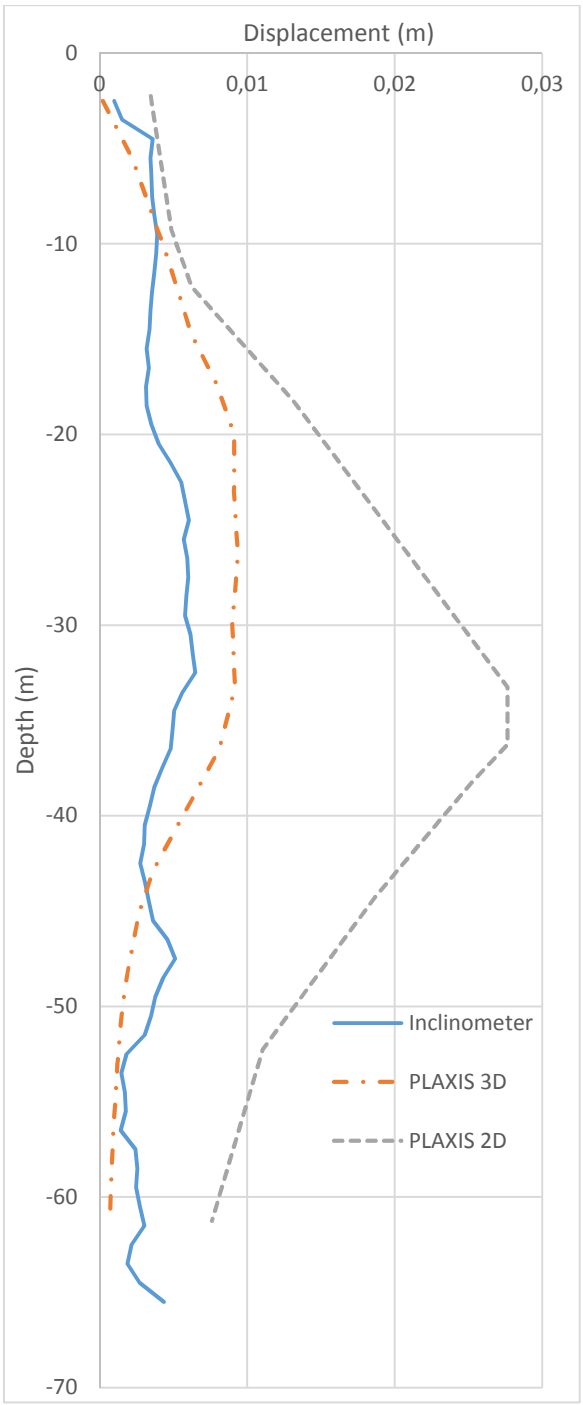

Figure D.6. Comparison of Displacements for Excavation Stage 6 (Inclinometer 1 Region)

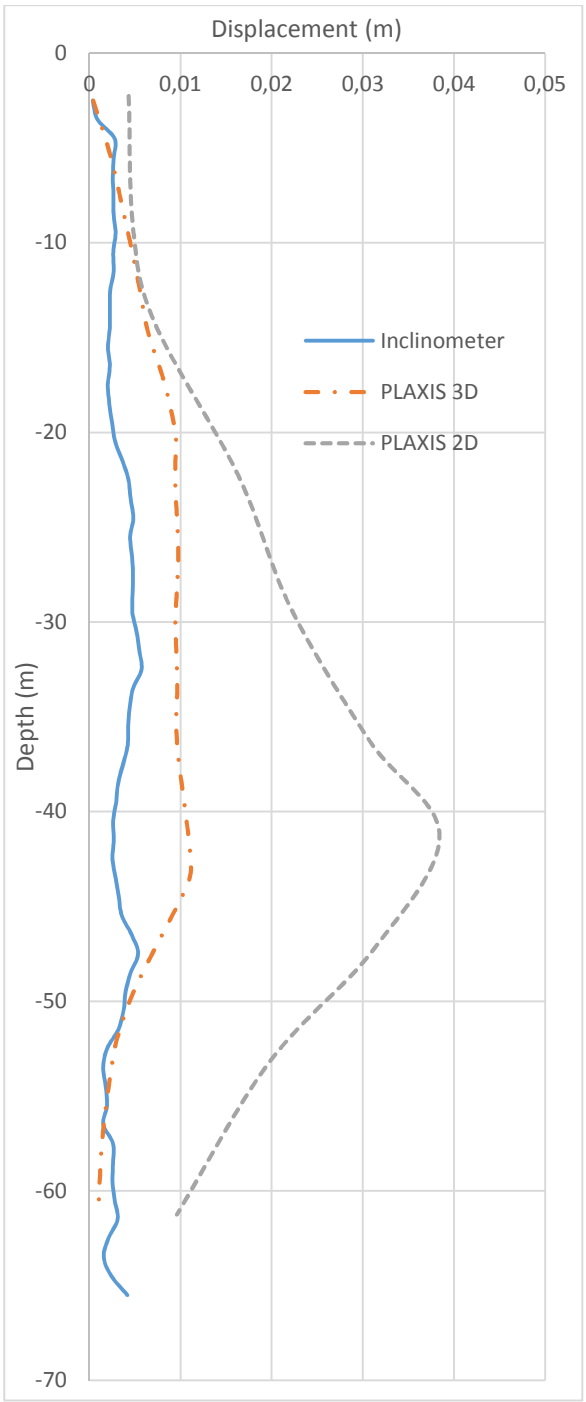

Figure D.7. Comparison of Displacements for Excavation Stage 7 (Inclinometer 1 Region)

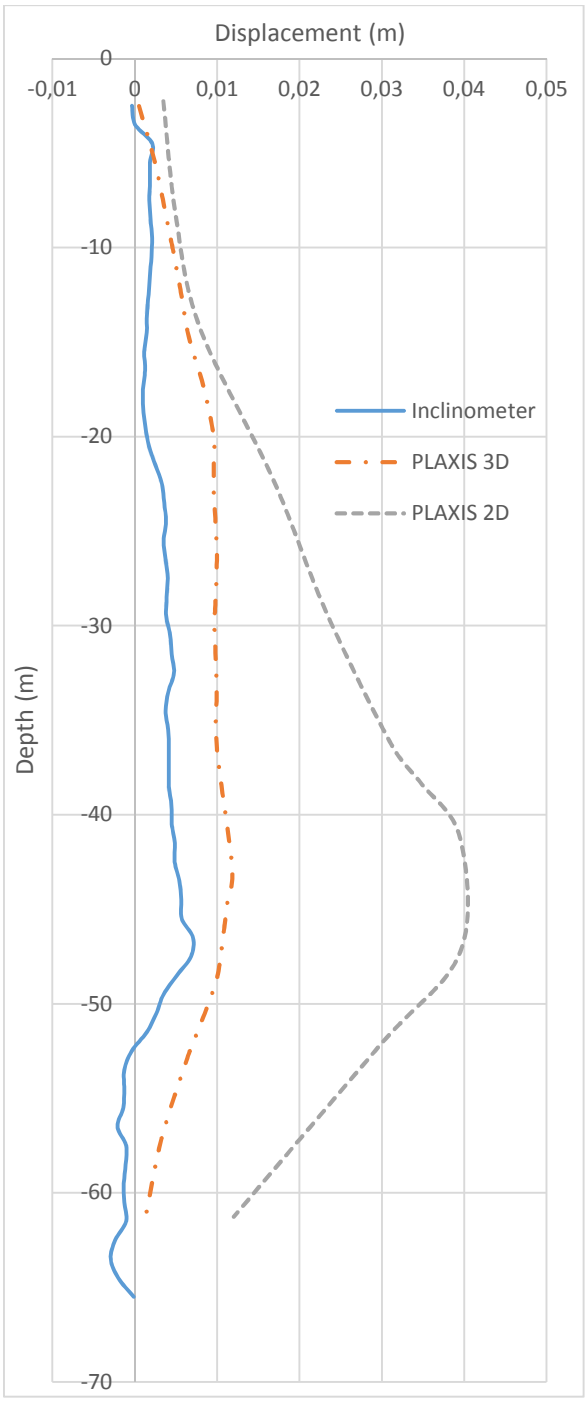

Figure D.8. Comparison of Displacements for Excavation Stage 8 (Inclinometer 1 Region)

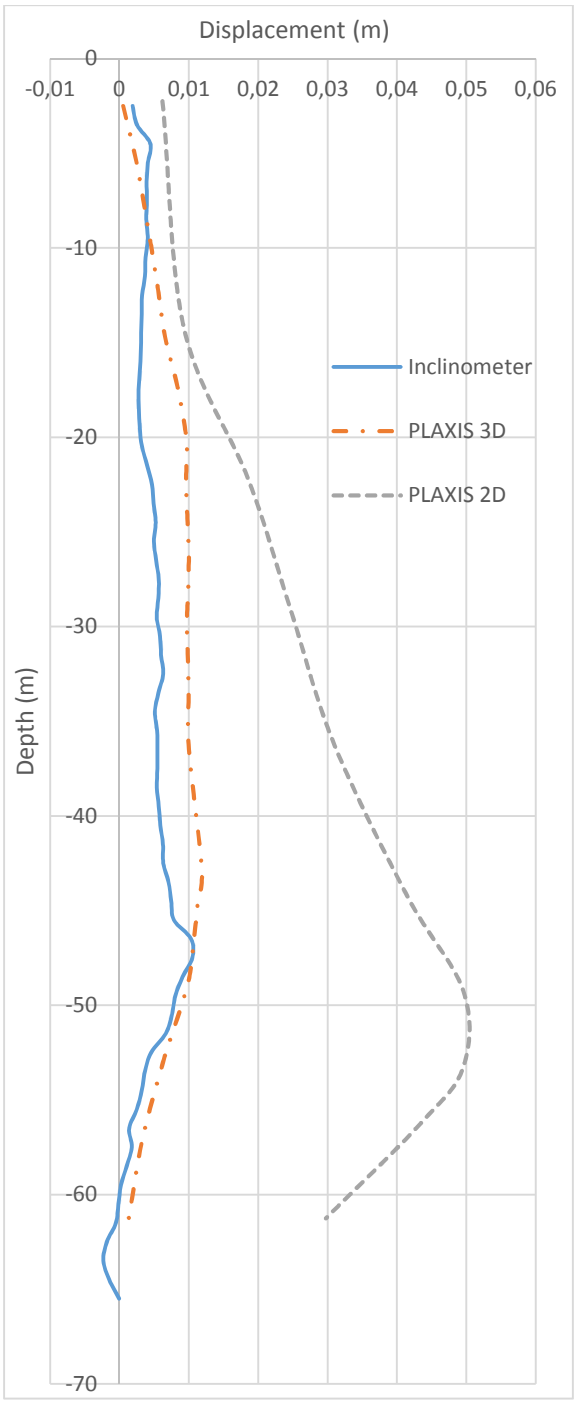

Figure D.9. Comparison of Displacements for Excavation Stage 9 (Inclinometer 1 Region)

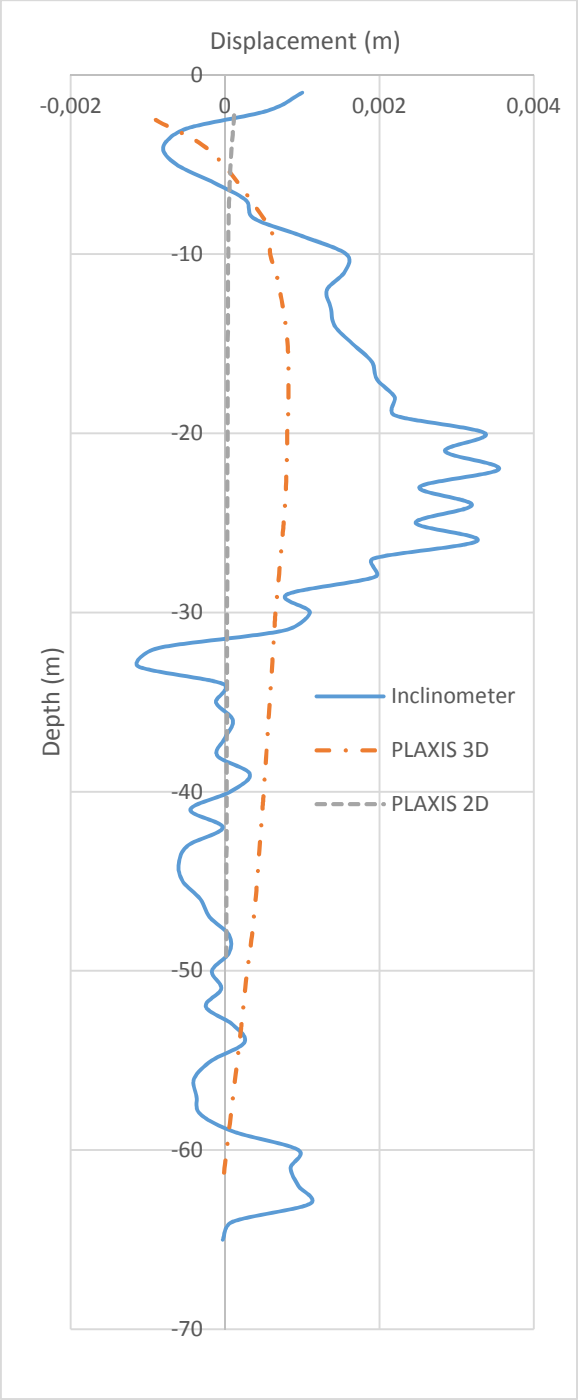

Figure D.10. Comparison of Displacements for Excavation Stage 1 (Inclinometer 2 Region)

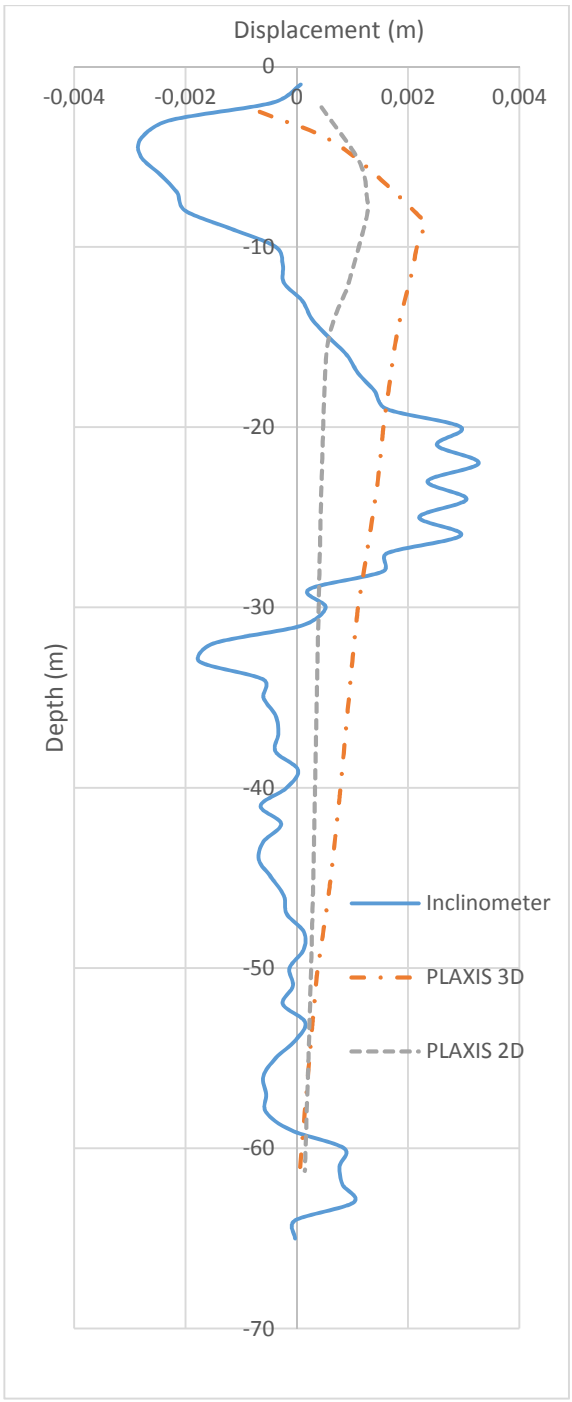

Figure D.11. Comparison of Displacements for Excavation Stage 2 (Inclinometer 2 Region)

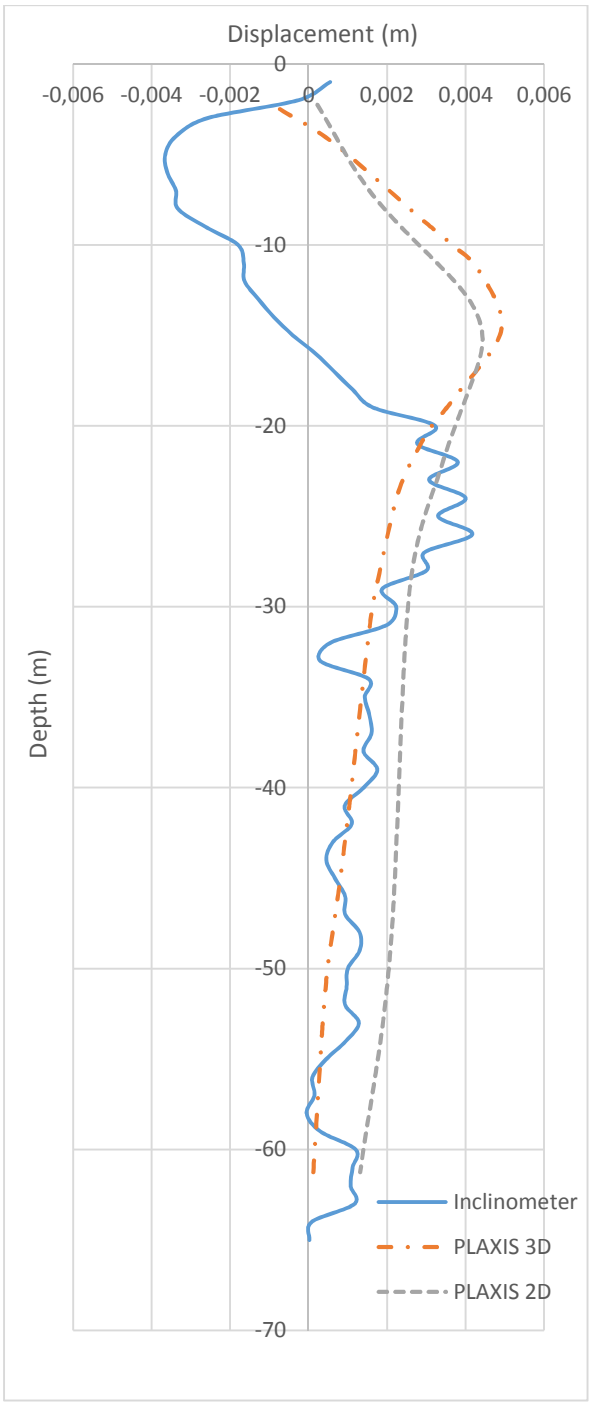

Figure D.12. Comparison of Displacements for Excavation Stage 3 (Inclinometer 2 Region)

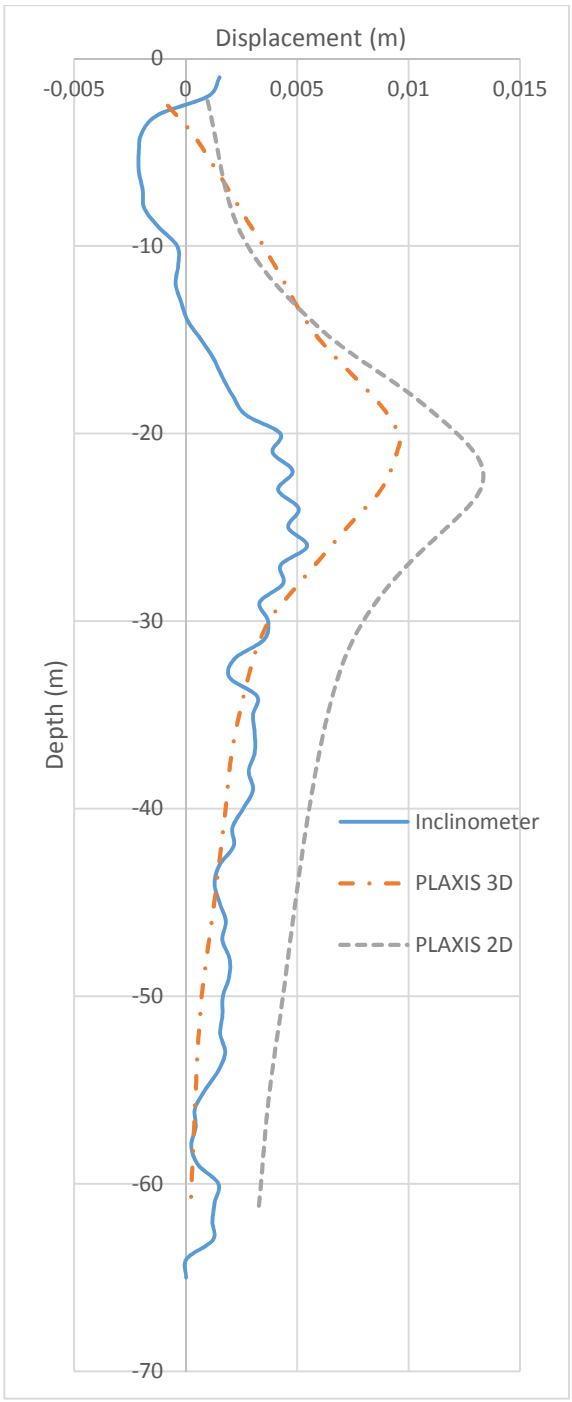

Figure D.13. Comparison of Displacements for Excavation Stage 4 (Inclinometer 2 Region)

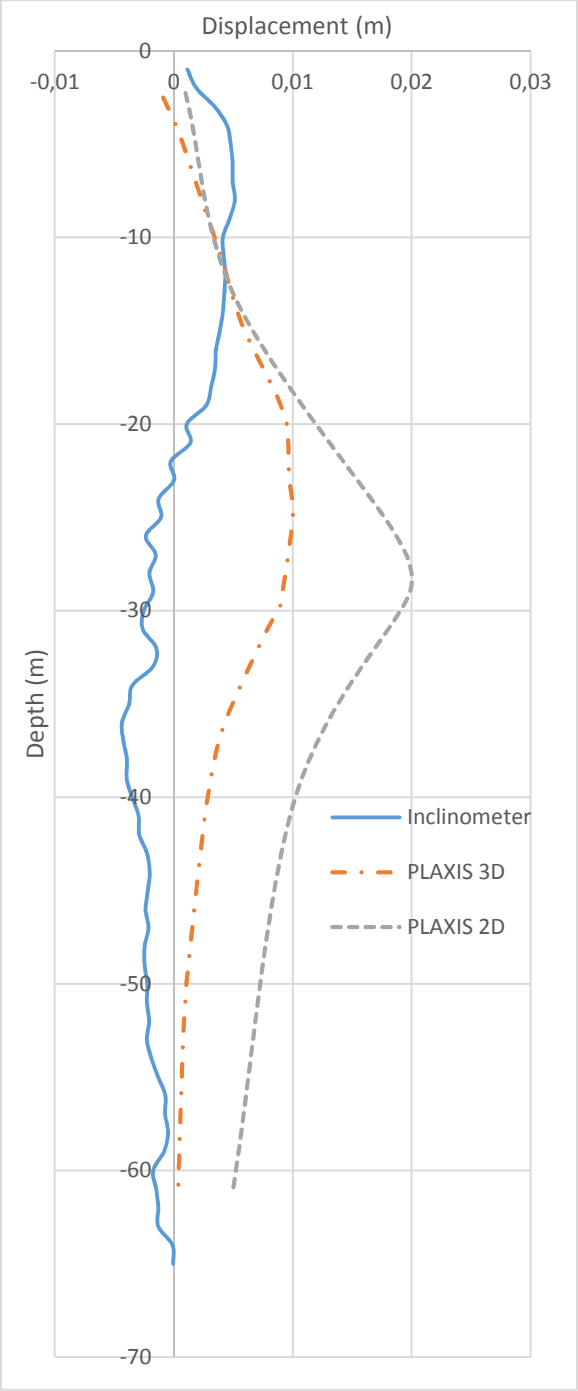

Figure D.14. Comparison of Displacements for Excavation Stage 5 (Inclinometer 2 Region)

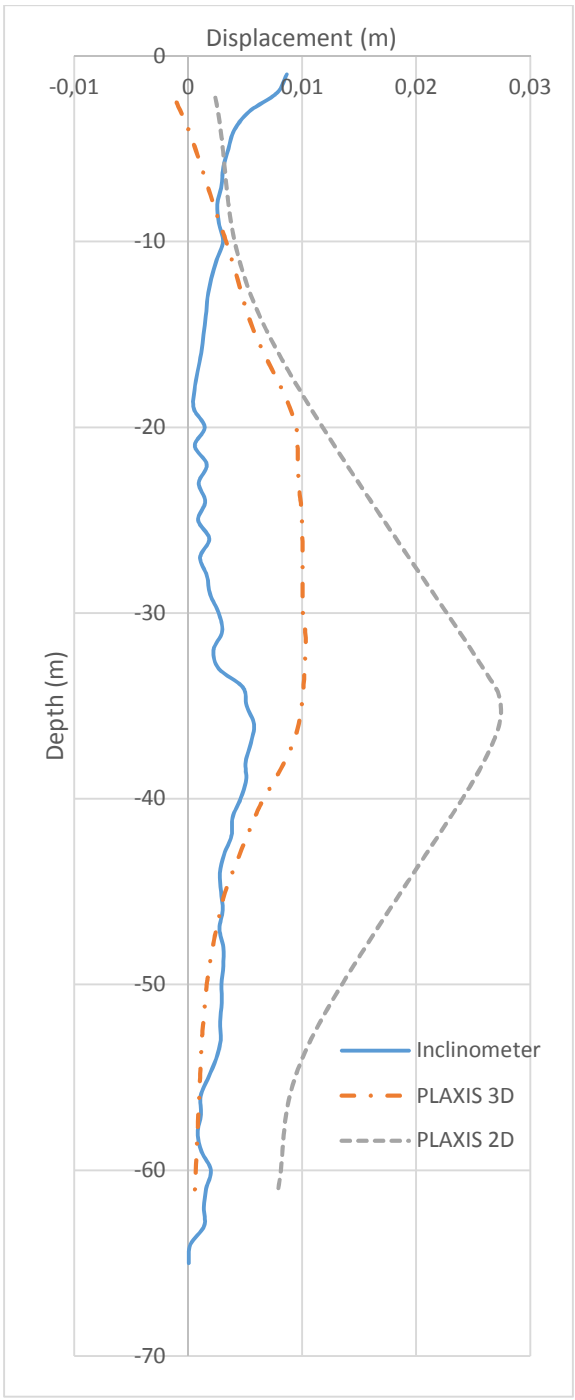

Figure D.15. Comparison of Displacements for Excavation Stage 6 (Inclinometer 2 Region)

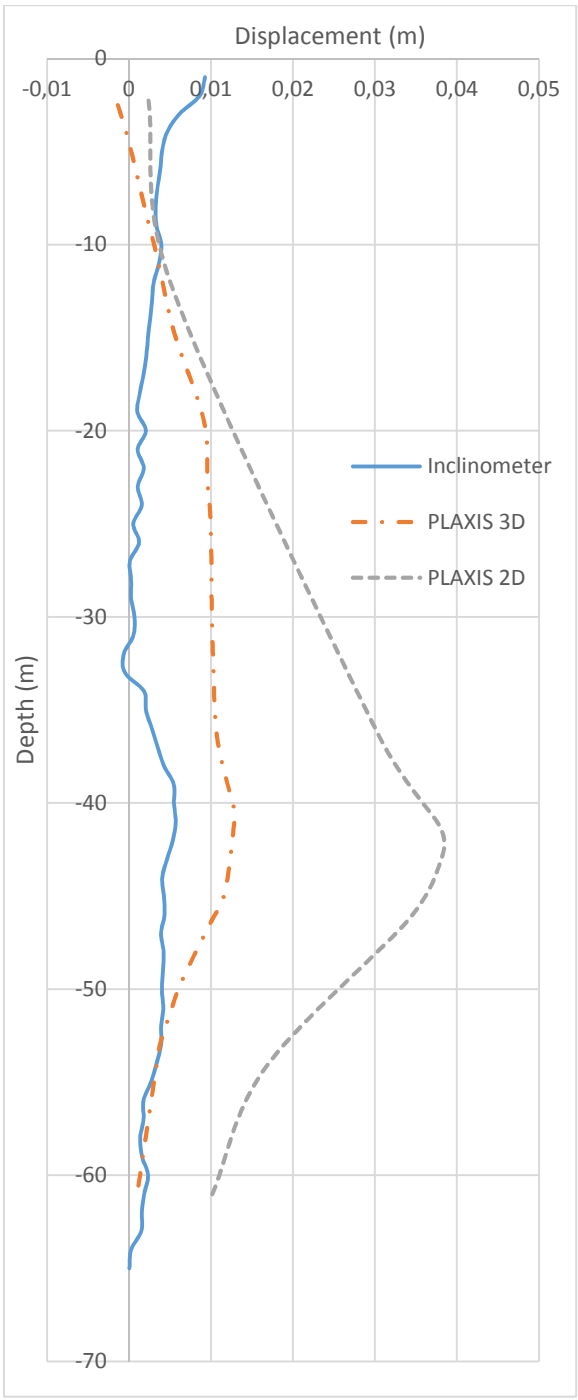

Figure D.16. Comparison of Displacements for Excavation Stage 7 (Inclinometer 2 Region)

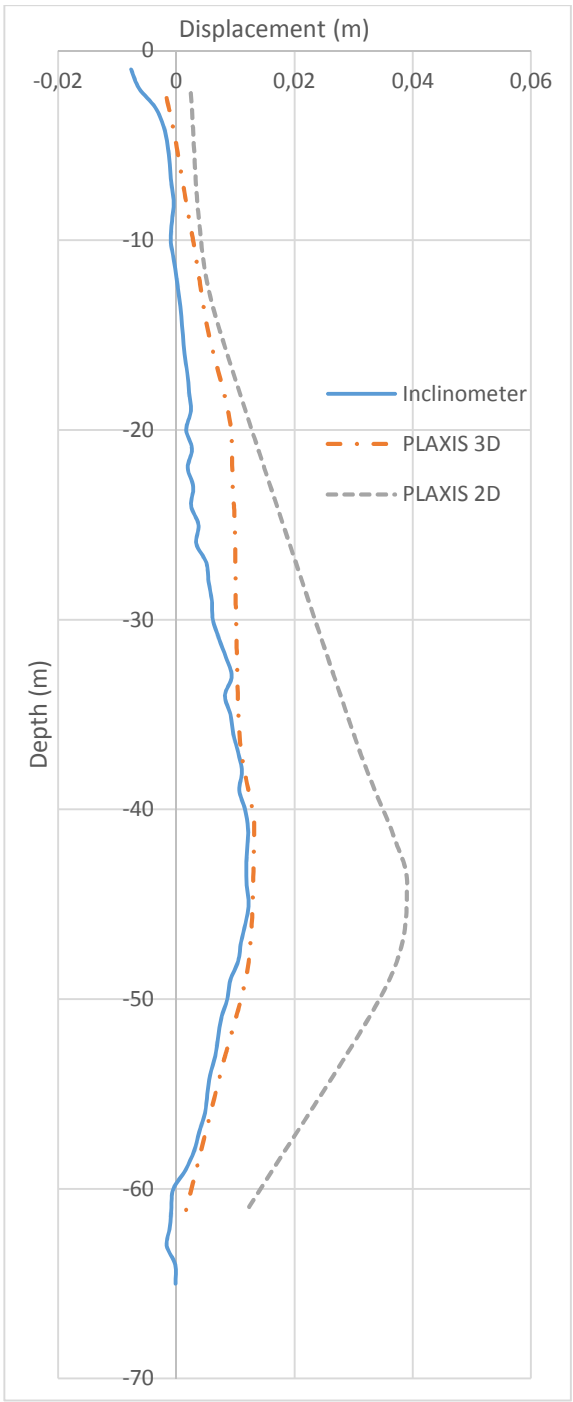

Figure D.17. Comparison of Displacements for Excavation Stage 8 (Inclinometer 2 Region)

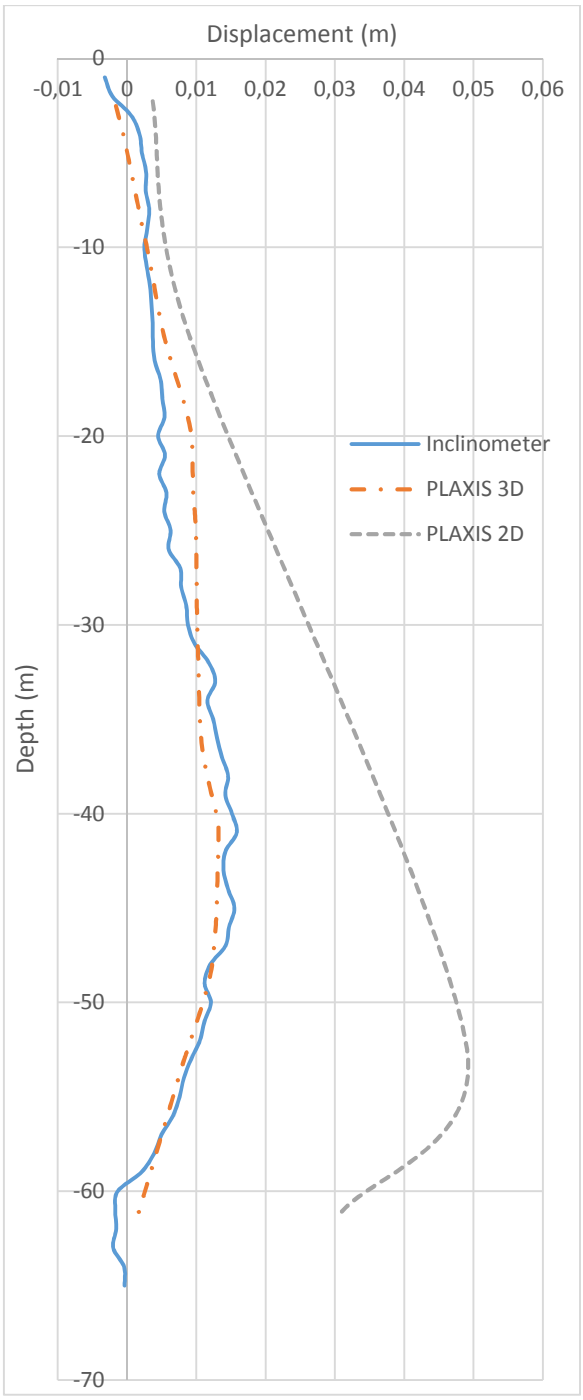

Figure D.18. Comparison of Displacements for Excavation Stage 9 (Inclinometer 2 Region)

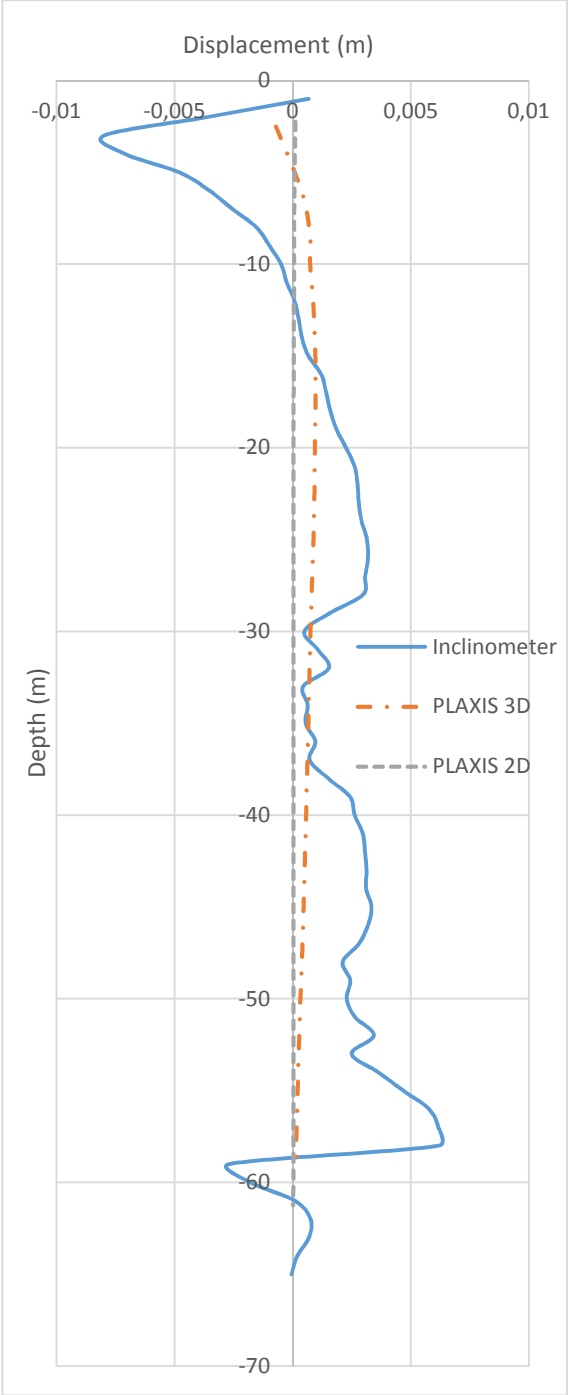

Figure D.19. Comparison of Displacements for Excavation Stage 1 (Inclinometer 3 Region)

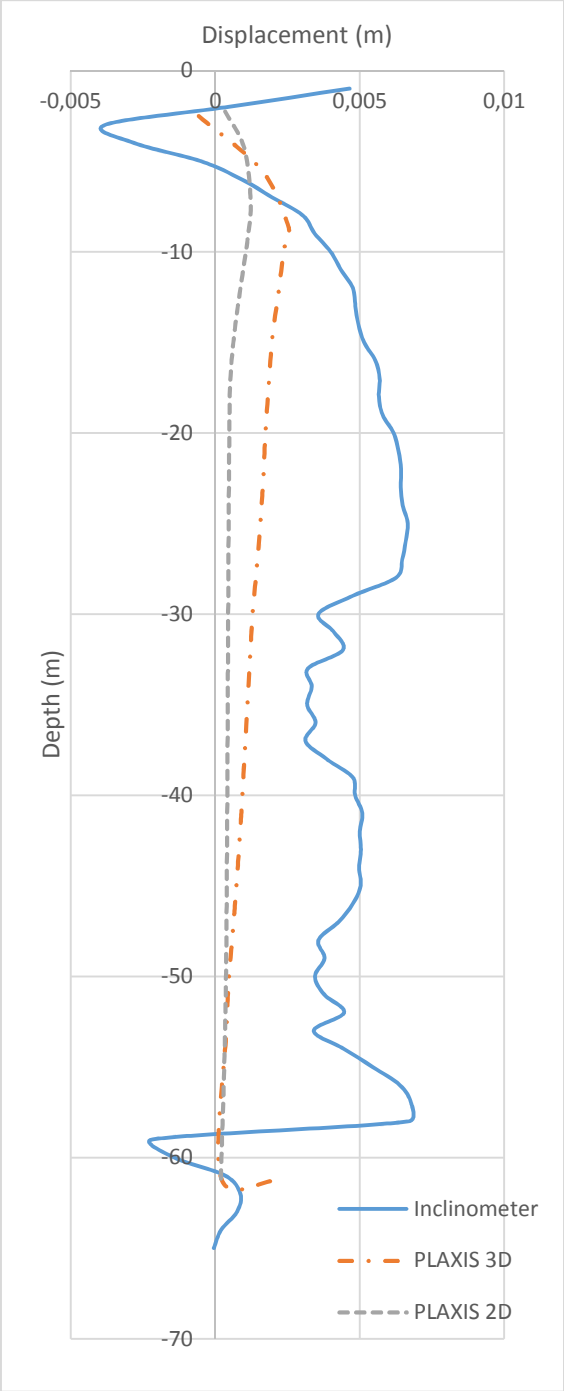

Figure D.20. Comparison of Displacements for Excavation Stage 2 (Inclinometer 3 Region)

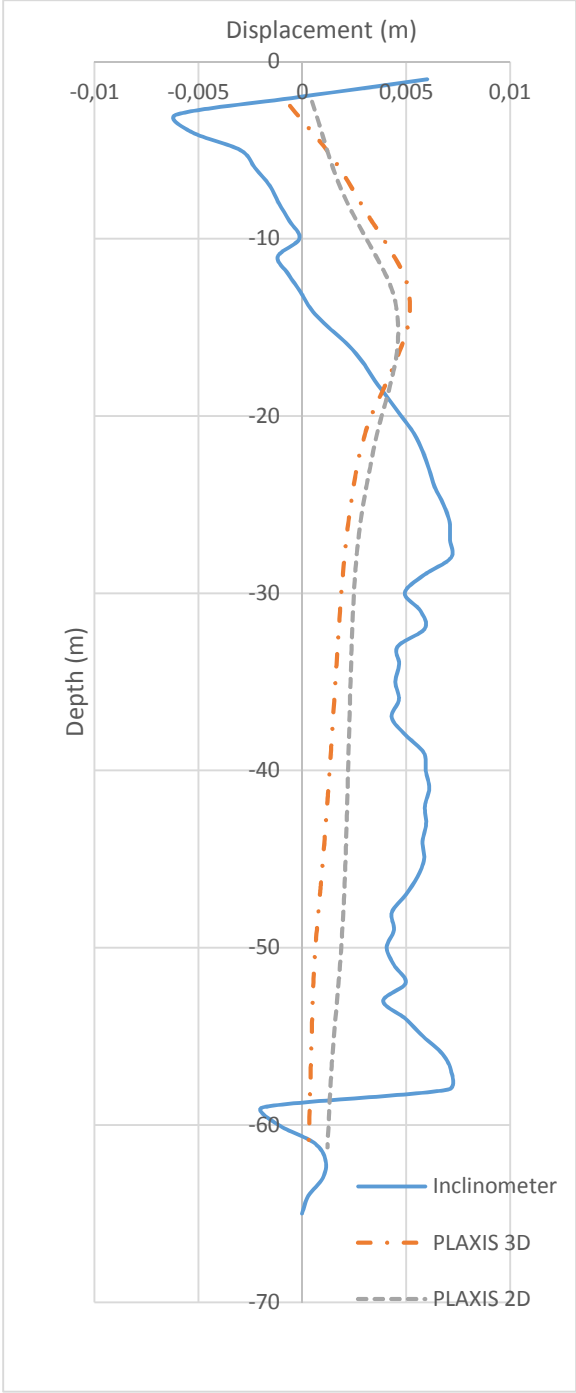

Figure D.21. Comparison of Displacements for Excavation Stage 3 (Inclinometer 3 Region)

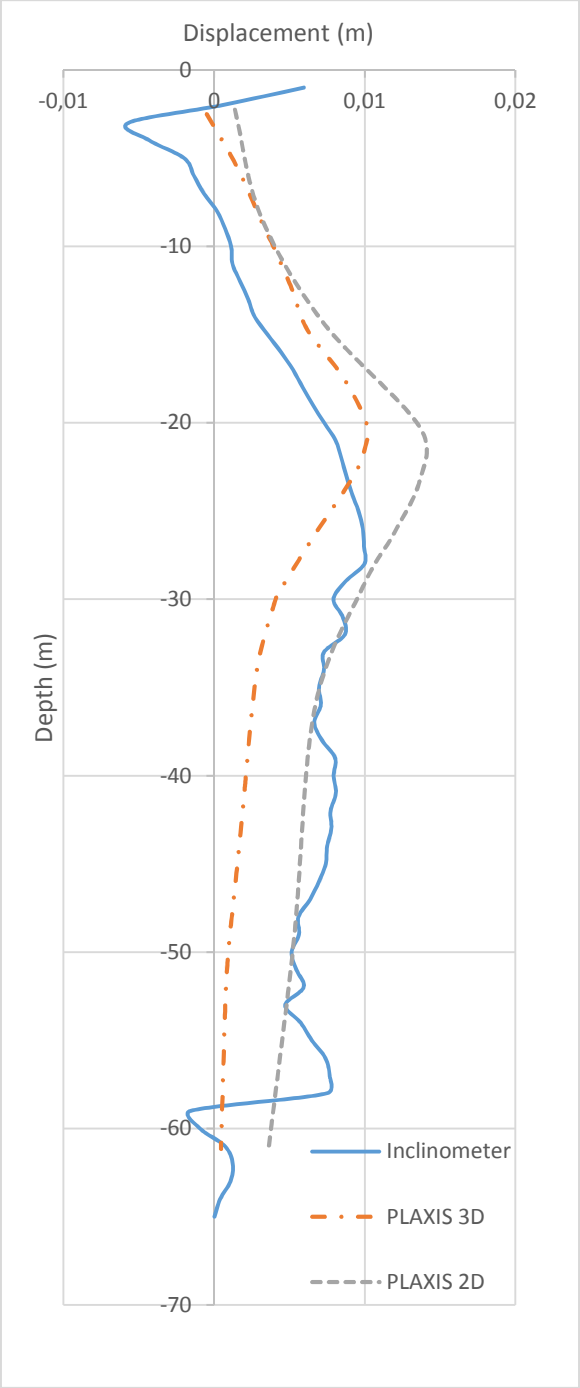

Figure D.22. Comparison of Displacements for Excavation Stage 4 (Inclinometer 3 Region)

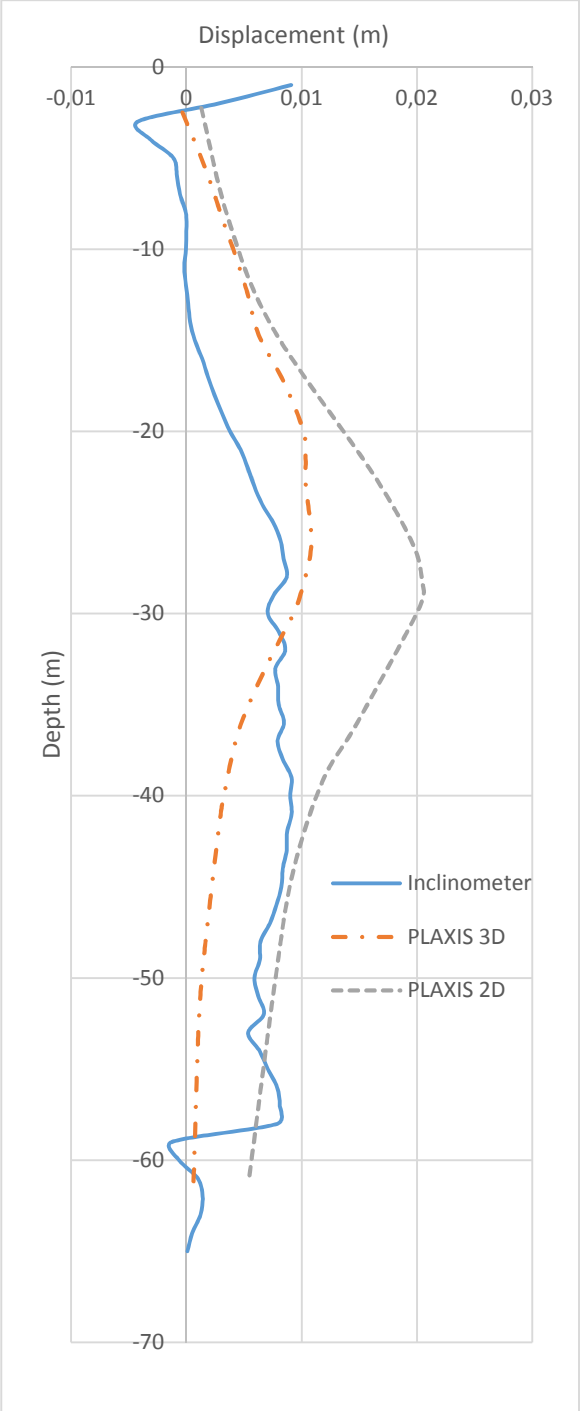

Figure D.23. Comparison of Displacements for Excavation Stage 5 (Inclinometer 3 Region)

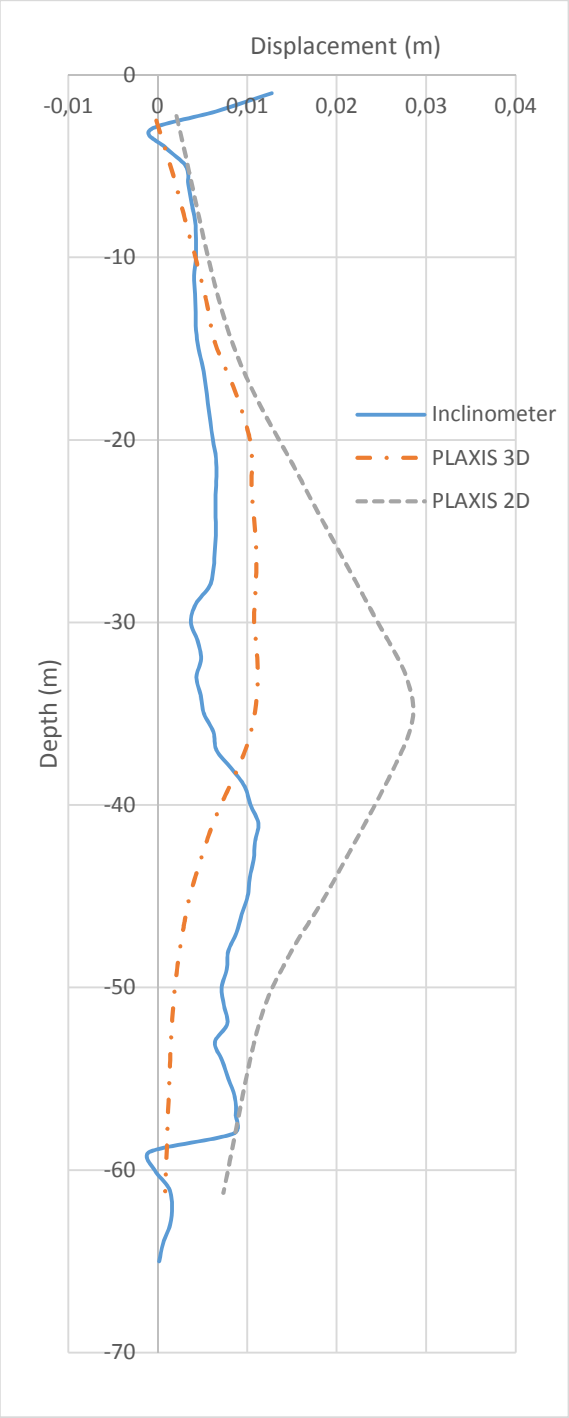

Figure D.24. Comparison of Displacements for Excavation Stage 6 (Inclinometer 3 Region)

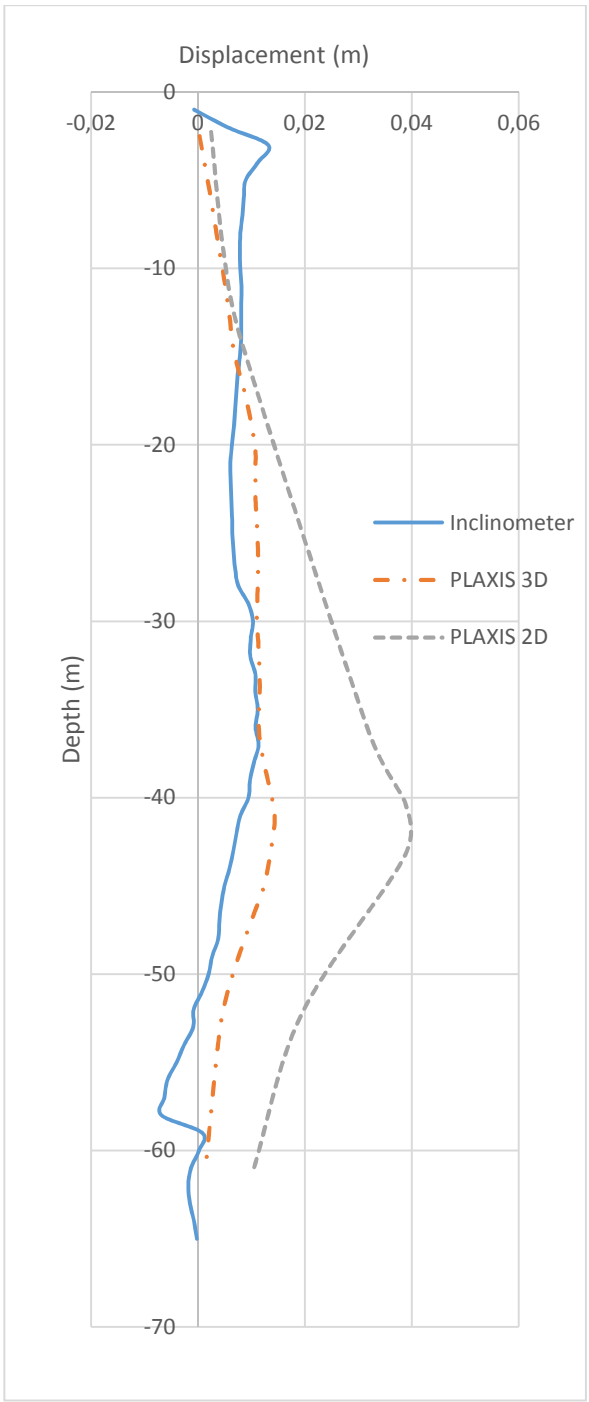

Figure D.25. Comparison of Displacements for Excavation Stage 7 (Inclinometer 3 Region)

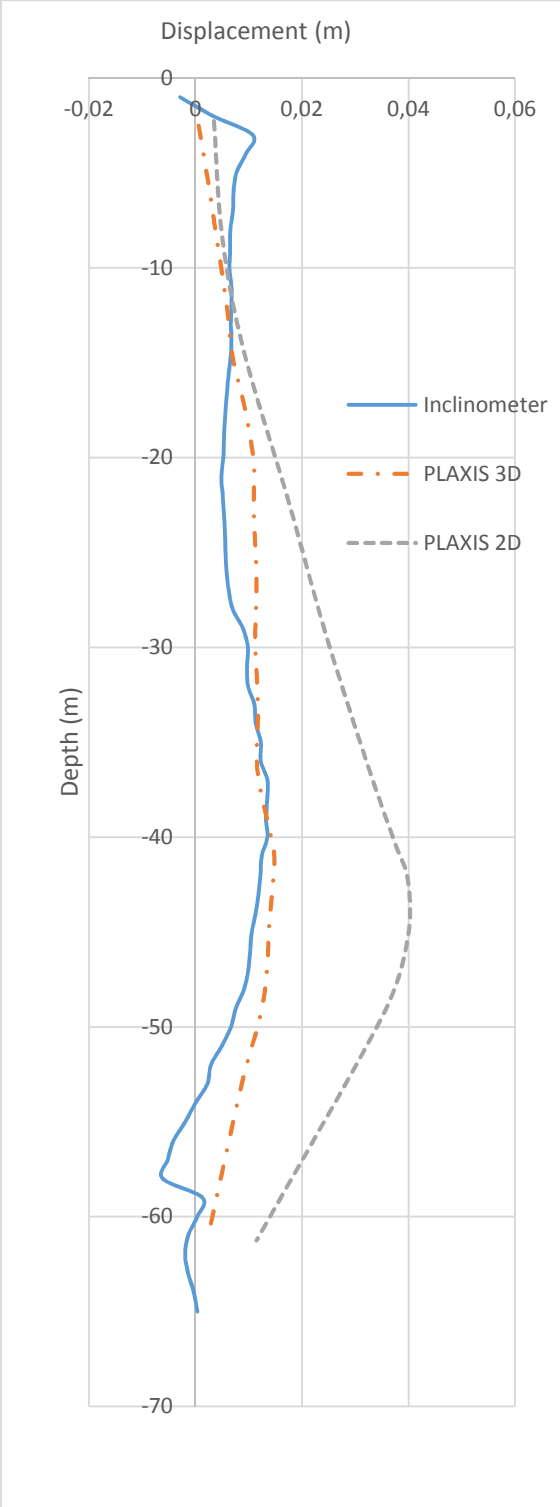

Figure D.26. Comparison of Displacements for Excavation Stage 8 (Inclinometer 3 Region)

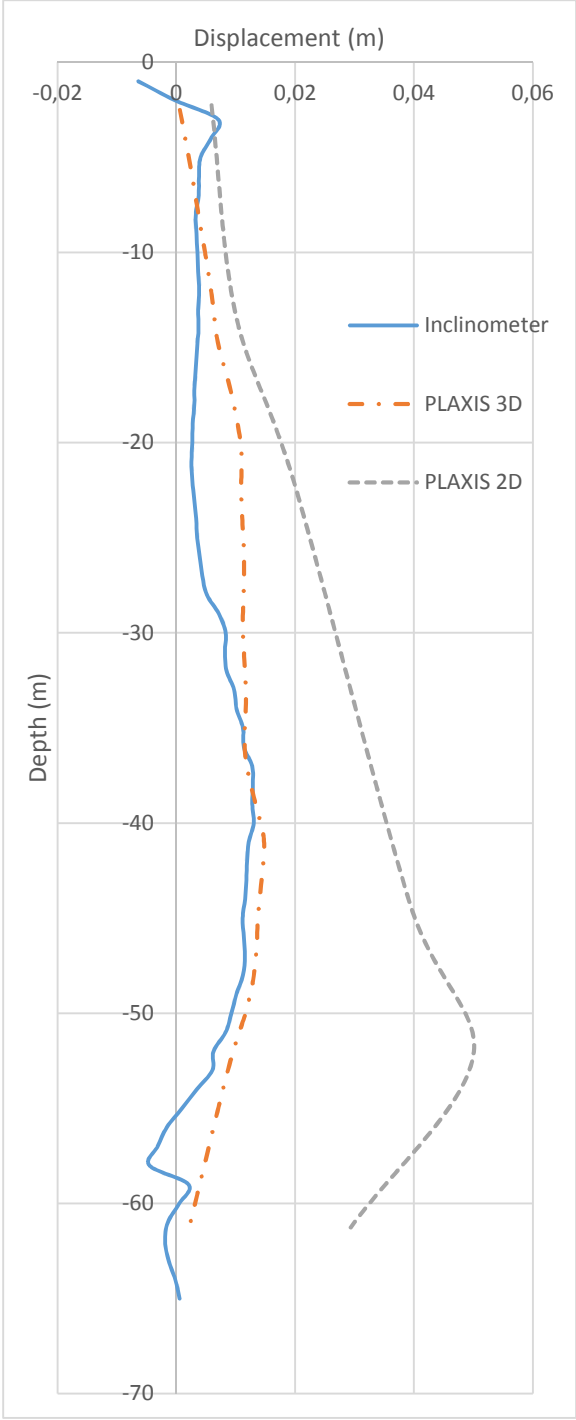

Figure D.27. Comparison of Displacements for Excavation Stage 9 (Inclinometer 3 Region)

APPENDIX E

INCLINOMETER MEASUREMENT GRAPHICS

The graphs in the following pages show the displacement versus depth graphs for 3 inclinometers separately. In each graph, inclinometer readings for all excavation stages are presented.

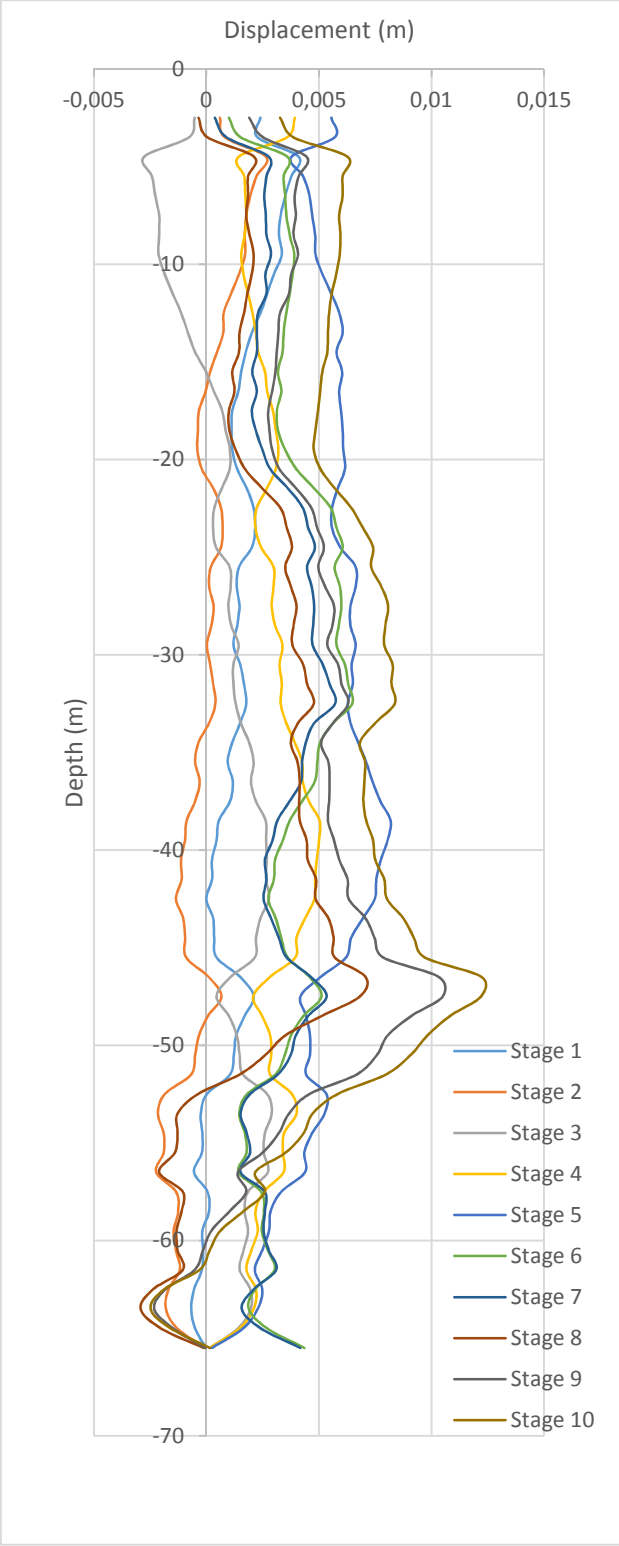

Figure E.1. Displacement vs Depth Graph for Inclinometer 1

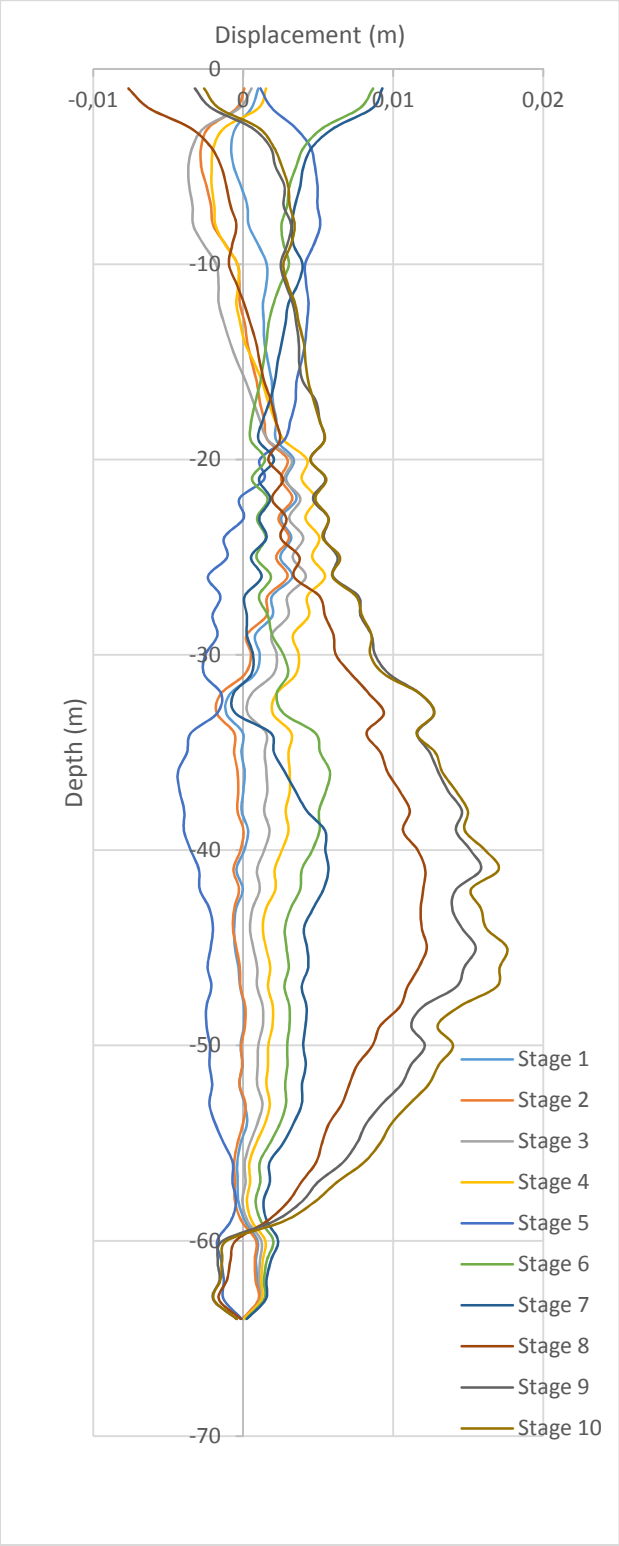

Figure E.2. Displacement vs Depth Graph for Inclinometer 2

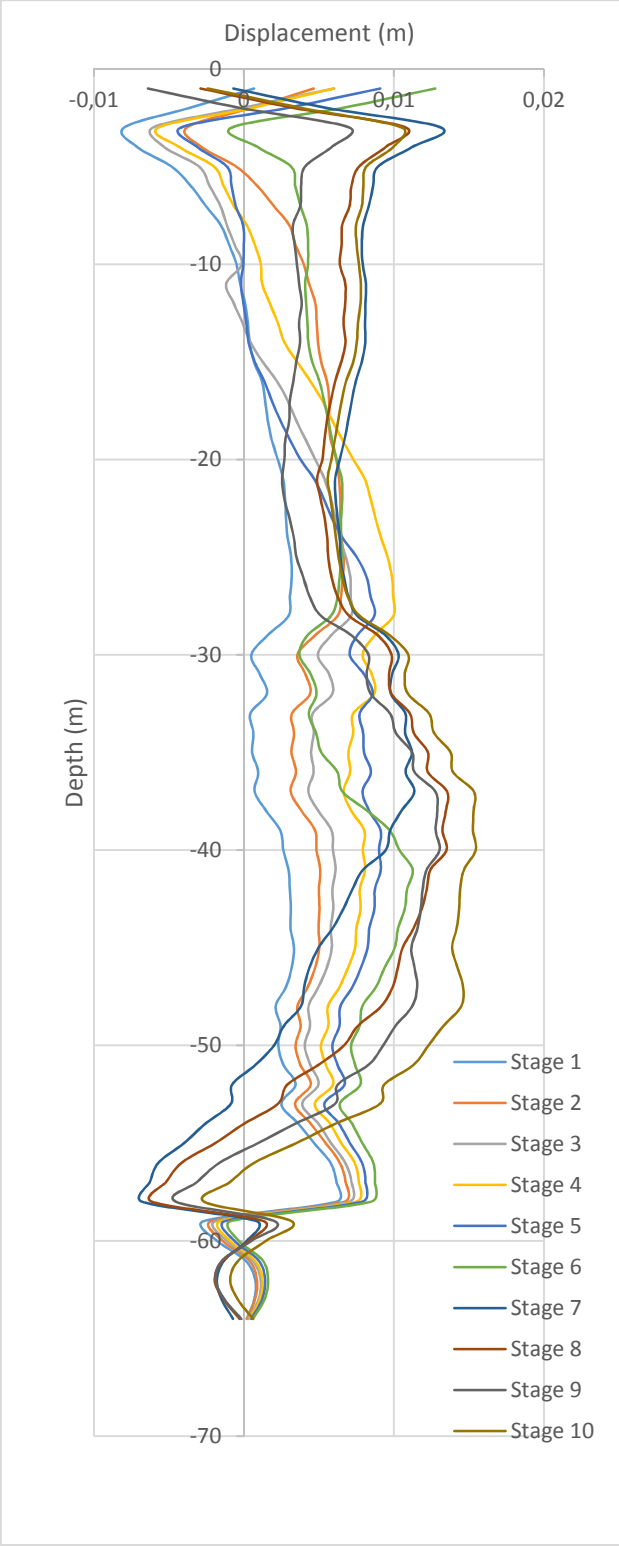

Figure E.3. Displacement vs Depth Graph for Inclinometer 3